1989

New development of laser-based techniques in applications of thin-layer chromatography, microprobe elemental analysis and gas phase pyrolysis

Jianzhong Zhu
Iowa State University

INFORMATION TO USERS

The most advanced technology has been used to photograph and reproduce this manuscript from the microfilm master. UMI films the text directly from the original or copy submitted. Thus, some thesis and dissertation copies are in typewriter face, while others may be from any type of computer printer.

The quality of this reproduction is dependent upon the quality of the copy submitted. Broken or indistinct print, colored or poor quality illustrations and photographs, print bleedthrough, substandard margins, and improper alignment can adversely affect reproduction.

In the unlikely event that the author did not send UMI a complete manuscript and there are missing pages, these will be noted. Also, if unauthorized copyright material had to be removed, a note will indicate the deletion.

Oversize materials (e.g., maps, drawings, charts) are reproduced by sectioning the original, beginning at the upper left-hand corner and continuing from left to right in equal sections with small overlaps. Each original is also photographed in one exposure and is included in reduced form at the back of the book. These are also available as one exposure on a standard 35mm slide or as a 17" x 23" black and white photographic print for an additional charge.

Photographs included in the original manuscript have been reproduced xerographically in this copy. Higher quality 6" x 9" black and white photographic prints are available for any photographs or illustrations appearing in this copy for an additional charge. Contact UMI directly to order.

U·M·I

University Microfilms International
A Bell & Howell Information Company
300 North Zeeb Road, Ann Arbor, MI 48106-1346 USA
313/761-4700 800/521-0600

Order Number 9014972

New development of laser-based techniques in applications of thin-layer chromatography, microprobe elemental analysis and gas phase pyrolysis

Zhu, Jianzhong, Ph.D.

Iowa State University, 1989

U·M·I
300 N. Zeeb Rd.
Ann Arbor, MI 48106

New development of laser-based techniques in applications of thin-layer chromatography, microprobe elemental analysis and gas phase pyrolysis

by

Jianzhong Zhu

A Dissertation Submitted to the
Graduate Faculty in Partial Fulfillment of the
Requirements for the Degree of
DOCTOR OF PHILOSOPHY

Department: Chemistry
Major: Analytical Chemistry

Approved:

Signature was redacted for privacy.

In Charge of Major Work

Signature was redacted for privacy.

For the Major Department

Signature was redacted for privacy.

For the Graduate College

Iowa State University
Ames, Iowa
1989

TABLE OF CONTENTS

GENERAL INTRODUCTION

The advent of the laser has made possible development of many new technologies because of its unique properties not found in conventional radiation sources. For example, laser enhanced ionization(LEI) spectroscopy, coherent anti-stokes Raman spectroscopy(CARS) and intracavity enhanced absorption spectroscopy are all relatively new techniques which require laser sources(1). Laser radiation is characterized by high directionality, monochromaticity, coherence and radiance.

Another important application of laser is for solid sample analysis(2,3). In general, this application can be classified into three categories according to the laser power density used: laser spectrochemical analysis, laser desorption or pyrolysis and laser plasma or microprobe.

Spectroscopic methods, measuring the optical properties of the samples, normally require less laser power, since too much higher power may damage the samples. For solid samples, absorption, fluorescence and scattering are the three most common modes of measurements(4-8). A typical example of this kind of application is the detection of the separated zone on thin-layer chromatography or electrophoresis. The optical measurement in an opaque solid media is much more difficult than that in a homogeneous liquid solution because of the scattering background. The heating effect is often ignored in these experiments except that photoacoustic or thermal

deflection methods(9) are applied to measure the absorption phenomena where the small thermal expansion formed by the absorption of photons is taken as the advantages(10-13).

Laser desorption and pyrolysis are performed at a much higher power density(10^4-10^6 W/cm^2)(14-16), consequently the temperature of the sample surface often reach a few hundred degrees or even over thousands degrees. The studied solid samples, particularly, the organic compounds, may be thermally decomposed or/and vaporized into gas phase. Laser desorption and pyrolysis methods are widely used in mass spectroscopy analysis of non-volatile compounds(17-21), such as polynuclear aromatic hydrocarbons(PAHS), amino acids, oligosaccharides, peptides and nucleosides(22-24). Samples are prepared in a thin film with the organic matrix and vaporized by a pulsed laser. Molecular ions could be found without auxiliary ionization sources.

Laser pyrolysis coupled with GC, MS or GC/MS, has been used to identify biomass materials and polymers(25-30). The GC provides usually a fingerprint characterization.

As the laser power increases much further and reach the throughput energy of most metals at around 10^6 - 10^8 W/cm^2, atomization occurs. At this time, a laser plasma is formed, where the temperature could be as high as 10,000 degrees(31-32). Since a laser beam can be focused into a very small spot(a few μm), laser has been used as an ideal microsampling tool to generate atoms, ions and particles for elemental analyses. In fact, laser microprobe analysis(LMA) was developed two years immediately after the invention of laser(33).

Lasers are also efficient energy sources to pyrolyze the gas phase molecules, particularly infrared laser because of the general efficient rate of vibrational deexcitation(34). As the sensitizer molecules(a very stable absorbent gas) absorb energy from laser radiation, through collisions, a high temperature region is created along with the laser path, where the studied compounds are pyrolyzed. One of the most important features of this laser-induced pyrolysis method is no surface interaction, since gas molecules are pyrolyzed as the cell wall remains virtually at room temperature(35).

Introduction to Thin-layer Chromatography

Thin-layer chromatography(TLC) is a separation method in which uniform thin layer of sorbent or selected media are used as a carrier medium(36). The sorbent is coated on an inert rigid backing plate of suitable size to obtain a stable layer, the stationary phase. The sample to be separated is applied to the surface of the sorbent layer as a spot, near the bottom edge of the plate. The separation is carried out in an enclosed chamber by contacting the bottom edge of the plate with a solvent, the mobile phase, which advances through the stationary phase by capillary forces. A separation of the sample is produced by the differential migration of the sample components in the direction traveled by the mobile phase.

TLC as an oldest form of chromatographic method continues to be widely applied in routine analysis(37), probably due to the following reasons:

(1) Capable of handling multisample simultaneously. It is not

difficult to demonstrate that 30 - 40 samples can be simultaneously separated on a 20 cm X 5 cm TLC plate. In fact, it is probably because of that, TLC has remained as the routine procedure in racing chemistry today to examine the drug abuse(38). This is the most significant feature of planar chromatography that competes with column chromatography in which only one sample is separated at a time.

(2) Separation of complex sample with relatively low cost. A TLC experiment could be set up with only a few hundred dollars. It would be easy to start at any level of research laboratories. Even for a long term consideration, TLC is still the cheapest separation method.

(3) Very simple instrumentation. It can be none at all for the entire experiment that consists of a plate, a container and a solvent. The detection can simply be done with a naked eye probably with the help of a few hundred spray reagents.

(4) Easy to perform two dimensional separation. Multidimensional chromatography can dramatically increase the separation efficiency. This is another important feature of plenary method in which the plate can be turned 90^{o} after the first separation to spread the sample in another direction. This sometime gives better separation than column chromatography methods because the mobile phase can be changed easily in the second dimensional development to optimize the separation for a particular application.

(5) Disposable. TLC is used only one time and then through away. Thus it is often employed as a preparative method to remove the highly retained compounds and the large matrix backgrounds for GC or HPLC

analyses of complex samples to avoid quick degradation of the columns.

(6) Easy change of mobile phase. This has advantage TLC as a scouting technique for HPLC to optimize the eluent composition, since in principle, the separation mechanisms of TLC and LC are the same.

However, in spite of its strength, TLC suffers from many limitations, such as labor and time consuming, inefficient separation and lack of universal and sensitive detections.

The big difference between TLC and LC is the detection methods. Because of the nature of the method of development, LC is performed in a sequential manner so analytes are detected as they elute. In TLC, detection is a completely independent step. Although this sometimes may be recognized as the advantage because the TLC plate can be saved for all different kinds of analyses, the processes are tedious. LC detection is performed under a transparent solution, however, TLC detection is carried out in the opaque non-uniform solid particles with a large scattering interferences. LC detection can be done with a variety of methods, including the universal refractive index detector, polarimetry detector and all different types of electrochemical detectors. In contrast, TLC detection is limited to only a few optical methods such as absorption and fluorescence, except the use of radioactive technique. Without doubt, results would highly rely on the optical properties of the analytes. In addition the highly scattering background of the thin layer material has further hampered the improvement of these detection methods. Direct identification of the analytes on the TLC plate has been extremely difficult.

Densitometry in situ on TLC represents the direct determination of the concentration by absorption(39). The plate is scanned by a beam of light of predetermined wavelength, and the proportion of the reflected or transmitted light by the thin layer is measured photoelectrically. Although it is similar to the conventional spectrophotometry, Beer's law is not followed due to the solid scattering(40). Kubelka and Munk equations must be used for correction. Detection limits are varied from 10 ng to 1 μg(39).

Fluorescence measurement offers larger linear dynamic range and sensitivity(4-6). However it suits only to those fluorescent compounds or those compounds which can be conveniently derivatized to become fluorescent. To expand the applicability of this method, fluorescent quenching has been used, where the TLC plate is prepared by the fluorescent material. The analytes will appear to be a dark spot under the UV lamp, since the samples absorb the incident light and as a result, the fluorescent intensity decreases. This is actually similar to the absorption method, but it helps visualization in the UV region.

Visualization is the most simple and straightforward method to observe the separation if the compounds are color or strong UV absorbent(37). However for most non-color compounds or weak UV absorption compounds, all above mentioned detection methods are not possible unless through a color development or spraying process, such as amino acids, sugars, pesticides, steroids and hydrocarbons(37). Hours of heating or even UV radiation are frequently required to promote the "color reaction". The reproducibilities of these processes are also very hard to control. This

is the most undesirable step in TLC and is also the second major reason to the scattering background that limits the further development of TLC.

In recent years, many research have been focused on development of new TLC detection methods. An indirectly fluorescent method has been investigated recently(41), in which a fluorescent solvent is used. A dark spot is created by displacement of the fluorescent compounds by analytes during the migration process. By this method, non-absorbed substances can be detected.

The use of the well collimated and high power laser in TLC detection has made two very important impacts. First of all, it improves the fluorescence detection sensitivity since fluorescence intensity is proportional to the strength of the excitation light and most of lasers have at least 100 times as many as photons by conventional light sources. The first application of laser to TLC, in fact, is published in the fluorescence method by Berman and Zare(4) in 1975 with subnanogram detection of aflatoxins. The detection has been improved later to about 10 pg(5). Secondly, the collimated nature of the laser beam allows for better focusing and easy instrumentation to improve the resolution and the scanning. With a photoacoustic beam deflector, a laser can scan a 10 cm as fast as 1 ms. By repeat scanning, one can decrease the scattering background because of the averaging effects. It also allows for two dimensional scan of the plate in a few seconds(44).

Laser has also been employed to address the identification problems. Fluorescent line narrowing is another newly applied laser-based technique for direct identification of TLC separated spots(45). The TLC plate is

placed in helium temperature in which most of molecules are in the v = 0 state, and irradiated by laser. The fluorescent spectra showed very sharp peaks and has been used to characterize carcinogen compounds.

Flame ionization detector(FID) and electron capture detector(ECD) are the most successful detectors developed today for GC, because of their sensitivity and generosity. Effort has been made to incorporate them to LC and TLC(41a - 41e). The application on TLC plate was very unsuccessful because a heater was used to vaporize the samples which was not able to provide the satisfied lateral resolution on the TLC plate. Thus a TLC rod was developed in order to use the FID detection(42), in which the rod can be moved along on the flame between two electrodes that collect the ion signals. Since the powerful FID detection, the research and application of this technique grown so rapidly that it have even been developed into a independent TLC method which is now called chromarod(43).

A new laser-based TLC detection method is proposed here based on laser pyrolysis and laser desorption in which the laser is used to vaporize the samples separated on TLC plate into gas phase. Then the sensitive and universal GC detectors can be easily facilitate for TLC detection.

Multidimensional chromatography has been a very attractive due to the increase of separation efficiency(46). The combination of GC to GC, LC to LC and even LC to GC have been widely accepted in practical applications. However, direct coupling of TLC to GC has been difficult, probably because of the sample transfer which involves solid to gas phase transition and require spatial resolution on the TLC plate. With the laser desorption and pyrolysis technique, these difficulties have been overcome. A

successful demonstration of coupling of TLC to GC will be shown with pesticides as the samples, since pesticides analyses have been the very important issue of environmental and food industries.

Laser Microprobe Analysis

Determination of trace element distribution is a very important field of analysis, as a result of the dependence of many properties of new and special materials such as semiconductor as well as biological and biochemical process on the presence of trace elements. Laser is a very adequate tool to be used in this application, because the laser can vaporize a very small amount of material(μg to pg) to give good lateral resolution and depth information. The advantages of laser include the ability to handle both electrically conductive and non-conductive samples which are difficult to deal by other microprobe techniques.

The laser interaction with solid is a very complicated event, which are affected by a large numbers of variables, including the heat capacity and thermal conductivity of the samples as well as the laser beam properties, such as wavelength, power density and temporal profile of the energy.

When the laser beam strikes the surface of a sample, a percentage of the beam will be reflected, dependent on the nature of the sample surface. The reflection will decrease as the sample absorb the incident radiation and begin to heat. As the temperature increases, the absorption increase abruptly(29). At the beginning of the plume before the actual

vaporization of the sample occurs, a very high temperature can be attained in a very thin layer(47). This temperature can be much higher than the boiling point of the metals. The further absorption of the laser energy is described by inverse bremsstrahlung(free-free electron photon interaction)(48). Finally due to the pressure gradient, the plume expands and leaves the sample surface into atmosphere. The thermal energy than converts into kinetic energy of the orderly expansion.

During the expansion, collision between the vaporized particles and the ambient gas molecules will create acoustic waves. The strength of the sound wave is proportional to the amount of material vaporized. This has been demonstrated to be a sort of internal standard to correct the errors introduced by laser power fluctuation and matrix effects for quantitation.

Since the temperature of the plasma is so high(over 5,000 ^{o}C), a large continuum plasma emission would be observed in which most of the energy is in the UV range.

The success of the laser microprobe analysis relys on the detection methods. Many techniques associated with the detection of the laser generated plume have been developed. The analysis is either directly taken in the plume or taken after it has been transferred for secondary excitation. Since the atoms and ions within the plume are excited, the simplest method is emission spectroscopy measured directly from the plume(33). However, the sensitivity is limited because of the high plasma emission background and the self absorption. One method to improve the signal to noise ratio is by the use of auxiliary excitation, often by a

spark discharge. An electrical discharge can pass through the laser plume by positioning a pair of electrode above the sample on either sides of the plume. Formation of the discharge can either be triggered passively by the breakdown when the ionized vapor from the sample bridges the electrode gas or activated by setting a switch delay so that the discharge is externally triggered to control it more reproducible. However, it may introduce contamination from the impurities of the electrodes and it also worsens the reproducibility because of the additional fluctuation of the discharge.

Laser enhanced ionization has been employed directly in the plume as a diagnostic tool(49). If the excitation laser wavelength is tuned in resonance with the absorption band of the analyte, ionization is enhanced significantly. Atoms or molecules can be excited by absorbing one or more photons, then the highly excited species are ionized by collision process. The ions are collected with a pair of copper electrodes. Over 70 times of ionization enhancement was observed in sodium samples. However, the analytical application of this technique is still ambiguous since to trace elements, this enhancement will be totally buried in the large ionization signals of the major components.

Atomic absorption measured the large population of the ground state atoms, therefore, might potentially sensitive. It can operate either on the plume or after transfer. For direct plume measurement, the light source is usually focused on 10 mm above the surface to decrease the plasma interference. The temporal resolution can be applied to further reduce the background since the plasma emission disappears quickly and

the ground state atoms will remain longer. With sample transfer by a gas flow, the atomic absorption can be measured in a normal graphite furnace(50,51).

The samples can also be transferred to ICP for emission spectroscopic measurement, called laser ablation solid sample introduction ICP. For any sample transfer method, however, the mass sensitivity is limited by the dilution caused by the gas flow.

In a laser energy of 5 X 10^9 W/cm^2, the degree of ionization can approach 100%(52). Of cause, the most sensitive and selective method to detect ions in the plume is by mass spectrometry. A pulse laser will generate a transient signal that can be rather easily measured by time of flight(TOF) MS. The TOF device has been incorporated an ion reflecting mirror to help compensate for the kinetic energy spread of the ions. The sensitivity is in ppb range. Fenner proposed the first mass analyzer for the laser plume, where the method was primarily used for the measurement of the distribution of inorganic ions in biological samples. Another variation of this method is called laser microprobe mass analyzer(LAMMA).

A chemiluminescence method is proposed in this dissertation for the elemental detection in the laser generated plume. The chemiluminescence is produced by the chemical reaction of analyte atoms formed in the laser plume with the ambient gas reagent. The chemical reactions of metal atoms with oxidant molecules are normally high exothermic. The excessive energy will be released by heat as the ground state products are formed. However, the high reaction exoergicity often entails the presence of the electronically excited products which give emission as they return to the

ground state. Chemiluminescence can be a very attractive method due to the following reasons:

(1) This technique is relatively simple. As in atomic emission, chemiluminescence can be directly measured in the plume without additional excitation instruments and without sample transfer. No sample transfer sometimes means mass sensitive because the amount of material vaporized can be controlled to a minimum.

(2) This technique has relatively low background. Chemiluminescence as observed, taken place at the top periphery of the plume, might spatially separated from the plasma emission by simply blocking a few mm from the sample surface. in addition, temporal resolution can be used since the possible time delay of the reaction and the relatively longer life time of the chemiluminescence species, while plasma emission lasts only very short time.

(3) This technique is chemical selective. Chemical selectivity can be introduced by selecting different reagent gases.

Laser-induced Gas Phase Pyrolysis

Pyrolysis is a thermal degradation process in which complex molecules are broken apart into simpler unites by the use of heat. It is a very important chemical process in industry as the pyrolysis of heavy oil to make gasoline. Pyrolysis is also a very useful organic synthesis method such as in dehydrogenation and retro-Diels-Alder reactions(53). The study of pyrolysis reaction has been the fundamental interest and industry

values for products control. Furthermore, the pyrolysis products distribution may help one to interpret the mass spectra since there are so many similarities between them(54-54a).

The conventional types of apparatus used for pyrolysis study can be either furnace type or filament type. The furnace type is normally operated in a continuous mode, where samples flow through a hot tube or a chamber, or sit simply in a holder if they are solid. Flash vacuum pyrolysis, a widely used gas phase pyrolysis method, is one of the furnace type devices. The vapors of the organic compounds are pumped through a hot quartz tubing and the pyrolysis reactions take place under vacuum pressure(a few torrs to 10^{-5} torrs), in which the secondary reactions could be minimized. The products are trapped by liquid nitrogen on the vacuum line for further analyses.

Filament type pyrolyzer, often operated in pulse mode, is used for study of non-volatile compounds. In essence, it consists of a small coil of electrically resistive wire and electrical lead. The compounds are coated in the filament surface, then decomposed while the filament is heating up with a pulsed current. The temperature which is the critical point in pyrolysis experiments, however, is difficult to control here and thus reproducibility is poor.

To better control the temperature profile, a Curie-point pyrolyzer is designed(55-57), where a ferromagnetic wire is centered in a glass or quartz tube, a high frequency induction coil surrounds the tube and heats the wire by induction. The wire heats up till its Curie-point is reached (This is the temperature at which the wire becomes paramagnetic and its

energy intake drops thus holding the temperature of the wire at this point.). Different pyrolysis temperature are obtained by using wire of different Curie-point. Many pyrolysis experiments have been successfully demonstrated in its applications, including for gas pyrolysis(58).

In all these conventional techniques, surface catalysis effect is always questioned because molecules are likely decomposed on the hot surface of the heating devices(59-62). The interpretation of the product distribution and the reaction mechanisms would be difficult. The true kinetic energies of reactions would hardly be estimated.

The development of lasers, particularly infrared laser, has opened a new possibility to revolutionize the pyrolysis methods(35,63-67). It is known the use of high-flux infrared laser to excite a special vibrational band has made the possible to affect the chemical conversion(68,69). However, there are essential limitations because of the generally efficient rate of vibrational deexcitation. But, the rapid intermolecular vibration-translation energy transfer, on the other hand, is advantaged to rapidly heat the gaseous mixtures of reactants to a pyrolysis effective temperature(500 - 1500 ^{o}K). This provides a strictly homogeneous reaction condition wherein the cell walls remain at low temperature. Silicon tetrafluoride and sulfur hexafluoride are often used as the sensitizer to absorb the laser photons and convert them into thermal energy. It is because that (1) they are inert and very stable, so they do not dissociate at the temperature below 1,600 ^{o}K(70); (2) they possess large absorption cross sections for the infrared radiation at the available wavelength.

A model is developed to predict the temperature profile of the laser-induced heating in the pyrolysis cell, in taking into account of the explicit temperature dependence of heat capacities, thermal conductivities, molar absorptivities, and gas densities. Then, this pyrolysis method is applied to study the thermal decomposition of tetralin which has been a very important chemical in the coal industry(71).

SECTION ONE:

QUANTITATIVE THIN-LAYER CHROMATOGRAPHY BY LASER PYROLYSIS AND FLAME IONIZATION OR ELECTRON-CAPTURE DETECTION

Introduction

Thin-layer chromatography (TLC) is a simple, rapid and versatile separation technique. Features of two-dimensional separation and multiple sample handling have also contributed to its widespread application. TLC readily provides qualitative results. For quantitative determinations, densitometry, fluorimetry, fluorescence quenching, visual comparison, spot area measurement, and radioactive methods are representative of the methods currently available (1).

Laser-based fluorimetry is the most sensitive technique. Detection limits are often in the 1-10 pg range (2). Fluorescence detection is however limited to those compounds which fluoresce or can be conveniently derivatized to become fluorescent. Densitometry is the most common quantitation method in TLC. Detection limits with commercial scanners and high-performance plates are typically at the nanogram levels for compounds that absorb visible or UV light strongly. With the recent development of a laser photo-acoustic densitometer (3,4), detection limits of 7.5 pg for α-ionone and 170 pg for orange G have been reported. All the quantitative techniques except radioactive methods are highly dependent on the optical properties (absorbance or fluorescence) of the analytes. Sensitivity

varying over several orders of magnitude is observed.

Many interesting applications of TLC are for "colorless or very weakly absorbing compounds, e.g., hydrocarbons, lipids, pesticides, carbohydrates, amino acids, proteins and glycols. Normally a "color" developing is needed. "Color" developing processes are often undesirable. Heating and even UV radiation are usually involved to promote the reaction. For example, one determination of amino acids with densitometry was described as follows: spray with ninhydrin reagent at a distance of 30 cm from the plate; heat it in an oven for 15 minutes at 60½C; and place it in a dark cupboard for 4 h before scanning (5). Two spray reagents and two heating procedures were proposed recently for amino acids analysis with a limit of detection of 0.5 - 1.0 μg (6). Quantitative results rely on the choice of spray reagent, spraying skill, heating temperature and heating time. Reproducibility is therefore poor. Even after spraying, optical detection on an opaque and intensely light scattering TLC plate is a difficult task. The Kubelka-Munk correction is often needed for nonlinear effects, although implementation is not difficult with the help of personal computers.

In this paper we describe a new quantitative TLC method: laser pyrolysis scanning (LPS). This technique is simple, rapid, highly instrumental, and has little dependence on the optical properties of the analytes. There is no need for spray reagents and "color" developing, and is applicable to all organic compounds. Briefly, a TLC plate after separation of the analytes is irradiated with an infrared laser to produce a high-temperature spot. The analyte is thus pyrolyzed and swept

into a flame ionization detector or an electron-capture detector by a carrier gas.

Experimental Section

Apparatus

The schematic arrangement of laser pyrolysis scanning with a flame ionization detection (LPS-FID) system is shown in Figure 1a. A CO_2 cw laser (Molectron Model C250, Sunnyvale, CA, U.S.A.) was used and the laser beam was focused on 2.5 mm on the TLC plate with a 1.0-m focal length concave mirror. Either a flame ionization detector or an electron-capture detector [both were dismounted from a Model 550 gas chromatograph (Tracor, Austin, TX, U.S.A.)] was directly connected to one end of the cell. The carrier gas used was hydrogen-helium (1:2) for FID and argon-methane (9:1) for electron-capture detection (ECD), and the flow-rate was 80-100 ml/minutes. The signal was collected by an integrator (CI 3000).

Figure 1b shows the details of the pyrolysis cell. The cell was made of copper and has a 70-mm long, 12-mm wide, and 7-mm high chamber to accommodate a 50 mm x 12 mm TLC plate. The open end of the cell can be closed with an O-ring seal. A potassium chloride window (50 mm in diameter) was attached to the cell with epoxy (Eccobond, Waltham, MA, U.S.A.).

Chemicals

The test compounds were phenylalanine, serine, p,p-DDT, and methoxychlor. These were obtained from Aldrich and used as received. The

Figure 1. Experimental Setup

a) Schematic diagram of quantitative TLC with laser pyrolysis scanning and flame ionization detection.

b) details of the laser pyrolysis cell. M = mirror, int = integrator.

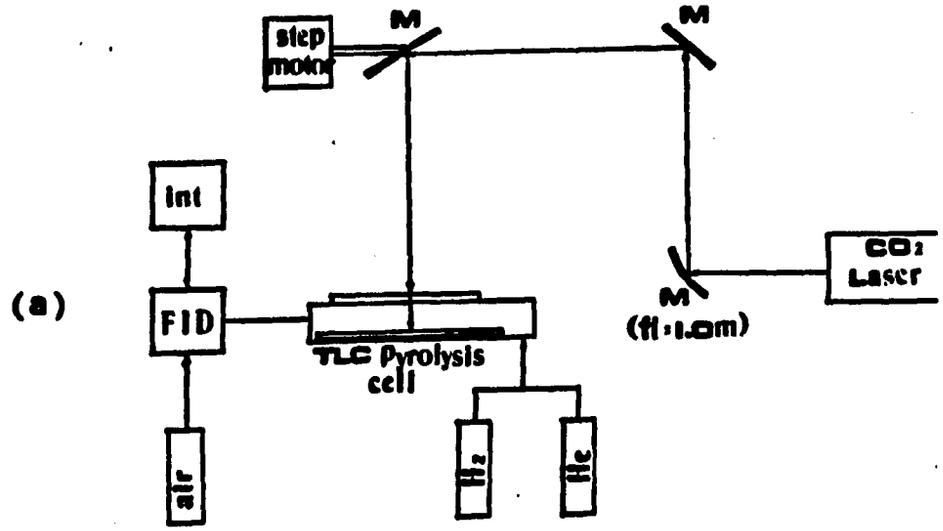

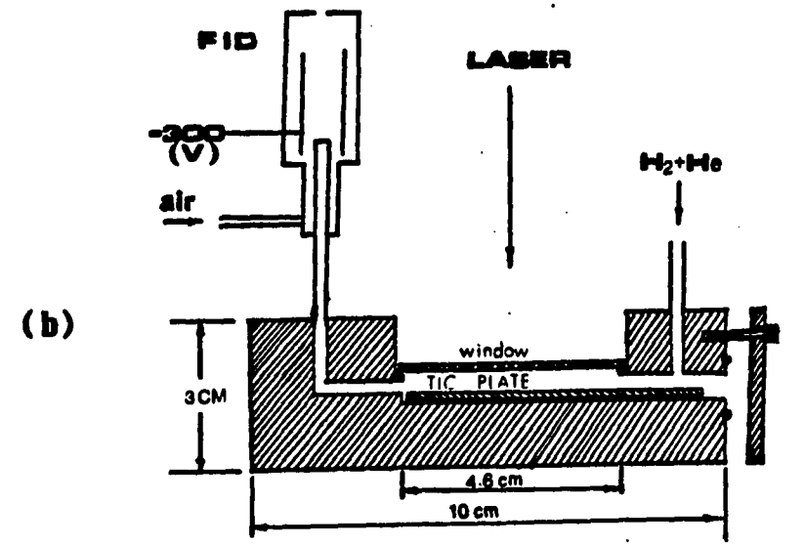

TLC PYROLYSIS CELL

amino acids were dissolved in water (pH = 4 with nitric acid) and the pesticides were dissolved in methanol-hexane (95:5). All solvents used were high-performance liquid chromatographic (HPLC) grade. Samples at various concentrations were prepared by dilution with the solvent used.

TLC separation

Two kinds of silica glass-backed plates were used, one with calcium sulphate binder (Alltech, Deerfield, IL, U.S.A., Adsorbsil HPTLC) and the other without binder (Alltech, Adsorbsil-plus, soft layer). Plates were cut to the desired sizes with a glass cutter. The soft layer plate was cleaned with methanol and the plate with binder was treated with concentrated nitric acid overnight, washed with pH 10 buffer and then with deionized water, dried under a 200-W infrared lamp and passed quickly over a flame. Plates were stored in a beaker filled with nitrogen.

Mixtures of the test compounds were applied as 0.2-μl spots with a 10-μl Hamilton microsyringe. Plates were developed in a 30-ml beaker covered with aluminum foil, and dried under an infrared lamp in a nitrogen-filled beaker for about 3 minutes to evaporate the solvents. The plate was scanned as soon as possible. Both flame ionization and electron-capture detectors were stable within 2 minutes after the TLC plate was introduced.

Scanning

The laser beam was controlled by a rotating mirror driven by an EPC-012 stepping motor (Hurst, Princeton, IN, U.S.A.). A 46-mm length of the TLC plate was scanned with a speed of 20 mm/minute in a direction opposite to the carrier gas-flow. The laser power varied from 1.0 to 5.6 W.

Results and Discussion

Flame ionization detection

Figure 2 shows the thin-layer chromatogram of LPS-FID for two amino acids, serine and phenylalanine, both ca. 1.0 μg. They were separated on the TLC plate with binder, with water as developing solvent. R_F values were 0.85 for serine and 0.7 for phenylalanine. The response factors were in close agreement with the carbon content of the amino acids, which was expected for FID. The laser power used was 3.5 W.

The dependence of the FID signal on laser power has been examined and is shown in Figure 3. Higher laser power gives more efficient pyrolysis and shows large FID signals. However, the background is also increased. For the best signal-to-noise ratio, 3.5 W was used. The limit of detection (LOD) is 100 ng for phenylalanine and 500 ng for serine. Linear calibration curves were obtained from the detection limits to 16 μg.

Electron-capture detection

The mixture of the organochlorine pesticides, p,p-DDT and methoxychlor, was separated on the TLC plate without binder. The developing solvent was hexane-methanol (99:1). R_F values were 0.6 for p,p-DDT and 0.1 for methoxychlor. Figure 4 shows the thin-layer chromatogram of the pesticides with LPS-ECD. The laser power used was 2.5 W. The dependence on laser power is shown in Figure 5. For laser powers above 2 W, the samples were almost completely pyrolyzed due to their low thermal stability. The LODs are 20 ng for methoxychlor and 50 ng for p,p-DDT. The response for methoxychlor was linear from 50 ng to 2.5 μg and that for p,p-DDT was linear from 200 ng to 2.5 μg. As one approaches the LOD, the

Figure 2. Thin-layer chromatogram of two amino acids with LPS-FID. The sample contains 0.96 μg serine and 1.02 μg phenylalanine. Laser power, 3.5 W; AUTZ = auto-zero to denote start of scan.

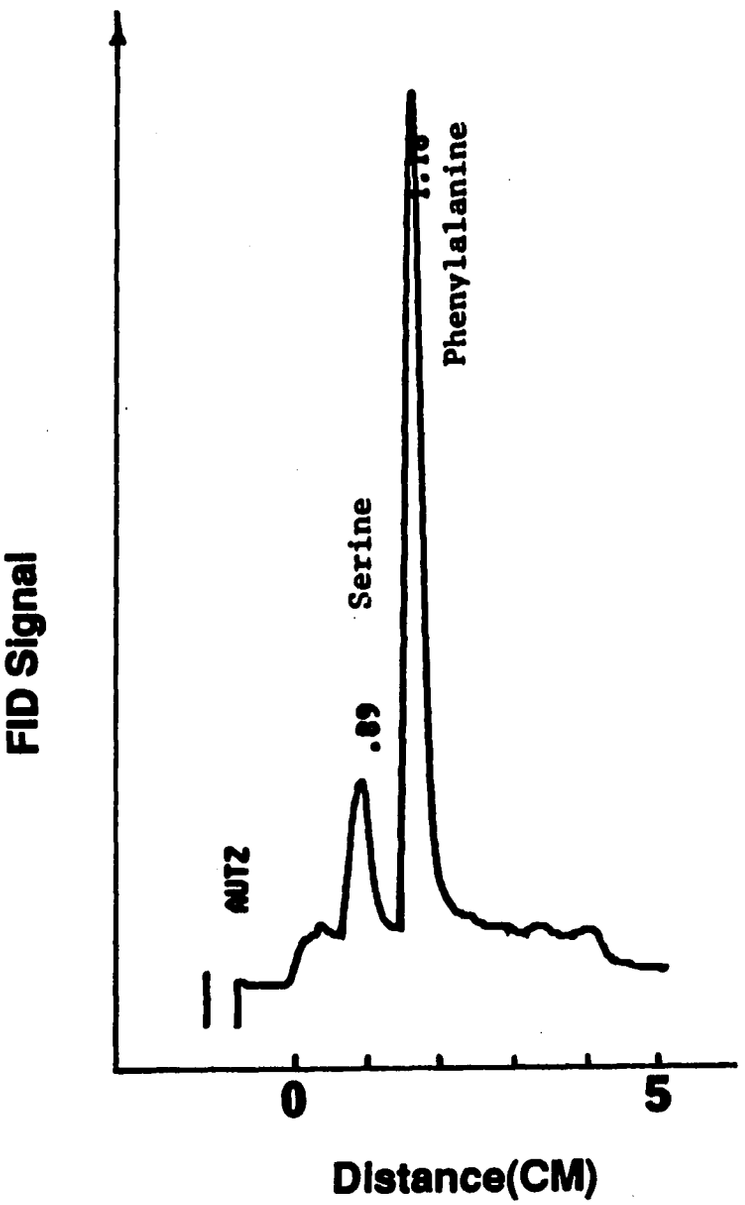
FID Signal
Serine
.89
Phenylalanine
0
5
Distance(CM)

Figure 3. Laser power dependence of signal in LPS-FID. S = serine, 0.96 μg; P = phenylalanine, 1.02 μg; B = background taken from the largest noise peak.

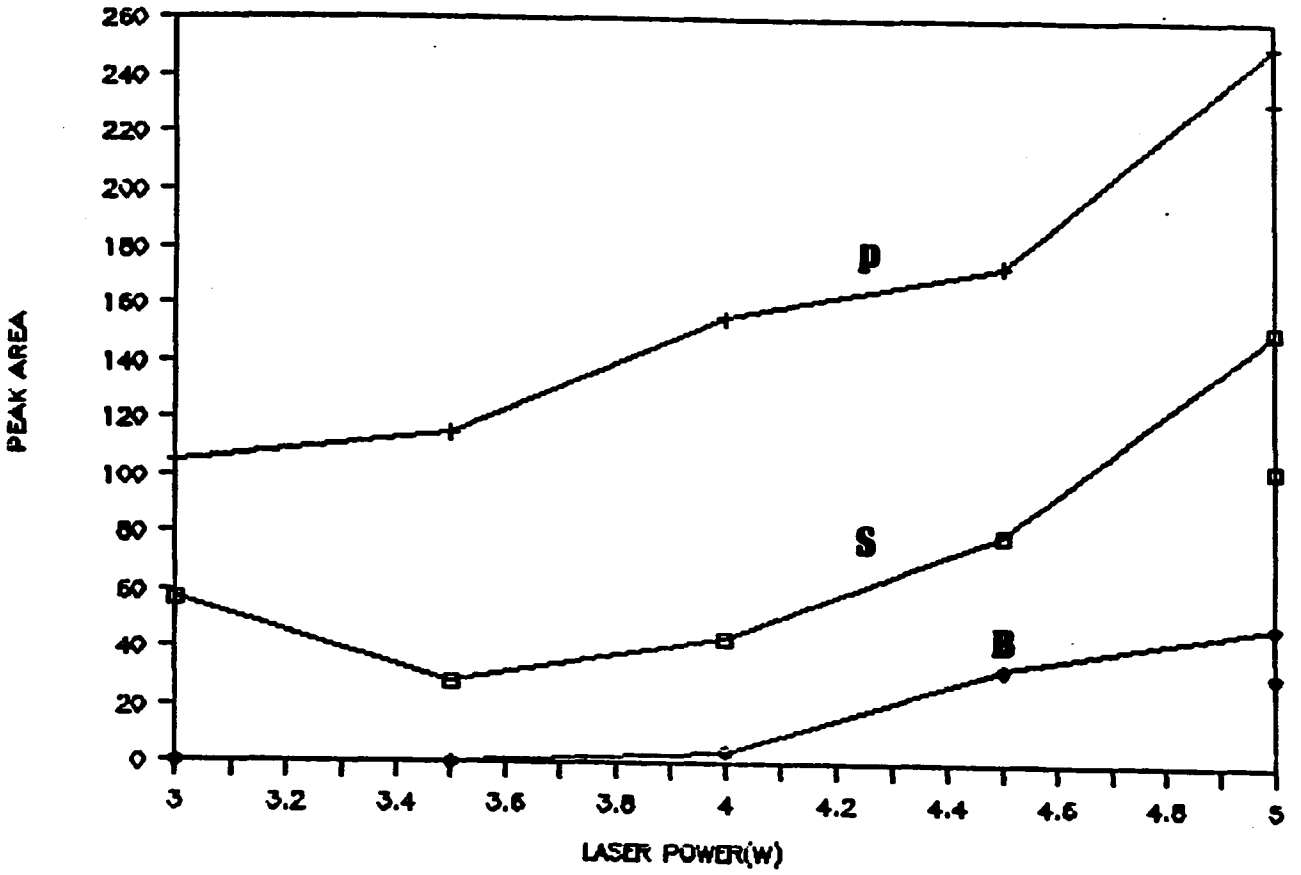
PEAK AREA
260
240
220
200
180
160
140
120
100
80
60
40
20
0
3
3.2
3.4
3.6
3.8
4
4.2
4.4
4.6
4.8
5
LASER POWER(W)
P
S
B

Figure 4. Thin-layer chromatogram of two pesticides with LPS-ECD. The sample contains 220 ng p,p-DDT and 270 ng methoxychlor. Laser power: 2.5 W.

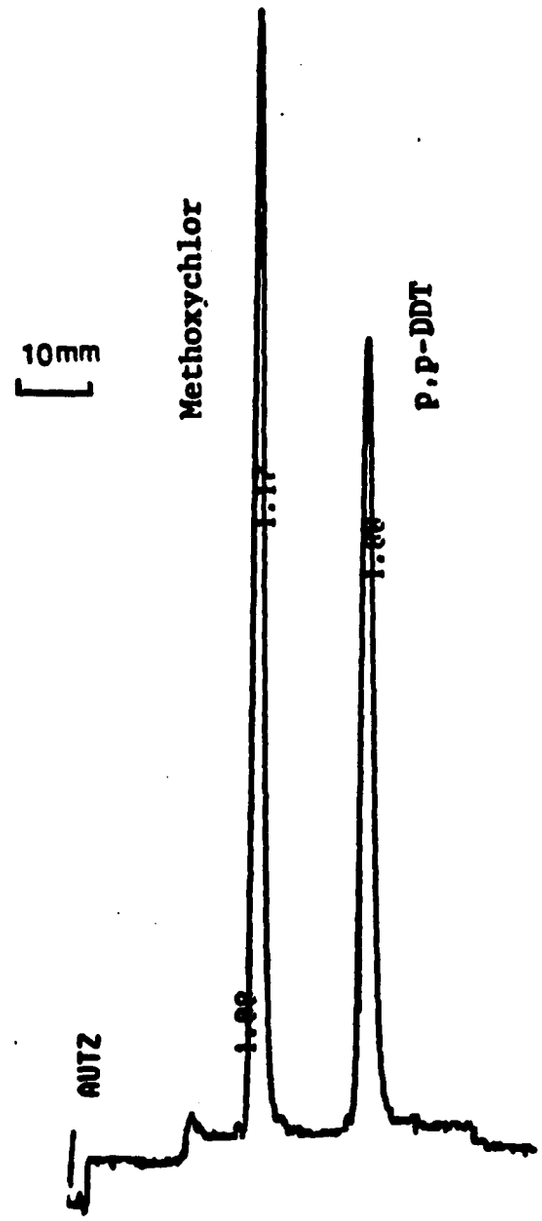
10mm
Methoxychlor
P,p-DDT
AUTZ

Figure 5. Laser power dependence of LPS-ECD. ( ) p,p-DDT, 440 ng; (+) methoxychlor, 530 ng.

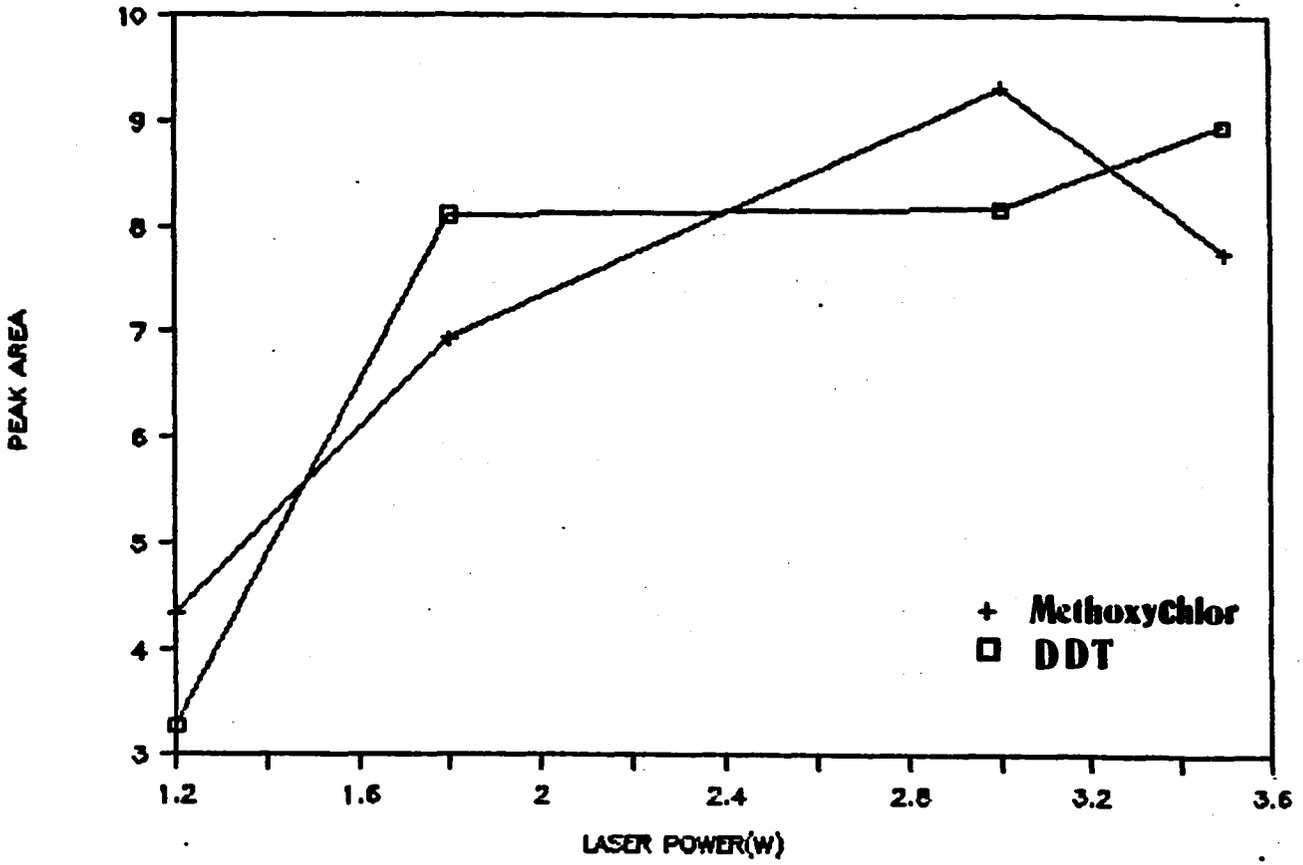
PEAK AREA
10
9
8
7
6
5
4
3
1.2
1.6
2
2.4
2.8
3.2
3.6
LASER POWER(W)
+ MethoxyChlor
DDT

signal was found to become non-linear and decrease rapidly.

The sensitivity and the linearity obtained are not very impressive compared to fluorescence (2) of photothermal methods (4). However, they are comparable to, or even better than those obtained with conventional densitometers. In densitometry, the detection limit of amino acids was 0.1-0.5 μg with ninhydrin spray reagent and a commercial densitometer at 490 nm (5,7). Proline and hydroxyproline are not detectable by that method because of the lack of reactivity. Independent determination was recommended using another spray reagent and scanning at 620 nm. With LPS-FID, all amino acids separated can be detected in one scan. This is because the laser light is absorbed by the TLC plate. Heating is guaranteed regardless of the analytes involved. Most importantly, no spray reagents are needed for LPS-FID.

The calibration curve for amino acid in densitometry is obtained by plotting the peak area vs. the square root of the amount and is linear up to 5 μg only. With LPS-FID, peak area is linearly related to the amount of amino acids and the linearity was improved by a factor of three.

The organochlorine pesticides can be detected at the 0.1-μg level with silver nitrate followed by UV photochemical reaction and a fiber-optics densitometer (8). The linear plot obtained was only over one order of magnitude. With LPS-ECD, both sensitivity and linearity are improved.

Further improvement of this technique relies on having a clean TLC plate, since the signal levels obtained are quite large. Contamination is believed to be the major source of the background. This includes impurities incorporated during the manufacturing process, exposure in the

laboratory atmosphere, and impurities in the developing solvent. The background decreased 62 times after the cleaning procedure for the TLC plates with binder. The plates without binder had a much lower background and thus required only a simple cleaning process. Okumura and co-workers (9,10) have discussed FID background in different types of silica gel quartz rods and found that sintered thin layers have low background. They burned the rod on a flame, which can be moved to scan, and collected ions on the top of the flame. Sintered TLC plates have also been made (11) and have been shown to possess good separation power.

Optimization of the experimental conditions is very important. This includes carrier gas flow-rate, laser scan rate, laser power and pyrolysis cell body temperature. These have not been fully explored in this work. Fast carrier gas flow will provide better resolution, but the sensitivity will decrease due to dilution. Higher laser power is better regardless of the background, for efficient pyrolysis and rapid vaporization. But, here it is limited to below 5 W, beyond which the glass-backed TLC plate may break. The scan rate is limited by the vaporization rate. The volume of the pyrolysis cell may be necessary since the analytes may evaporate before pyrolysis and deposit on the cell wall.

Low nanogram detection for LPS-FID and picogram detection for LPS-ECD are certainly possible. In gas chromatography (GC), FID is capable of detecting 10^{-11} g/s of methane with 10^{8} linear range (12), and ECD is capable of detecting as little as 10^{-14} g/s of sulfur hexafluoride with 10^{4} linear range. So, it may be possible to eventually improve on the LOD here. Most compounds can be easily pyrolyzed using laser powers of 5

W. The laser power (3.5 W) used in our experiments may produce a 600-700°C spot (estimated by the brightness of the spot).

Direct identification in TLC is an even more difficult task than quantitation. TLC-LPS should allow one to identify the separated compounds from the gas-phase fragments. For example, by connecting to a gas chromatograph, it is ready for pyrolysis-GC fingerprint identification. It should also be possible for mass spectrometry (MS), GC-MS and GC-Fourier transform IR analysis. For complex mixtures, the additional TLC step provides one more dimension for separation.

The LPS technique is presently limited to silica gel and alumina plates. Reversed-phase plates, cellulose plates and those plates with organic binder are not suitable for FID because of the high organic contents. Also, low boiling point solvents must be used for easy solvent evaporation in LPS-FID to minimize the background. Broad use of TLC-LPS will depend on new types of TLC plates with low background for FID or ECD.

In summary, we have presented a novel quantitation method for TLC based on LPS. No spray reagent is necessary. The analysis time was reduced from several hours to 20 minutes. The test samples were chosen for demonstration of the technique. The same principle should apply to all other organic compounds because pyrolysis is a universal mechanism for transferring species to flame ionization or electron-capture detectors.

Literature Cited

1. Kirchner, J. G. Thin-layer Chromatography; Wiley: New York, 1978.
2. Coddens, M. E.; Butler, H. T.; Schuette, S. A.; Poole, C. F. LC Mag. 1983, 1, 282.
3. Kawazumi, H.; Yeung, E. S. Appl. Spectrosc., 1988, 42, 1228.
4. Chen, I. I.; Morris, M. D. Anal. Chem., 1984, 56, 19.
5. Touchstone, J. C.; Sherma, J. Densitometer in Thin-layer Chromatography; Wiley: New York, 1979.
6. Laskar, S.; Basak, B. J. Chromatogr. 1988, 436, 341.
7. Fried, B.; Sherma, J. Thin-layer Chromatography; 2nd ed.; Marcel Dekker: New York, 1986.
8. Sherma, J.; Bloomer, K. J. Chromatogr. 1977, 135, 235.
9. Okumura, T; Kadono, T. Bunseki Kagaku (Jap. Anal.) 1973, 22, 908.
10. Okumura, T.; KAdono, T.; Iso'o, A. J Chromatogr. 1975, 108, 329.
11. Okumura, T.; Kadono, T.; Nakatani, M. J. Chromatogr. 1972, 74, 73.
12. Grob, R. L. Modern Practice of Gas Chromatography; 2nd ed.; Wiley: New York, 1985.

SECTION TWO:

DIRECT COUPLING OF THIN-LAYER CHROMATOGRAPHY TO GAS CHROMATOGRAPHY BY LASER DESORPTION

Introduction

Thin-layer chromatography (TLC) is a widely employed analytical technique which provides a simple, rapid and inexpensive separation method. In terms of instrumentation, detection, separation and identification, TLC is not as well developed as column liquid chromatography, although some aspects have been improved by the recent development of high performance TLC and novel methods of detection (1-15). TLC still plays an important role in the separation of complex samples. For example, highly retained compounds may eventually degrade a column but are compatible with TLC since the plates are disposable. Because TLC is capable of handling multiple samples in a short time, it is extensively used in routine clinical and drug testing, where hundreds of samples are analyzed every day and only a few TLC-test-positive samples are sent to HPLC or GC/MS for confirmation (16-19). Also, many GC analyses of environmental and biomedical samples directly or indirectly rely on TLC for sample clean-up to protect the GC column or to avoid background interference. Therefore, direct coupling of TLC to GC should find broad applications in many areas of analysis.

On-line multidimensional chromatography has attracted increasing

attention recently because of increased separation efficiency. The on-line combinations of HPLC/GC, HPLC/TLC and GC/TLC were reported (20-24). In off-line combinations, the TLC spot was scraped off, redissolved, and then injected into LC or GC. Direct coupling of TLC to GC or to HPLC has not been reported in the literature, probably because of the sample transfer difficulties, where a solid to gas or solid to liquid transition with spatial resolution (on the TLC plate) is required.

An ion source has been used for direct solid-gas phase transfer in TLC/secondary ion mass spectrometry (SIMS) to extract samples from the plate without loss of resolution (25-27). However, SIMS is only sensitive to the first few atomic layers of the sample and thus most of the sample on the TLC plate (buried in the silica particles) was inaccessible unless it is first extracted. Some other techniques including fast atom bombardment (FAB) and laser microprobe analyzer (LMA) were also applied in TLC/MS for direct identification of the TLC spotted compounds (8, 28). High TLC adsorbent backgrounds were observed. Identification become even more difficult if the compounds are not well separated. The combination of TLC/GC to MS should be free from most of these problems, since GC would further discriminate against the TLC background and distinguish between non-separated compounds.

The purpose of present work is to develop an interface for direct coupling of TLC to high-resolution GC based on laser desorption. Without the GC column, this technique should also work as a universal quantitative scanning method for TLC by taking advantage of any of the existing GC detectors.

Experimental Section

Apparatus

The schematic diagram of the TLC/GC interface is shown in Figure 1a. The laser was a model HyperEX 460 (Lumonics, Ottawa, Canada) and operates at 308 nm. The laser repetition rate was varied from 10 Hz to 200 Hz. The pulse energy ranged from 10 mJ to 18 mJ as measured by a radiometer (Laser Precision, Utica, NY, Model Rj-7200) with an energy probe (Laser Precision, Utica, NY, Model Rjp-734). The laser beam was focused to about 2 x 3 mm with a quartz lens (f.l. - 50 cm) and directed by a mirror driven by a stepping motor.

The TLC cell was constructed with copper and consisted of either a 50 mm (long) x 50 mm (wide) x 8 mm (deep) or a 50 mm (long) x 10 mm (wide) x 8 mm (deep) chamber to accommodate the TLC plate. The top of the chamber was covered by a quartz window sealed with an o-ring. The details of the TLC cell are shown in Figure 1b. The carrier gas (argon + 10% methane) enters from three corners of the chamber, passes above the surface of the TLC plate and then flows out of the corner to a GC inlet or directly to a GC detector. The flow rate was about 100 ml/minute during GC separation.

Thin-Layer Chromatography

Normal phase silica gel plates (Alltech, Deerfield, IL, Adsorbsil HPTLC) were used. The plates were cut to the sizes required and cleaned with methanol only. A 0.2 μl of the pesticide sample was spotted on the plate by a 1.0-μl Hamilton microsyringe.

In the experiments involving quantitative scanning without GC

Figure 1. Experimental Setup

a) Schematic diagram of the laser desorption interface.

b)Details of the TLC cell. L: lens (f.l. = 50 cm); M: mirror; s.m.: stepping motor; I: integrator.

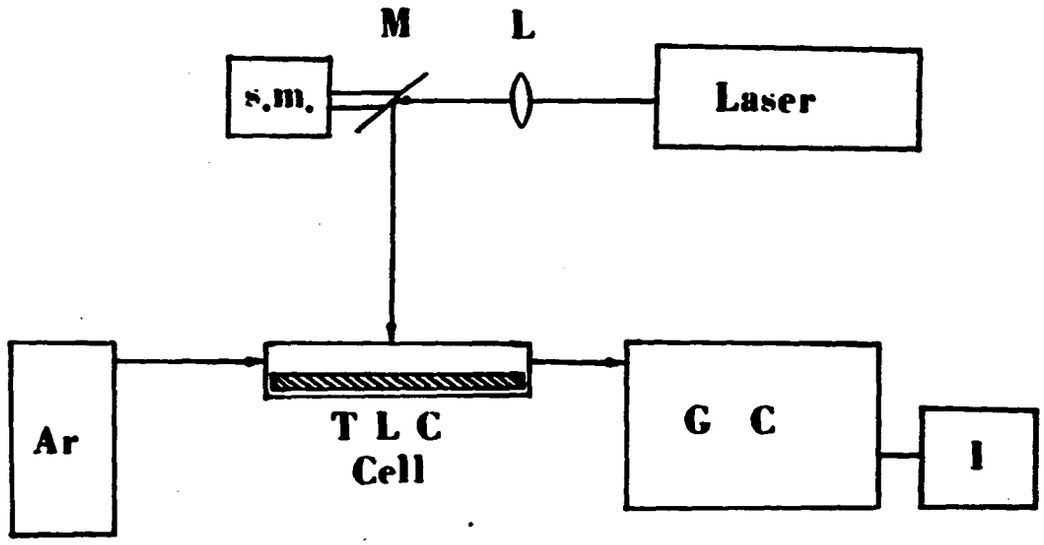

Schematic Diagram of the Laser Desorption Interface

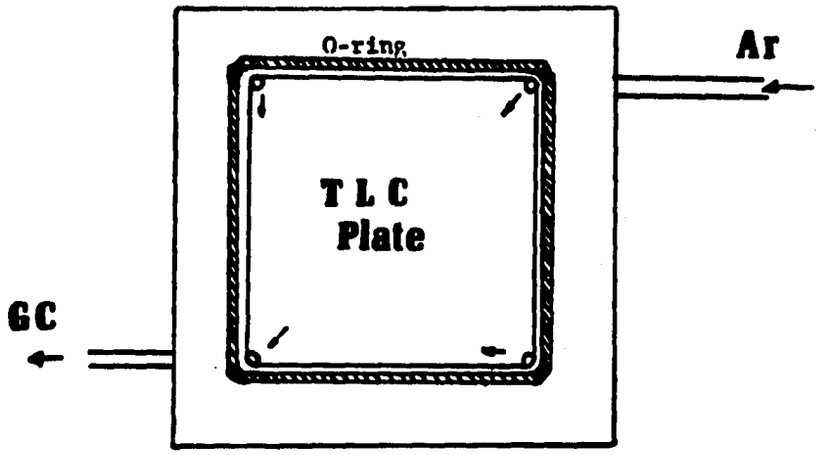

TLC Cell

(Top View)

Figure 1 (Continued)

separation, for a lower background, the plate was prescanned with the laser and the sample introduction and TLC separation were performed in a glove box filled with nitrogen to avoid contact with air. Plates were developed with hexane and dried under a 200-W infrared lamp for 2 minutes to evaporate the solvents. A carrier gas flow rate of 300 ml/min was used.

Gas Chromatography

A model 550 gas chromatograph (Tracor, Austin, TX) with an electron capture detector was equipped with a 30 m x 0.53 mm (i.d.) DB-1701 fused silica column (J&W Scientific, Folsom, CA). The oven temperature was programmed at 30°C for 5 minutes, then raised 10°C/min to 200°C. The data collection was accomplished with an integrator (LDC, Riviera Beach, FL, CI 3000). The column was directly connected to the TLC cell through a stainless steel tubing via the GC inlet. The tubing was heated by a heating tape to around 250°C to prevent sample deposition.

Chemical

The pesticide standards were purchased from Alltech Associates, Inc. (Deerfield, IL) and used as received. They were dieldrin, p,p-DDT, lindane, and methoxychlor. Samples were dissolved in hexane and diluted to various concentrations. All solvents used were HPLC grade.

Results and Discussion

Laser desorption (LD), particularly with pulsed lasers, is an attractive technique for rapid vaporization of solid molecular samples. It has been widely investigated as a sampling method in mass spectrometry for both volatile and nonvolatile organic compounds (29-30). Laser desorption is simply based on the rapid heating effect in which the molecules desorb before they have time to kinetically decompose (11-25). However, certain kinds of fragmentation processes have also been observed. These are related to laser power density, laser wavelength and the thermal stability of the compounds (31). The same mechanism is expected in the laser desorption of TLC adsorbed molecules, although the experimental requirements may be very different. Quantitative transfer and the production of neutral molecules are the main concerns in TLC/GC, while enhancements of ionization processes are more important in laser desorption mass spectrometry (LDMS). Therefore, low laser power density (5×10^6 W/cm^2) and multiple pulses (around 1000 pulses) were used in this experiment instead of the high power density and single shot conditions in LDMS.

The gas chromatograms of four pesticides directly removed from TLC plates by laser desorption are shown in Figure 2. The experimental conditions of GC have not been optimized. For the first five minutes, the column was left at room temperature to trap the material from a given spot. This effectively provides a small injection volume. There are two intriguing features in the TLC/GC results shown in Figure 2. First, it

Figure 2. GC (with an ECD detector) chromatograms of laser desorbed compounds from the TLC plates. b: TLC background peaks; detector signal attenuation: x 32.

a) Lindane: 100 ng, laser: 18 mJ/30 Hz;

b) dieldrin: 200 ng, laser: 16 mJ/30 Hz;

c) p,p-DDT: 200 ng, laser: 14 mJ/100 Hz;

d) methoxychlor: 200 ng, laser: 14 mJ/50 Hz.

Lindane
21.49
20.32
18.39
17.84
15.69
13.22
12.51
11.86
10.81
9.41
3.87
3.23
OUT2

FIG. 2B

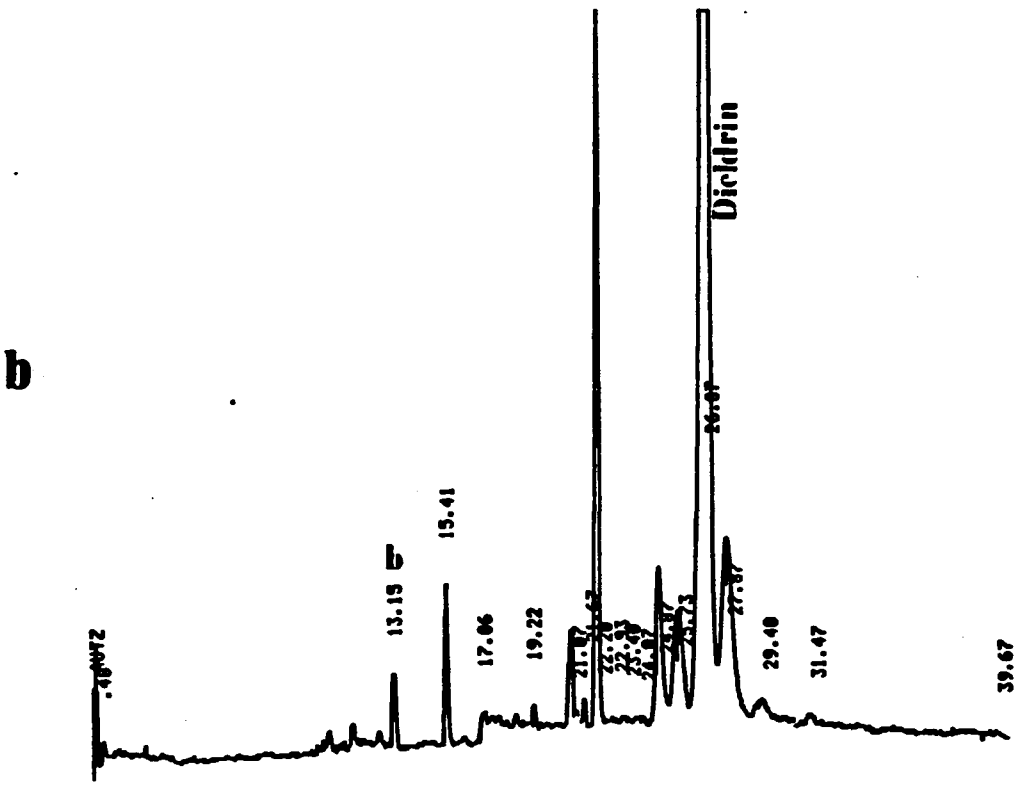

Figure 2 (Continued)

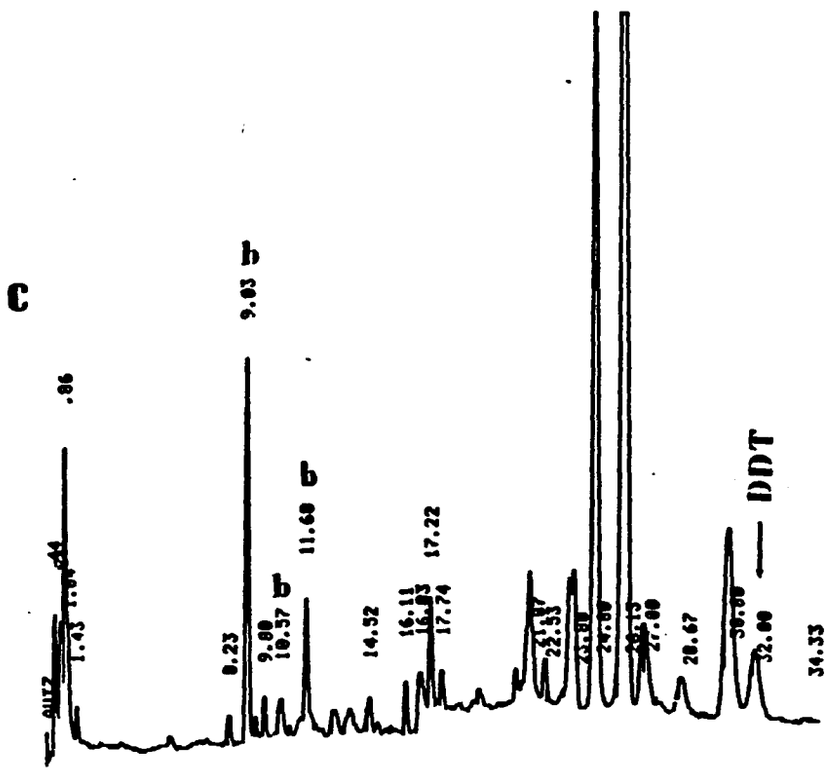

Figure 2 (Continued)

d)

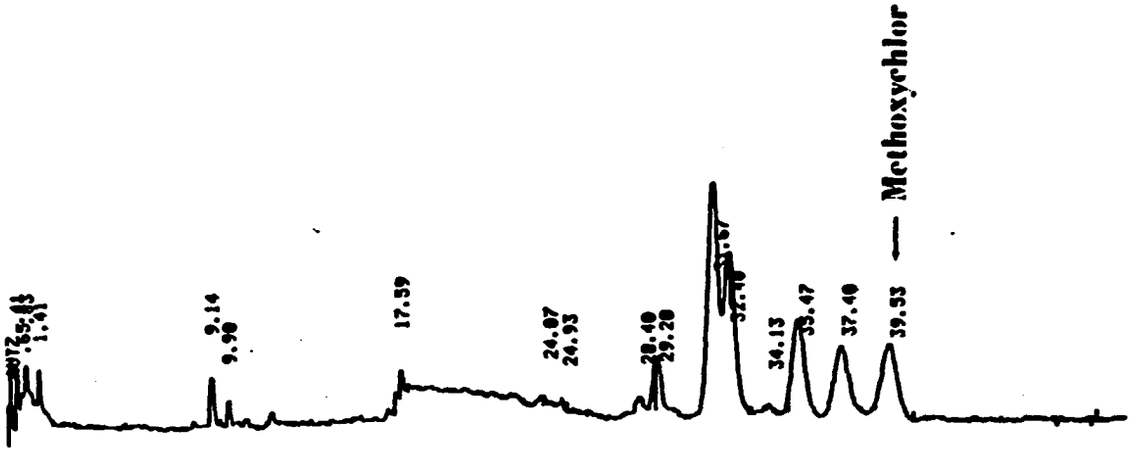

Figure 2 (Continued)

demonstrates sensitive detection for TLC by GC detectors without TLC adsorbent background interference. The background peaks were marked by "b" and they were identified by their GC retention times. There were four major background peaks. They correspond to the peaks at 9.03, 10.57, 11.68, and 13.15 minutes in Figures 2b and 2c. These are derived from breakdown of the TLC stationary phase by the laser. No attempts were made to identify them, however. The background peak at 9.03 increased dramatically at high laser repetition rates. This is due to a higher degree of heating of the TLC plate. Secondly, one obtains for each analyte a characteristic fingerprint that can be used for identification of the TLC-separated compounds. Direct identification of the TLC-separated zones has been a challenging task. TLC/GC may serve as a complementary method to TLC/MS, similar to the use of pyrolysis/GC for the identification of a polymer (32).

The transfer efficiency and the parent molecule peak ratio of each compound for the experimental conditions of Figure 2 are summarized in Table I. The transfer efficiency is defined as the ratio of the total peak area of the GC fragments in Figure 2 and the peak area produced by a sample containing the same amount of analyte tested but without TLC separation (normal GC injection). The parent peak ratio is defined as the ratio of the parent molecular peak area and the total peak area of all fragments including the molecular peak. The data in Table I are only rough estimates because the detector response of the fragments may not be the same as the parent molecule. As we can see, the volatile compounds have higher transfer efficiencies and less fragmentation at the same laser

power and pulse repetition rate. These are desorbed from the surface at lower temperatures.

The transfer efficiency was found to increase with increasing laser energy or with higher pulse repetition rates. At a repetition rate of 50 Hz (1000 shots total), the transfer efficiency of lindane increased from 47% to 62% when the laser energy is increased from 10 mJ/pulse to 16 mJ/pulse. The transfer efficiency was 76% at 16 mJ/pulse and 150 Hz. The laser pulse repetition rate seems to play a very important role in the surface temperature of the TLC plate because of the heat accumulation effect. That is, one pulse follows the other before the surface cools down. With a laser energy of 10 mJ/pulse, we estimate from the brightness of the spot that repetition rates of 50 Hz and 150 Hz produce surface temperatures of 400°C and 600°C respectively. Also, at a higher repetition rate, more fragmentation is expected, since at higher temperatures pyrolysis becomes more important relative to desorption. When the total number of laser shots were maintained at 1000 and the laser energy was constant at 10 mJ/pulse, the parent peak ratios for lindane were 72% and 32% at repetition rates of 30 Hz and 150 Hz, respectively.

Another crucial factor which will influence the transfer efficiency is readsorption. Compounds desorbed from the TLC plate may adsorb or condense on the cold surfaces again during the flow process before they enter the hot connecting tubing. Warming up the TLC cell to lessen the readsorption is not recommended because volatile compounds may desorb, causing a loss of signal. A proper design of the TLC chamber with a higher carrier gas flow should minimize this problem. The distance

between the TLC plate and the window is also critical. With a distance of 1 mm, less than 10% of lindane was detected, even though the linear flow rate in the chamber was higher with the smaller chamber volume. A distance of 5 mm was optimal for the flow rate used here. Still higher flow rates were not compatible with GC and the resulting pressure is too high for our particular TLC cell.

TLC/GC coupling offers one more dimension of separation. Figure 3 presents a well separated GC chromatogram of a mixture of four pesticides which was spotted on the TLC plate with no separation. This simulates overlapping components on the TLC plate. Here the analytes and their fragmentation fingerprints can be easily identified based on the individual chromatograms in Figure 2.

Quantitative Scanning

For laser scanning alone, the TLC cell was directly connected to a GC detector without the GC column. Quantitative scanning of TLC plates for detecting amino acids and pesticides by a continuous wave infrared laser with a flame ionization detector (FID) or an electron capture detector (ECD) has been demonstrated in an earlier paper (LPS, laser pyrolysis scanning) (6). The system here represents laser desorption scanning (LDS). The advantage of LDS is brought about by pulsed laser operation, which provides high power density, fast heating, and rapid cooling, leading to better scanning resolution and fewer fragments. For efficient transfer of the analytes, a higher laser power density is needed. But a high power cw laser would easily break the TLC plates. The scanning speed

Figure 3. Thin-layer chromatogram of four pesticides with laser desorption scanning and electron capture detection (no GC separation). D: dieldrin (12.6 ng); P: p,p-DDT (6.8 ng); L: lindane (5.0 ng); M: methoxychlor (6.8 ng); laser energy: 16.5 mJ/ pulse; repetition rate: 50 Hz; scan speed: 10 cm/min; flow rate of carrier gas: 300 ml/min; ECD output attenuation: x8; TLC plate: 5 x 5 cm. 0.1 μl of sample was introduced by 1.0 μl syringe and developed with hexane.

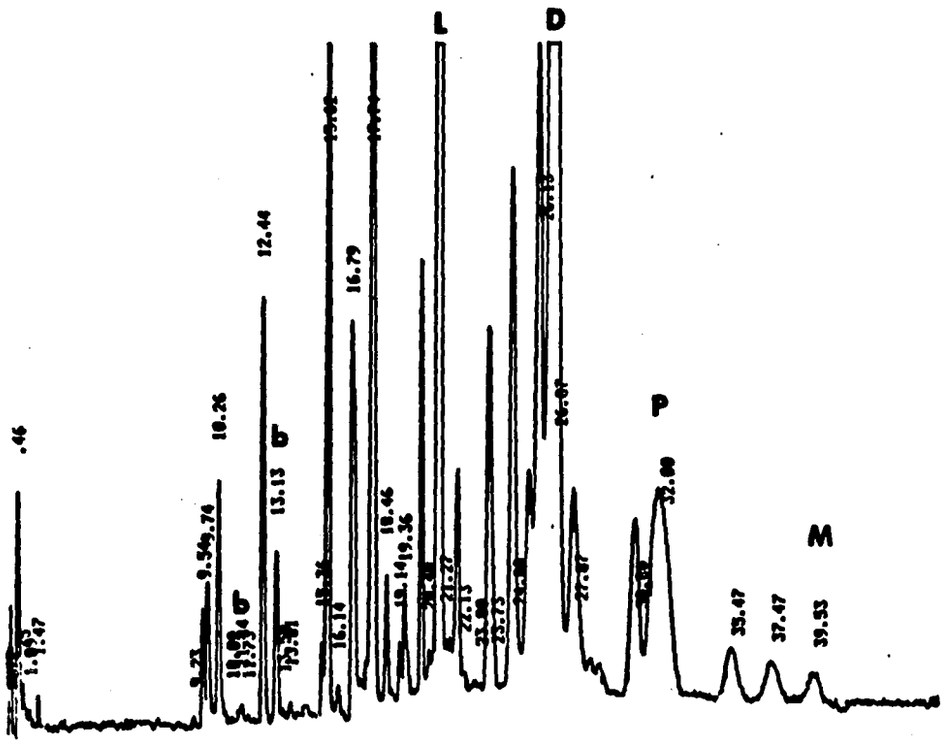

Mixtures of Lindane, Dieldrin, p,p-DDT and Methoxychlor

and spatial resolution are increased due to fast vaporization and less heat conduction to the neighboring spots. Figure 4 shows a demonstration of LDS for the four TLC separated pesticides: dieldrin, p,p-DDT, lindane and methoxychlor. The detection limit is in the one nanogram range and the scan rate was 10 cm/min. The detection limit is about a factor of 20 better than LPS reported earlier (8). To achieve this level of performance, the TLC plate was pre-cleaned, developed and detected in a nitrogen environment to avoid oxygen, moisture and other laboratory contamination.

The signal dependence on laser energy and the laser pulse frequency in a scanning mode is shown in Figure 5 for 250 ng of lindane. It should be noted that the signal level was also position dependent. When the spot was in a location close to the outlet of the chamber, it produces larger signals, particularly for a 50 x 50 mm TLC plate. Readsorption and peak dispersion may be the causes f this spatial dependence. Samples were spotted at the same position in Figure 5 for comparisons. The results indicate that complete vaporization of the sample spot occurs above 40 Hz for 14 mJ/pulse and 16 mJ/pulse. On the other hand, it takes 200 Hz to vaporize the entire sample at 10 mJ/pulse. The thermal effects at higher repetition rates compensate for the lower powers of the pulses. Therefore, for maximum vaporization at low powers and low repetition rates, the scan rate will have to be reduced. However, the signal (Figure 3) may not increase because the material vaporized will then be more dilute at the detector. Figure 6 shows the amount of material desorbed over a series of laser pulses at 0.05 Hz without scanning. The slow

Figure 4. Gas chromatogram of a TLC spotted mixture (without separation) by laser desorption. The mixture contains L: lindane (200 ng), D: dieldrin (200 ng), P: p,p-DDT (200 ng) and M: methoxychlor (200 ng); laser: 14 mJ/50 Hz, 1000 shots; ECD detector attenuation: x32.

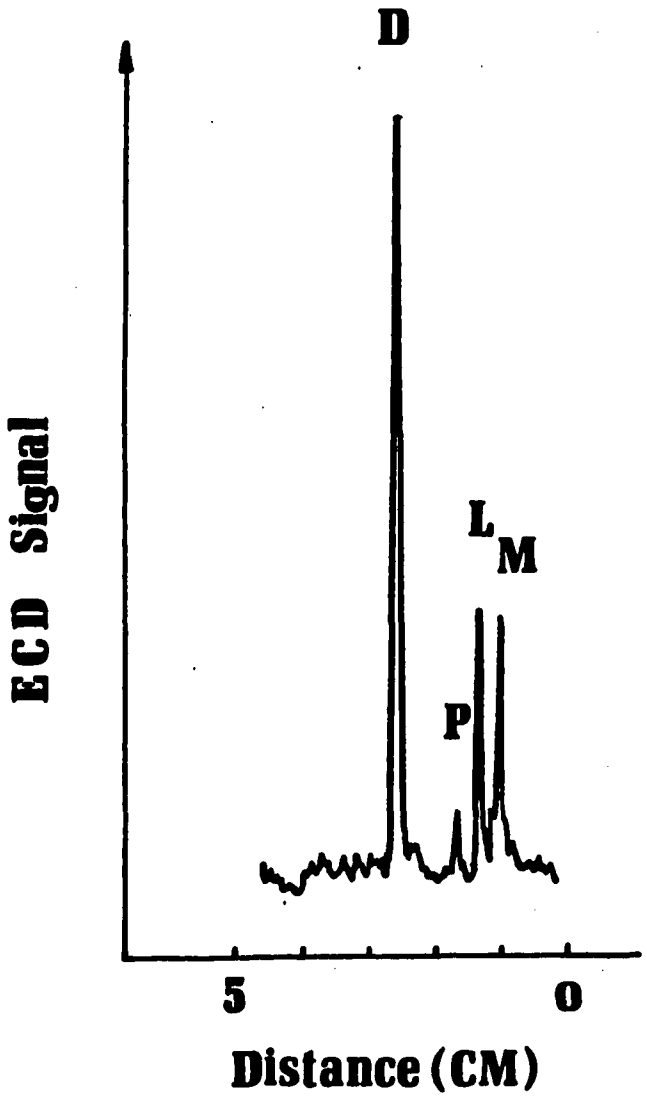
D
L
M
P
ECD Signal
5
0
Distance (CM)

Figure 5. ECD signal dependence on laser energy and repetition rate in laser desorption scanning TLC of 250 ng lindane. Attenuation: x512.

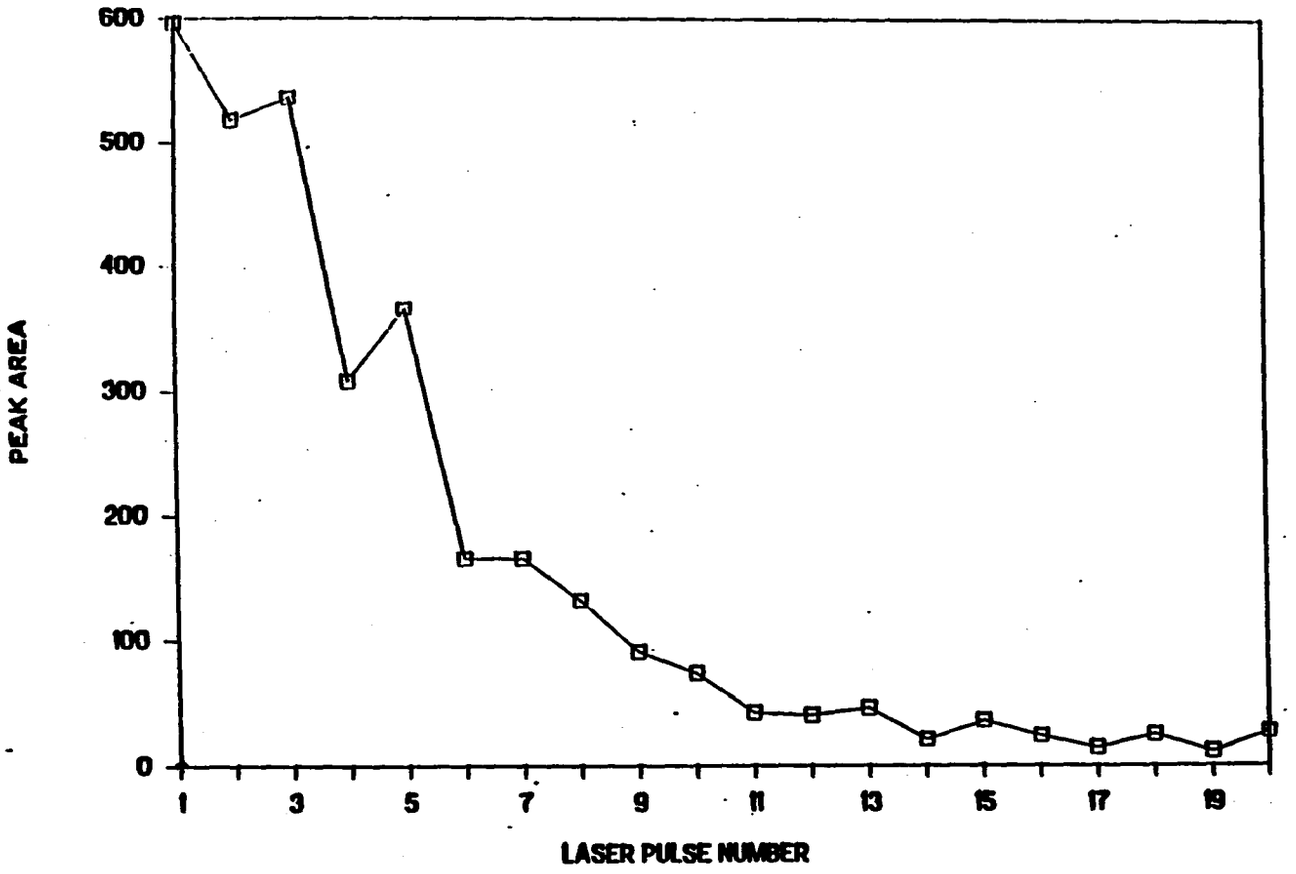
600
500
400
300
200
100
0
PEAK AREA
1
3
5
7
9
11
13
15
17
19
LASER PULSE NUMBER

Figure 6. ECD signal for consecutive laser pulses. Sample: lindane (200 ng); laser energy: 16 mJ/pulse; repetition rate: 0.05 Hz.

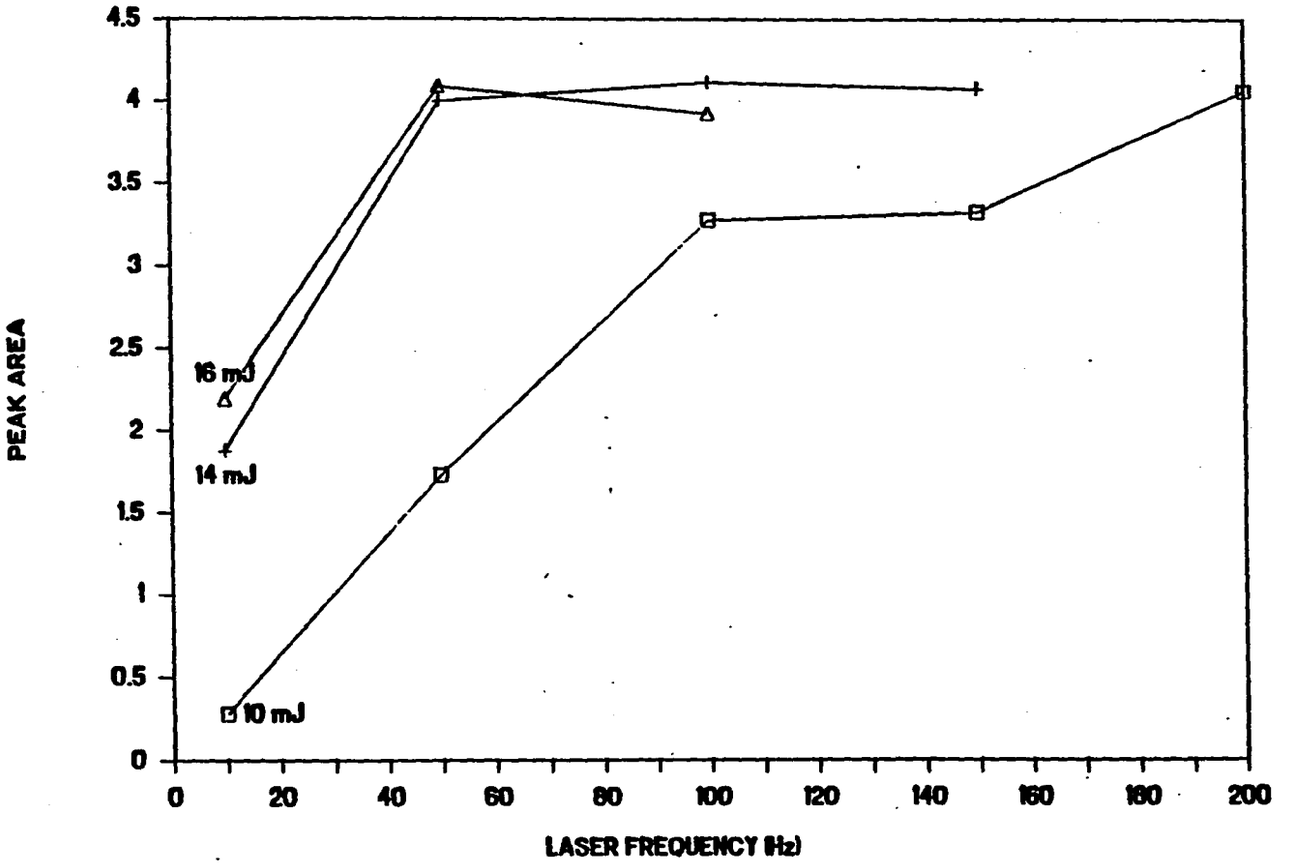
PEAK AREA
4.5
4
3.5
3
2.5
2
1.5
1
0.5
0
16 mJ
14 mJ
10 mJ
0
20
40
60
80
100
120
140
160
180
200
LASER FREQUENCY (Hz)

repetition rate guarantees that very little heat is generated by the laser on the plate itself. The primary vaporization mechanism is therefore desorption and not thermal pyrolysis (8). It is interesting that less than 1% of the sample (out of the integrated area in Figure 6) was detected in the first laser shot. The profile in Figure 6 will naturally be different at higher repetition rates, since surface temperatures will then be higher.

Registry No.

Dieldrin, 60-57-1; lindane, 58-89-9; methoxychlor, 72-43-5; p,p-DDT, 50-29-3.

Literature Cited

1. Kirchner, J. G. Thin-layer Chromatography; Wiley: New York, 1978.
2. Sherma, J. Anal. Chem. 1988, 60, 74R.
3. Bertsch, W.; Hara, S.; Kaiser, R. E.; Zlatkis, A.; Huthig, Heidelberg, Instrumental HPTLC, 1980.
4. Morris, M. D.; Chen, I. I. Anal. Chem. 1984, 56, 19.
5. Ma, Y.; Yeung, E. S. Anal. Chem. 1988, 60, 722.
6. Zhu, J.; Yeung, E. S. J. Chromatogr. 1989, 463, 139.
7. Kaiser, R. E., Ed. Proceedings of the 3rd International Symposium on Instrumental High Performance Thin Layer Chromatography. Institute of Chromatography: Bad Duerkheim, FRG, 1985, 509.
8. Novak, F. P.; Hercules, D. M. Anal. Lett. 1985, 18(A4), 503.

9. Ramaley, L.; Vaughan, M. A. Anal. Chem. 1985, 57, 353.

10. Iwabuchi, H.; Nakagawa, A.; Nakamura, K. J. Chromatogr. 1987, 414, 139.

11. Unger, S. E.; Vincze, A.; Cooks, R. G. Anal. Chem. 1981, 53, 976.

12. Busch, K. L.; Stanley, M. S. Anal. Chem. Acta 1987, 194, 199.

13. Ramaley, L.; Nearing, M. E.; Vaughan, M. A. Anal. Chem. 1983, 55, 2285.

14. Belchamber, R. M.; Read, H.; Roberts, J. D. M. J. Chromatogr. 1987, 395, 47.

15. Belenkii, B. C.; Gankina, E. S.; Adamovich, T. B.; Lobazov, A. F.; Nechaev, S. V.; Solonenko, M. G. J. Chromatogr. 1986, 365, 315.

16. Stahr, H. M.; Hyde, W.; Pfeiffer, R.; Domoto, M. Proc. Int. Symp. Instrum. High Perform. Thin Layer Chromatogr., 3rd, 1985, 447.

17. Scott, R. M. Clinical Analysis by Thin-layer Chromatography Techniques. Humphrey Science: Ann Arbor, 1969, 227 pp.

18. Touchstone, J. C. Advances in Thin Layer Chromatography: Clinical and Environmental Applications; Wiley: New York, 1982.

19. Garrett, E.; Tsan, J. J. Pharm. Sci. 1974, 64, 1563.

20. Raglione, T. V.; Hartwick, R. A. Anal. Chem. 1986, 58, 2680.

21. Hofstraat, J. W.; Engelsma, M.; Van De Nesse, R. J.; Gooijer, C.; Velthorst, N. H.; Brinkman, U. A. Anal. Chim. Acta 1986, 186, 247.

22. Casu, B.; Cavallotti, L. Anal. Chem. 1962, 34, 1514.

23. Janak, J. J. Gas Chromatogr. 1964, 15, 15.

24. Humphrey, A. M. J. Chromatogr. 1970, 53, 375.

25. DiDonato, G. C.; Busch, K. L. Anal. Chem. 1986, 58, 3231.

26. Stanley, M. S.; Busch, K. L.; Vincze, A. J. Planar Chromatogr. 1988, 1, 76.

27. Stanley, M. S.; Busch, K. L. J. Planar Chromatogr. 1988, 1, 135.

28. Bare, K. J.; Read, H. Analyst (London) 1987, 112, 443.

29. Kolaitis, L.; Lubman, D. M. Anal. Chem. 1986, 58, 2137.

30. Tembruell, R.; Lubman, D. M. Anal. Chem. 1986, 58, 1299.

31. Hillenkamp, F. Int. J. Mass Spec. Ion Phys. 1982, 45, 305.

32. Irwin, W. J. Analytical Pyrolysis Dekker: New York, 1982.

Table I. Fragmentation and transfer efficiency in Figure 2

Pesticides	Transfer Efficiencies[a] (%)	Parent Peak Ratios[b] (%)
A: Lindane	71	52
B: Dieldrin	89	62
C: p,p-DDT	64	3
D: Methoxychlor	29	14

[a]Transfer Efficiency = $\frac{\text{Area of all fragments}}{\text{Area without TLC step}}$.

[b]Parent Peak Ratio = $\frac{\text{Area of the parent peak}}{\text{Area of all fragments}}$ x 100%.

SECTION THREE:

ELEMENTAL ANALYSIS BASED ON CHEMILUMINESCENCE IN THE LASER MICROPROBE

Introduction

Direct solid analysis to provide local concentrations and depth profiles of trace elements has become one of the important applications of lasers (1,2). Because of the high irradiance, the laser microprobe is able to interrogate a variety of samples: electrically conductive or nonconductive. The ability to focus the beam to a diffraction-limited spot size allows two-dimensional profiling on the μm scale. Thus, the laser microprobe technique has been used for the identification of inclusions and for the analysis of elemental distributions in solid samples, such as alloys, semiconductor, wood, ore, polymer, ceramics and glass (3-6).

Laser microprobe analysis includes two processes: sample vaporization and signal detection. Upon irradiation, a tiny amount of material is removed from the surface and a microplasma is formed. This contains atoms, ions, electrons, molecular fragments and particles. Signals related to the analyte species in the plasma are then measured. Detection methods include mass spectrometry (7), atomic emission (8-10), atomic absorption (11,12), Raman spectrometry (13), inductive coupled plasma

atomic emission (14,15) and atomic fluorescence (16), etc. Among them, direct atomic emission is probably the simplest and the most straightforward detection scheme, since analyte atoms and ions contained in the plume are excited without additional sophisticated instruments. Moreover, no sample transfer process is involved and thus the amount of sample vaporized can be reduced to a minimum (nanograms or even picograms) to obtain high spatial resolution.

Direct observation of the atomic emission from the plume, unfortunately, often suffers from high background due to the continuum plasma emission, and from self absorption by the cooler vapor (ground state atoms) at the edge of the plasma. Consequently, the sensitivity is poor (9). To improve that, cross excitation by a spark discharge was developed, where a pair of electrodes is placed a few millimeters apart above the sample surface (8). This brings additional energy to excite the cooler wings of the plume and results in higher emission. Improvements of S/N by a factor of 10 is achieved (9). However, some disadvantages are present, for example, contamination by the electrode impurities. The reproducibility was reported to be twice as bad because additional discharge fluctuation is introduced upon laser vaporization (9). The variation in the fraction of sample reaching the spark region has also contributed to the uncertainty. The mass sensitivity may also be affected by the sample transfer efficiency (1).

A new detection method, chemiluminescence, is explored in this study for laser microprobe analysis. The chemiluminescence is produced by the reactions of the analyte atoms formed in the laser generated plume with an

ambient gas reagent. The potential advantages of this method are as follows. First, the chemiluminescence can be directly measured without additional excitation and without sample transfer. Therefore it is simple and potentially quite sensitive. Second, it should be possible to introduce chemical selectivity in addition to spectral selectivity for elemental analysis. Third, the chemiluminescence may be spatially separated from the plasma emission, since the reactions most likely take place at the top periphery of the plume where the atoms encounter the gas reagents while the plasma emission is mainly localized near the sample surface. Fourth, temporal discrimination can also be used because of the time delay of the reaction (collisions) and the longer lifetimes of the chemiluminescent species, while the plasma emission lasts only a very short time. It is hoped that one can eventually decrease the background to attain better signal-to-noise ratio by chemiluminescence detection vs. atomic emission.

The spectroscopy of diatomic fluorides has been of long-standing interest due to both the fundamental reactions and the potential development of chemical lasers (17-21). The generally high reaction exoergicity frequently entails the appearance of electronically excited products and produces chemiluminescence. Numerous examples of reactions:

$$M + F_2 \rightarrow MF^* + F \qquad (a)$$

$$MF^* \rightarrow MF + h\nu$$

where M is a metal atom, have been studied. The emission spectra of many fluorides (AlF, CuF, GeF, SiF, etc.) were reported, where the atoms were usually generated by oven-heating or prepared in volatile forms (metal

hydrides) (22-26). Therefore, it is our goal to explore fluoride chemiluminescence in a laser generated plume. Hopefully, the study may provide further understanding of the reaction and potential use as a detection scheme in laser microprobe analysis.

Quantitation is an important consideration for surface analyses. However, many factors such as laser power, focusing, sample composition, mechanical properties as well as sample surface conditions have contributed to the irreproducibility of the sampling process (27). Much effort has been made in recent years to improve the precision. Techniques including signal averaging, monitoring the laser power fluctuations or the size of the crater, use of standard material, and use of internal reference lines were employed (28-32). Recently, the acoustic wave generated in each laser shot has been used to correct for variations in the total amount of material evaporated (33). It was shown that variations in the intensity of atomic emission (without auxiliary electrodes) can be normalized by the acoustic signals over three orders of magnitude, regardless of experimental conditions. So, the correlation between the chemiluminescence and the acoustic signals is also investigated here to evaluate the utility of the latter as an internal standard for quantitation.

Experimental Section

The schematic diagram of the experimental arrangement is shown in Figure 1. A pulsed excimer laser (Lumonics, Ottawa, Canada, Model Hyper

Figure 1. Experimental arrangement for chemiluminescence measurement in a laser generated plume. A: Aperture, M: Mirror, L1, L2: Lens, S: Sample, Mo: Motor, F: Filters, WA: Waveform Analyzer, HV: High Voltage Supply, PMT: Photomultiplier Tube.

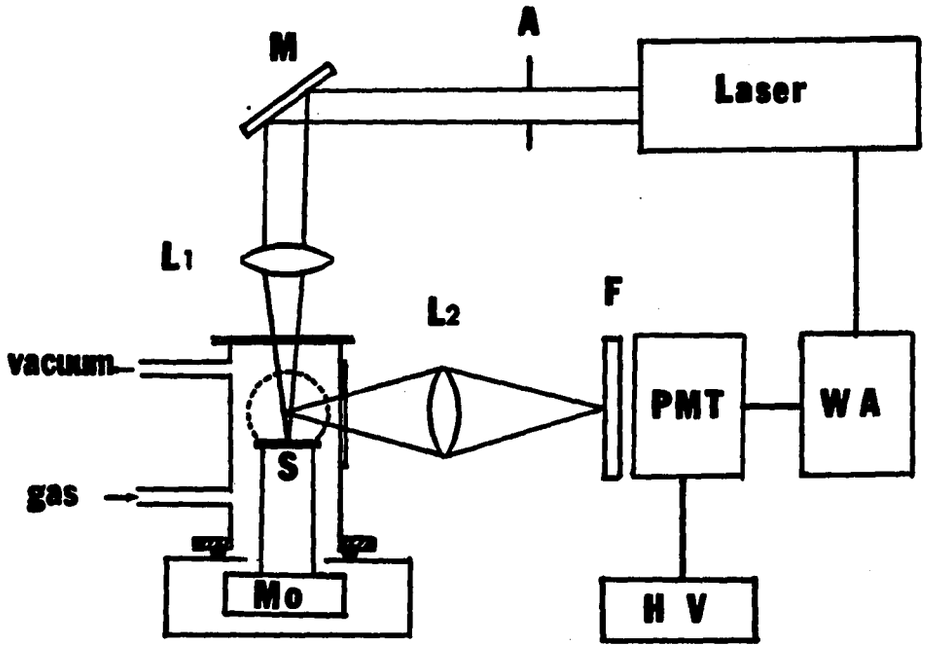
M
A
Laser
L1
L2
F
vacuum
PMT
W A
S
gas
Mo
H V

EX 460) operating at the 308 nm XeCl transition was used. The size of thelaser beam was confined by either a 6 mm or a 10 mm diameter aperture. The laser energy was directly regulated by varying the operating voltage and was measured by an energy radiometer (Laser Precision, Utica, NY, Model Rj-7200) with an energy probe (Laser Precision, Utica, NY, Model Rap-734) right after the aperture. The pulse duration was about 25 ns and the pulse fluctuation was found to be ±2% at an operating voltage of 20 KV. The reproducibility deteriorates to ±5% at the minimum operating voltage of 16 KV. The laser energies used varied from 0.5 mJ to 5 mJ. The laser beam was focused onto the sample surface by a 5 cm diameter and 15 cm focal length UV lens which has been mounted in a micrometer-transnational stage so that the focusing condition can be precisely adjusted.

The sample cell, made from a rod of 3 cm x 3 cm x 8 cm brass, has a 2.5 cm internal diameter x 8 cm cylindrical chamber with three 2 cm diameter side windows. A 0.5" diameter condenser microphone (Knowles, Franklin Park. IL, Model BT-1759) was attached to one of the side windows to measure the acoustic signal. The top of the cell (where the laser beam is introduced) and the other two side windows, one for emission measurement and the other for visual observation, were sealed with 3 x 3 x 0.2 (cm) quartz plates by 5 min epoxy. The sample cell was mounted against an o-ring on the bottom to an aluminum chamber where a stepping motor (Hurst, Princeton, IN) was accommodated, so that the whole system could remain air-tight. A finely adjustable needle valve was connected to a gas inlet of the sample cell to control the gas pressure. The vacuum was maintained

through a two-stage glass diffusion pump. The sample cut to 1 x 1 x 0.1 (cm) was placed on top of the axis of the motor and right in the middle of the cell. The stepping motor, driven by a motor controller (Hurst, Princeton, IN), was rotated at 0.1 degree per second to produce a new sample surface for each laser shot.

To ensure interference-free spectroscopy, several pure materials were used: silicon wafer (99.999%, SEH Inc.), germanium wafer (99.99%, Semiconductor Processing Company), copper (>99.5%), and aluminum (>99.5%). Three reference standard aluminum alloy samples were purchased (National Institute of Standards and Technology, SRM 1256a, SRM 1258 and SRM 1241a containing 9.2%, 0.78% and 0.16% of Si respectively). Samples were polished by #600 gritpaper and cleaned by methanol before used. F_2 (5% in Ne), SF_6 (99.99%) and NF_3 (99.9%) were examined as chemiluminescence reagents. The 5% SF_6 and 5% of NF_3 were made with He as a buffer gas and stored in glass chambers. All gases were obtained from Matheson (Seacaucas, NJ) and used as received.

The chemiluminescence emission was collected with a 1" diameter UV lens (f.l. = 2.5 cm) to assure better collection efficiency. Only the 10 mm to 20 mm region of the plume above the sample surface was imaged on the photomultiplier tube (PMT) to achieve spatial resolution and to avoid saturation by the intense plasma emission which was confined to a few mm from the surface. The PMT (RCA Electron Optics, Mount Joy, PA, Model 1P28) used was more sensitive in the blue to UV region. The high voltage power supply was normally set at 500 V. For SiF chemiluminescence detection, two 440 nm interference filters were used to collect the $A^2\Sigma$ -

$X^2\Pi$ band emission and to block most of the continuum background. The signal was directly sent to a waveform analyzer (Data Precision, Davers, MA, Model D6000) with a 1.4 KΩ terminator. The peak area can be calculated in any selected time period using the mathematical functions built into the waveform analyzer. The microphone signal was measured by an oscilloscope (Tektronix, Inc., Beaverton, OR, Model 7904 and 7A22) with a sensitive differential amplifier.

To acquire the chemiluminescence spectra, a monochromator (Heath Co., St. Joseph, MI, Model EU-700) was used to replace the filters. A 10 cm focal length lens was used to match the f-number of the monochromator. The signal of the PMT was sent to a boxcar averager (EG&G Model 162 with Model 164 gated integrator) in which the amplifier was gated at 1-6 μs. An effective time constant of 1 second and a laser pulse rate of 20 were used to obtain a reasonable signal-to-noise ratio. Plots were made on a strip chart recorder. The sample chamber and all the optical components were rigidly mounted on an optical table (Newport, Fountain Valley, CA, Model NRCXS-46).

Results and Discussion

Chemiluminescence spectra. Chemiluminescence of MX in the reaction of metal atoms with halogen or halogen containing compounds is by no means a rare event. However, we believe this represents the first investigation in a laser-generated plume. When the sample cell was filled with 200 mtorr of reagent gas (5% SF_6 in He), a strong bluish violet emission was

observed on the periphery of the plume produced by a laser shot on a silicon wafer. As the reagent gas pressure decreased, the emission region gradually expanded to a few cm in volume and the emission became weaker and vanished for pressures around a few mtorr. When pure SF_6 was used, the expanded bluish violet emission can still be seen in the low mtorr range. As the pressure increased, the emission region was confined and became merged with the plasma emission zone, and eventually could not be distinguished from it. The use of NF_3 as the reagent gas led to no observable differences from SF_6. However, the use of F_2 (5% in Ne) showed a weaker emission, although the same color and similar pressure dependence were obtained. A reddish band was also present just above the plasma region, the intensity of which increased with increasing Ne pressure, that was identified as the Ne atomic emission (632 nm) since it also appeared in pure Ne buffer gas. Germanium sample exhibits almost the same phenomenon as described above. However, the bluish violet emission could not be observed in either aluminum or copper samples in the presence of SF_6, NF_3 or F_2. Instead, a pale yellow emission was observed for aluminum samples using the three gases and the intensity was in the order of NF_3, F_2, then SF_6. The green atomic emission was predominant in copper.

The fact that the bluish violet emission was not observed in aluminum and copper samples can exclude the reagent gases themselves as the corresponding emitters. If the chemiluminescence was produced by dissociation or excitation of the reagent gases in the laser plasma, the chemiluminescence will not depend on the solid media as long as a laser

plasma was created. Since large amounts of reactive atoms are produced in the laser plume, it is quite clear that the atoms may react with the reagent molecules to yield electronically excited products.

Figure 2 shows the emission spectra responding to (a) Si, (b) Ge, (c) Al, and (d) Cu in the presence of SF_6. In all cases, the spectrometer was scanned in the wavelength region of 350 nm to 600 nm, but only the regions with chemiluminescence were shown in the figures. The emission spectra appeared similar in using F_2 or NF_3 as reagents. Since many of the metal oxides and metal fluorides possessing chemiluminescence reactions have been studied by beam-gas experiments, the emission bands can be easily identified by comparing with the literature. Their assignments are as follows: (a) SiF ($A^2\Sigma^+ - X^2\Pi$), (b) GeF ($A^2\Sigma^+ - X^2\Pi$), (c) AlF ($a^3\Pi - X^1\Sigma^+$, $b^3\Sigma^+ - a^3\Pi$) and (d) CuF ($C^1\Pi - X^1\Sigma$) (17,19,22,23,25,26). It should be noted that all reactions produced monofluoride emission.

One of the important features of laser-generated plumes is the extremely high temperature environment where large populations of species with high kinetic energy and reactive metastables can occur. Therefore, the study of chemiluminescence in a laser-generated plume may show interesting reaction pathways and unusual high energy state transitions. In a beam-gas experiment, Rosano and Parson were not able to observe the electronic transitions of monofluoride in Si + SF_6 reaction, where the Si atoms were thermally generated (34). Instead they reported the transition of dihalides in the reactions of Si, Ge and Sn with SF_4, SF_6 and ClF_3. It is not surprising since the formation of difluorides is highly exothermic (around 130 Kcal/mole), enough to reach the $^3B_1$ state of MF_2 around 75

Figure 2. Chemiluminescence spectra of metal monofluorides

(a) SiF,

(b) GeF,

(c) AlF,

(d) CuF.

Resolution: (a), (b): 0.3 nm, (c): 3 nm, (d): 0.6 nm.

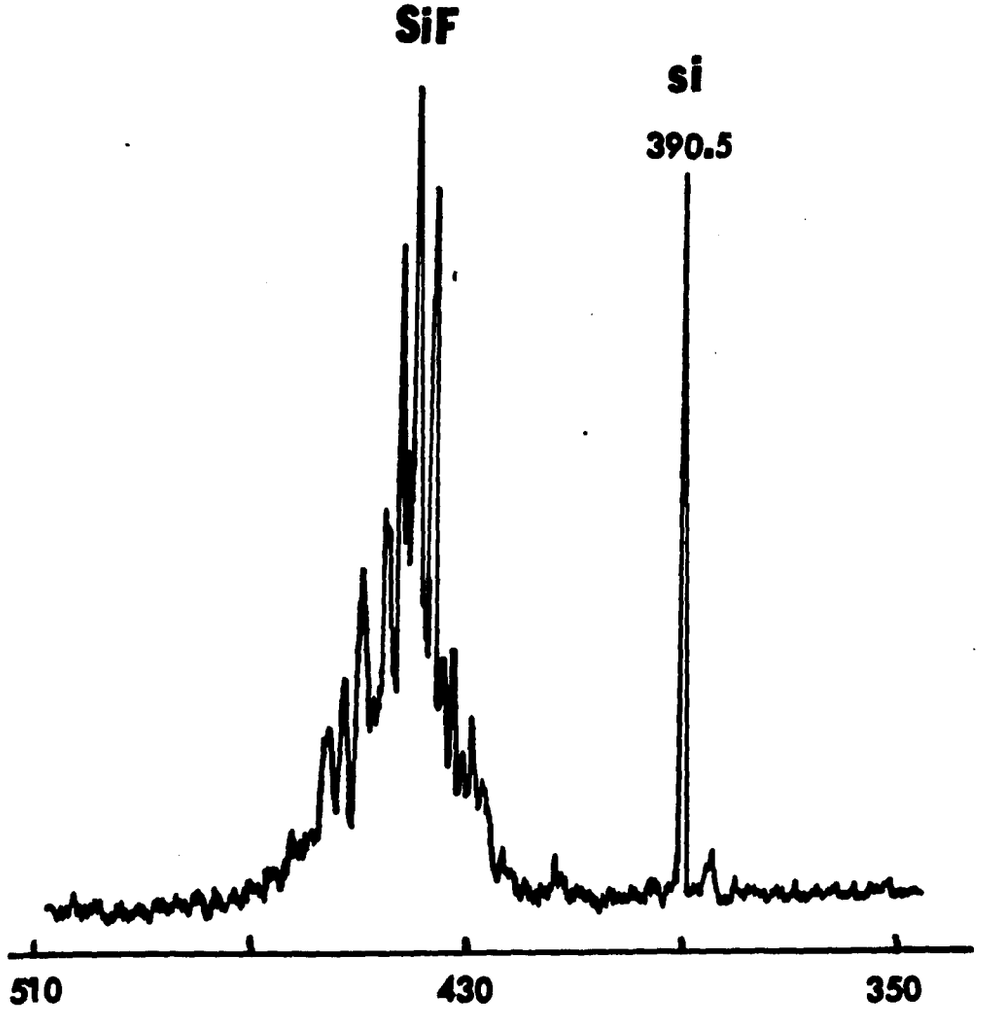

(a)

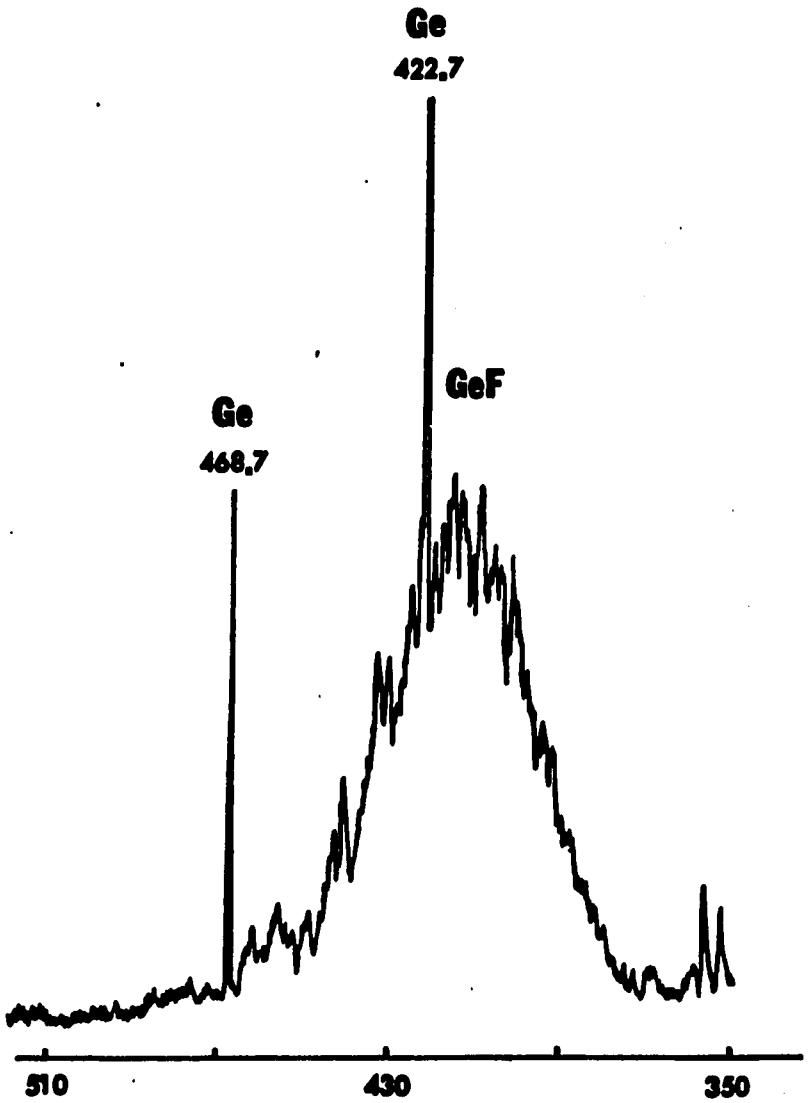

(b)

Figure 2 (Continued)

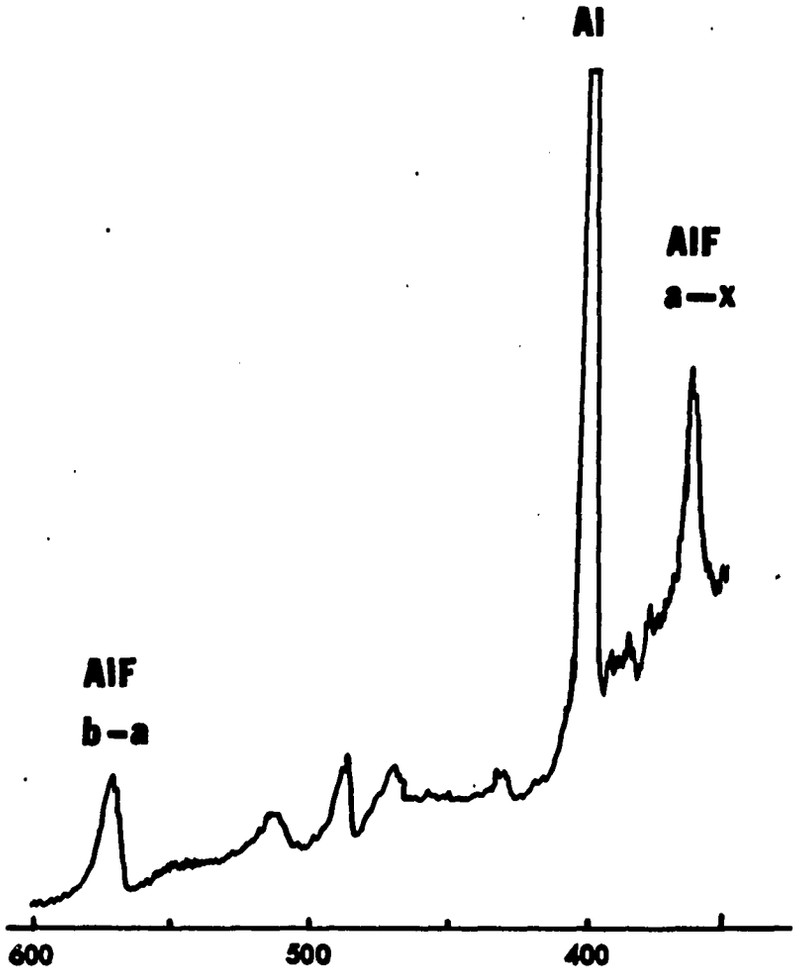

(C)

Figure 2 (Continued)

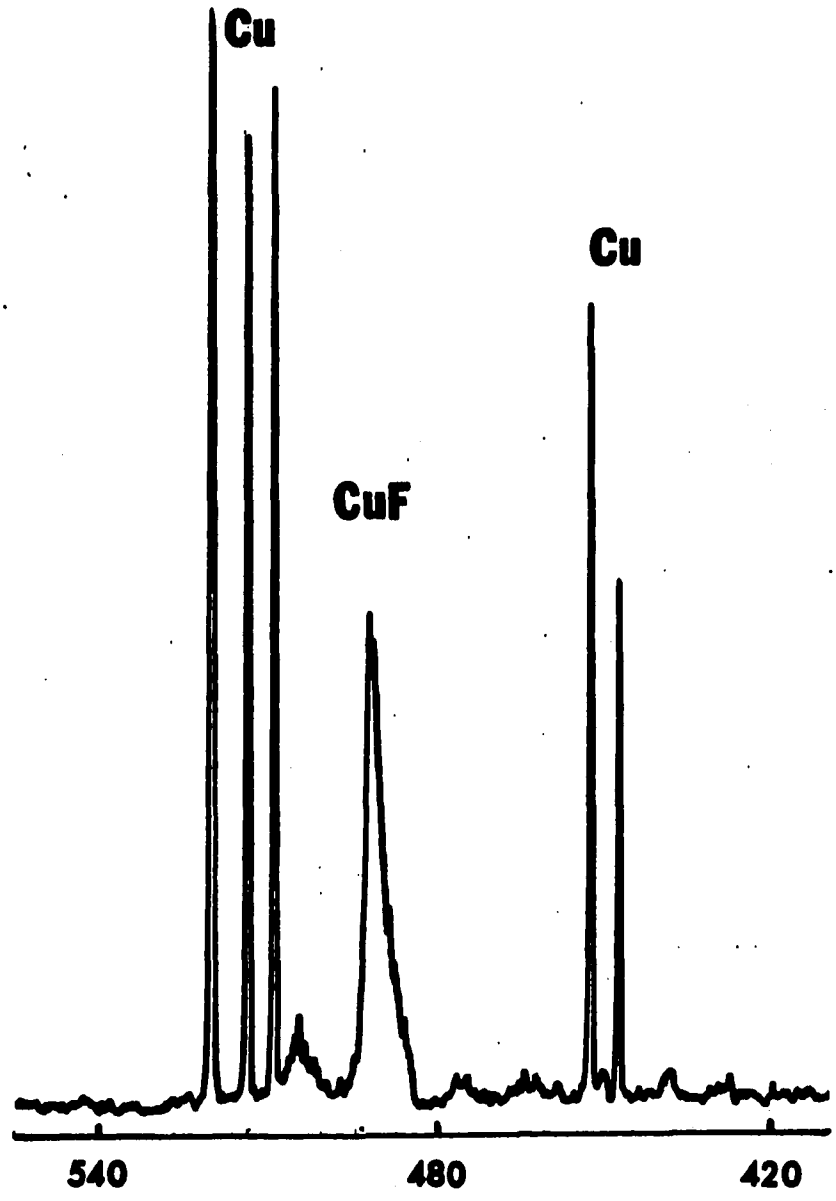

(d)

Figure 2 (Continued)

Kcal/mole.

From the reported bond strengths, the reactions of Si, Ge with Sf_6 are exothermic by 67, 47 Kcal/mole, and with SF_4 are exothermic only by 44 and 24 Kcal/mole, respectively (35). The energies required to reach the first electronically excited A state of SiF and GeF are 65 and 66 Kcal/mole. Thus, the transitions of monofluorides may not be observed.

In a laser-generated plume, however, the large kinetic energy and the existing metastable states will provide extra energy, so the reaction schemes:

$$M + SF_6 \rightarrow MF^* + SF_5 \qquad (b)$$

$$MF^* \rightarrow MF + h\nu$$

are energetically accessible. In fact, Verdasco, et al. has studied the reaction of metastable $Ca^*(^3P)$ with SF_6 and observed $A^2\Pi$ and $B^2\Sigma^+$ excitation of CaF. There, the metastable atoms were produced by heating and then further excited by a dc discharge (36).

In particular, it is worth noting that the spectra of SiF obtained here show vibrational structure, and the highest peak corresponds to the v(0,0) transition. This agrees with ref. 25 and 26, but is in variance with ref. 17, where one finds an essentially continuous spectrum. This is because the excitation and relaxation mechanisms in the different studies are different.

Reagent gas pressure dependence. If the chemiluminescence is first order relative to the reagent gas pressure, it can be described by the following equation:

$$I \propto p\, e^{-\alpha p} \qquad (1)$$

where I is the intensity of the emission, p is the reagent gas pressure and α is an attenuation factor related to the total cross-section for removal of atoms before entering the viewing region (17,37,38). The emission of SiF (440 nm) was studied as a function of SF_6 pressure over 0.5 - 30 mtorr (10 - 660 mtorr, 5% SF_6 in He). The plot of emission intensity against the pressure of SF_6 is shown in Figure 3. The solid curve represents the best fit curve of equation (1), with an α value of 0.1. These results indicate the reaction is first order relative to the reagent gas pressure.

The chemiluminescence temporal peak positions were also evidence supporting the reaction scheme in (b). Figure 4 shows a set of SiF emission signal traces for pressures of 10^{-4} to 5 torr (5% SF_6). As the pressure decreased, the peak maximum shifts from 1 to 6 μs. The peak corresponds to the amount of SiF* in the 1 - 2 cm viewing zone above the surface. This shift is expected if reaction is directly with SF_6. At high pressures, most of M reacted before entering and only small amounts of the luminescence species appeared in the viewing window, resulting in a small, early peak. At low pressures, many atoms passed into window without reaction, resulting in a late, broad peak.

Laser power dependence. Since the reagent gas may dissociate in the laser plasma before the chemiluminescence reaction, the following mechanism is still possible:

$$SF_6 \rightarrow F + SF_5 \qquad (c)$$

$$SF_5 \rightarrow F + SF_4$$

$$M + F \rightarrow MF^*$$

Figure 3. Chemiluminescence signal of SiF vs. SF_6 pressure.

Square : experimental data;

Solid curve: Simulation of equation (1).

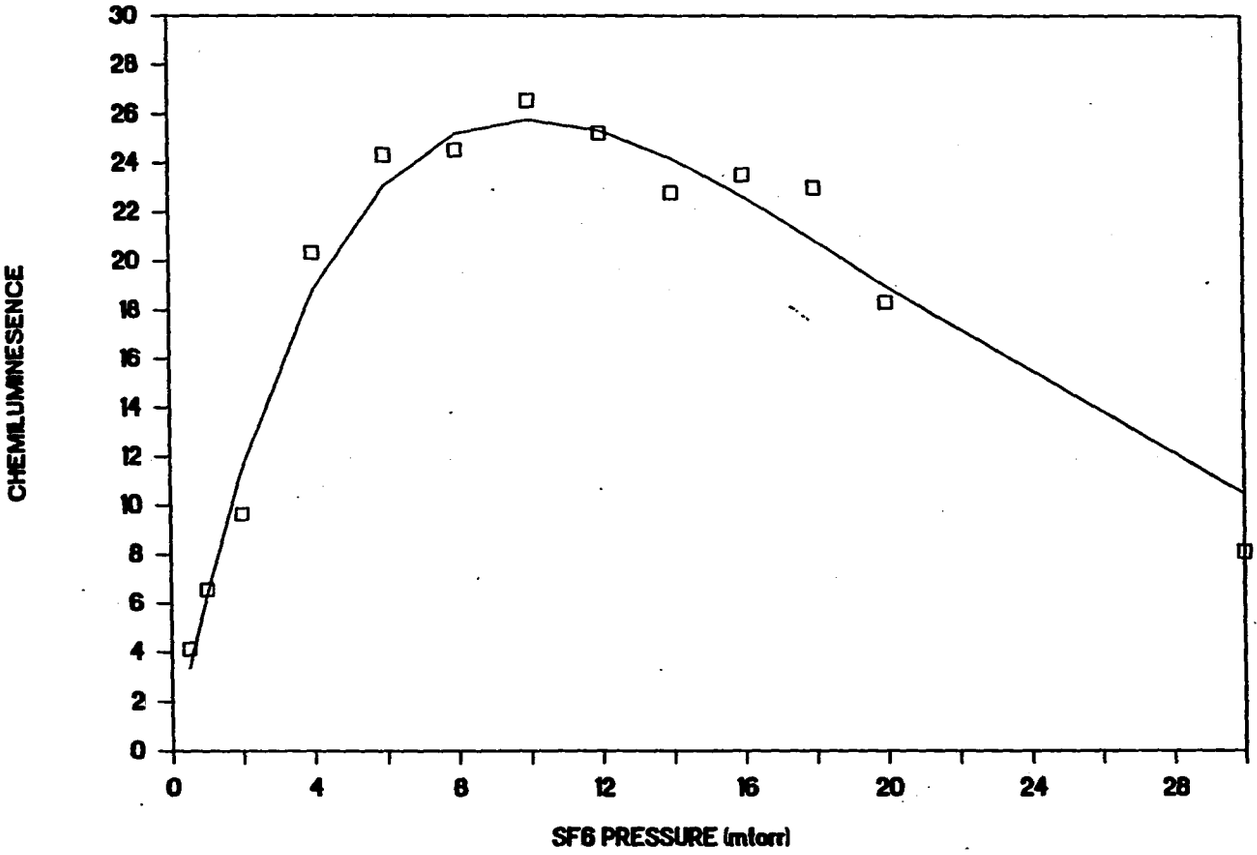
CHEMILUMINESCENCE
30
28
26
24
22
20
18
16
14
12
10
8
6
4
2
0
0
4
8
12
16
20
24
28
SF6 PRESSURE (mtorr)

Figure 4. Peak shift of SiF chemiluminescence with pressure (SF_6 5%).

Trace 1: 5 torr;

Trace 5: 0.1 torr;

Trace 10: 10^{-4} torr.

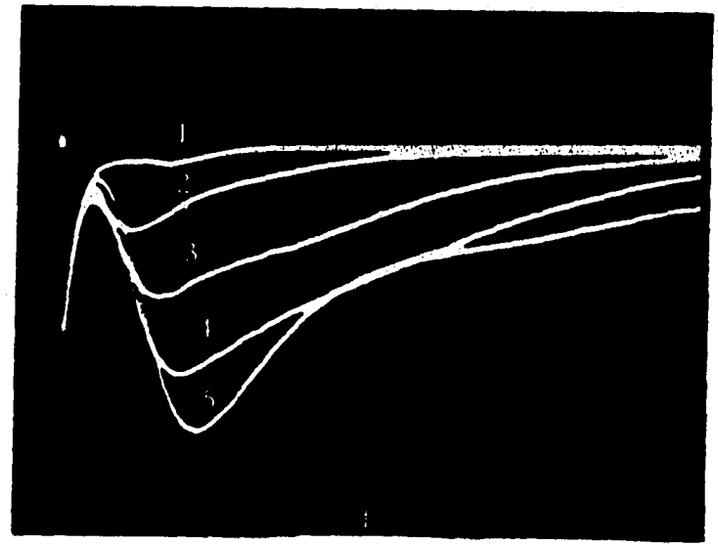
1
2
3
4
5

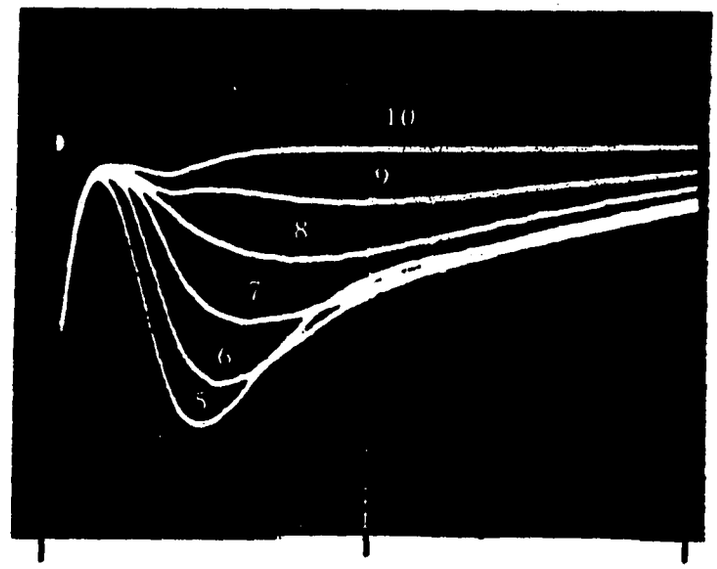
10
9
8
7
6
5
0
5
10
(us)

$$MF^* \rightarrow MF + h\nu$$

If this mechanism dominates, the emission intensity should have a high order dependence on laser power, because both the silicon and the reagent species are produced by the laser. However, if the chemiluminescence signal is directly proportional to the amount of silicon atoms, this reaction scheme must be unimportant.

In order to account for the amount of material generated at different laser powers, the acoustic signal was measured as the first peak height. The actual signal trace is shown in Figure 6. Figure 6 shows that the chemiluminescence signal is well delayed from the plasma emission at the left edge of the trace. The ringing pattern for the acoustic signal is an intrinsic resonance in the microphone diaphragm.

Figure 5 manifests a linear relation over nearly 80 fold change in chemiluminescence, except at low signal levels where uncertainties in integrating the signal become large. For 17 data points between 0.2 and 54 mV for the acoustic signal, a correlation $r^2 = 0.992$ was found. The results have two implications. First, the luminescence was produced by the reaction of atoms with reagent gas directly and not with F atoms dissociated from the fluorine containing compounds. The data in Figure 5 were produced over a large range of laser powers, and the signal only depends on the amount of Si produced. Second, the acoustic signal may be used as an internal standard in chemiluminescence detection for quantitation to improve precision.

Figure 7 shows the acoustic signal dependence on buffer gas pressure. The data continue to 71 torr with the acoustic signal staying constant at

Figure 5. Chemiluminescence signal of SiF vs. acoustic signal at a cell pressure of 150 mtorr.

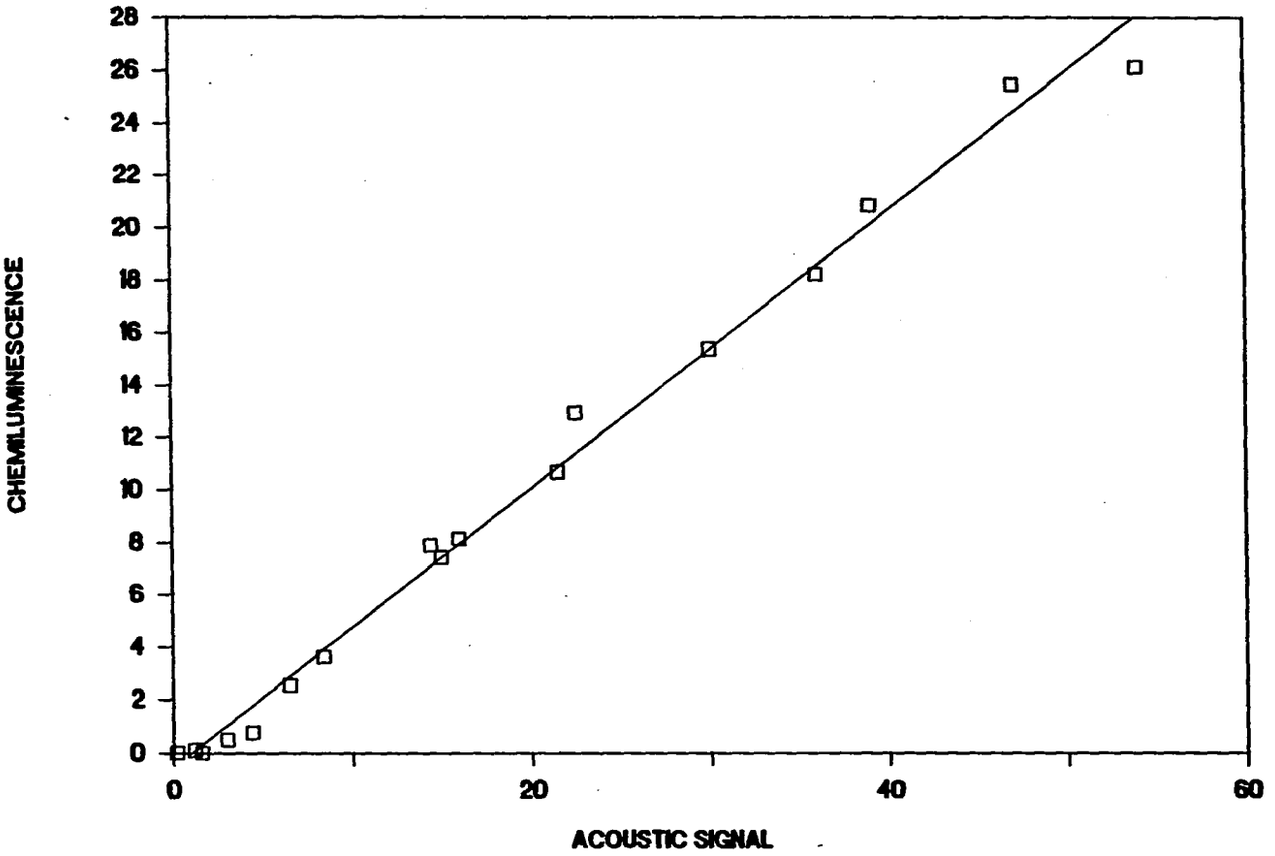
CHEMILUMINESCENCE
28
26
24
22
20
18
16
14
12
10
8
6
4
2
0
0
20
40
60
ACOUSTIC SIGNAL

Figure 6. Top trace: the temporal profile of chemiluminescence of SiF, Lower trace: acoustic wave. Sample: silicon wafer; pressure: 150 mtorr He (SF_6 5%); laser: 3 mJ/pulse.

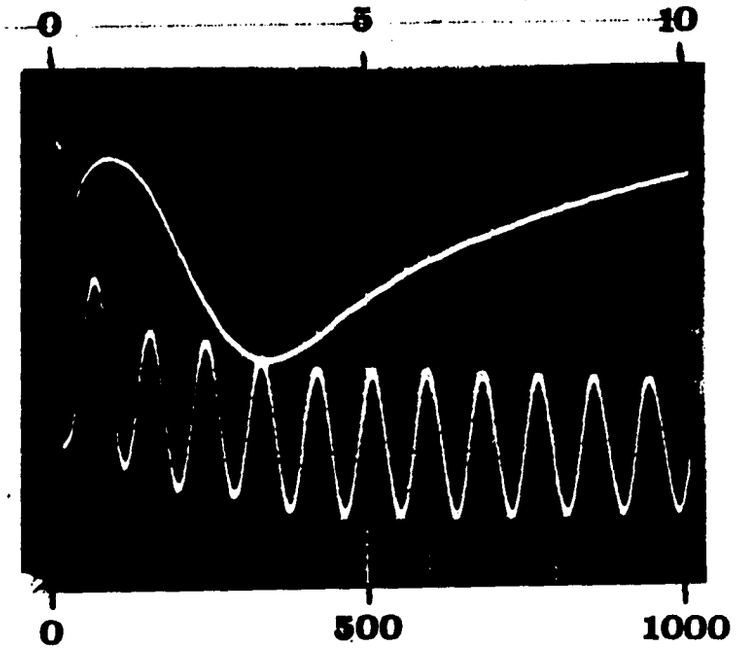
0
5
10
0
500
1000
TIME(uS)

170 units. This indicates that the gas coupling efficiency of the sound wave to the microphone has reached a plateau at around 1 torr. Figures 3 and 7 show that the reagent gas, SF_6, must be mixed with an inert gas to optimize both chemiluminescence and acoustic detection. Figure 8 presents the typical acoustic waveforms generated by a 3 mJ laser pulse at cell pressures (a) 100 mtorr and (b) 50 torr. Sound can be transmitted by gas collisions and also by the solid media. At low pressures, the solid media (sample, sample mount and cell body) transfer should be prevalent. The nice harmonic decay is characteristic of the microphone diaphragm, slightly damped. The acoustic frequency was found to be independent of cell pressures at low pressure. In contrast, the waveform became irregular at high pressures. It can be explained based on sound wave reflection, which is complicated by the irregular cell geometry. The gas coupling signal is very likely added to the solid transferred signal as the composite value observed in (b). The first peaks, which is invariant when the cell pressure is changed. This peak height was thus used in this study as the acoustic signal.

Laser microprobe analysis. In comparison with atomic emission, chemiluminescence occurs after a relatively long time delay. The Si atomic emission peak occurs at about 2 μs with peak width of 0.6 μs, while chemiluminescence lasts for about 30 μs. It was found that the area determined by integrating from 3 μs onwards showed better signal-to-noise ratio. An improvement of S/N of 6 was obtained over atomic emission, when the Si (390.5 nm) atomic emission and SiF (400 nm) chemiluminescence were compared. The chemiluminescence background was measured with inert gas

Figure 7. Dependence of acoustic signal on buffer (He) gas pressure.

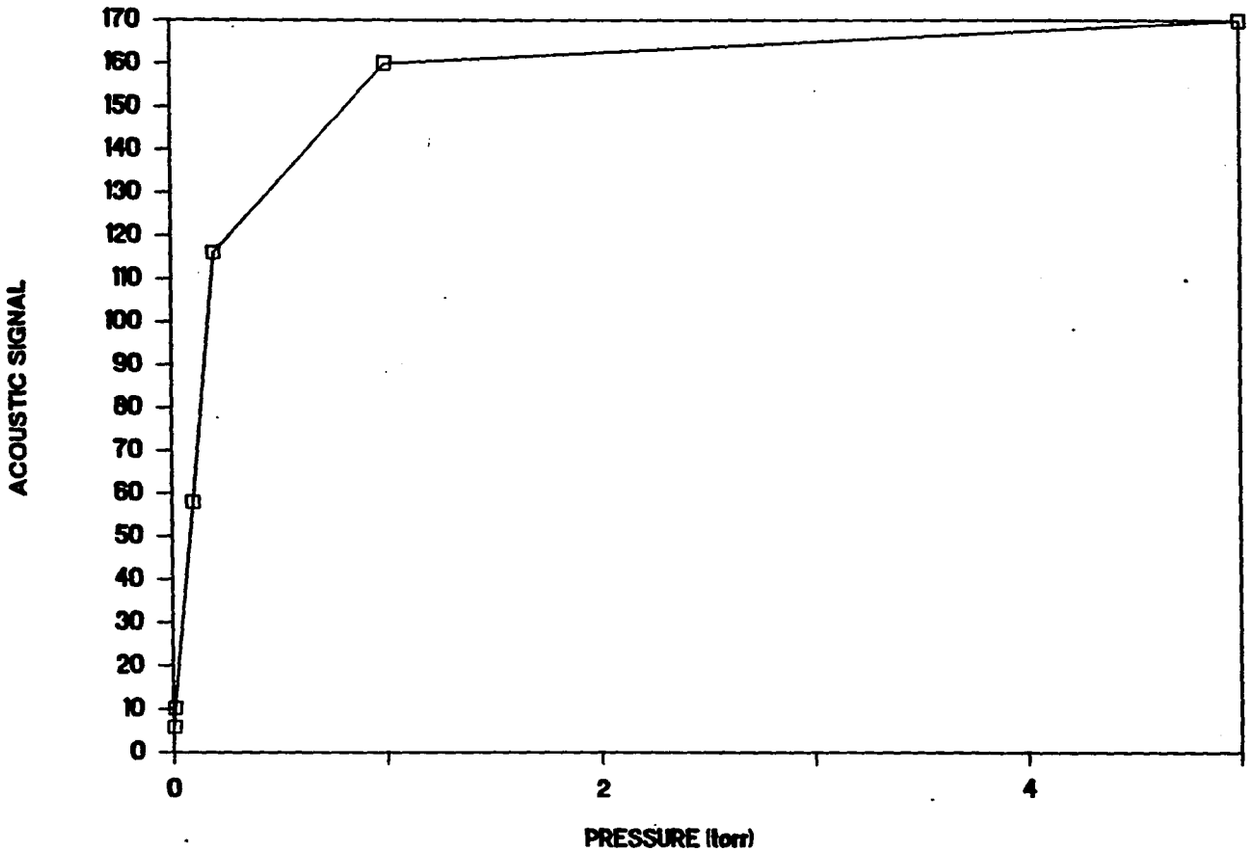
ACOUSTIC SIGNAL
170
160
150
140
130
120
110
100
90
80
70
60
50
40
30
20
10
0
0
2
4
PRESSURE (torr)

Figure 8. Acoustic wave

(a) cell pressure: 200 mtorr (X = 1 ms per division, Y = 20 mv);

(b) cell pressure: 50 torr (top: X = 0.1 ms, bottom: X = 0.5 ms, Y = 50 mv).

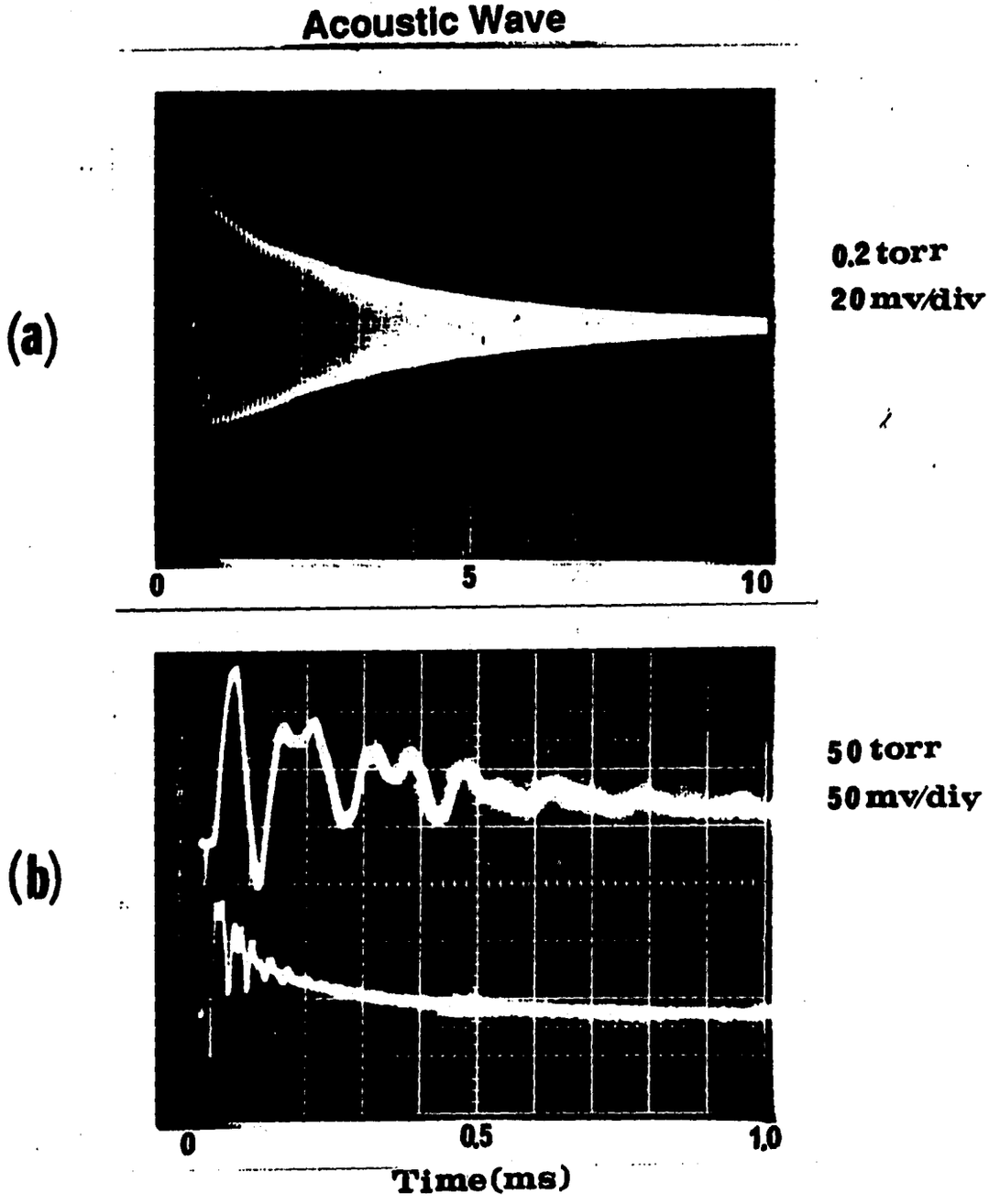
Acoustic Wave
(a)
0.2 torr
20 mv/div
0
5
10
(b)
50 torr
50 mv/div
0
0.5
1.0
Time(ms)

but without SF_6.

We studied the chemiluminescence determination of Si in aluminum alloys with acoustic signal as an internal standard. For the SRM samples studies, linearity was found over the range 10% Si to 0.1% Si. Two 440 nm interference filters were used and the cell pressure was maintained at 150 mtorr with 5% SF_6 in He. The laser pulse energy used was 2.7 mJ so that the amount of material vaporized can be kept in the low nanograms. The volume of material removed was estimated by measuring the size of the crater using an electron microscope and the weight removal was calculated from the density of the sample. 20 ng of sample is typically removed with a range of ±50%, for the laser energies used here. The mass detection limit of Si was in the 10^{-11} g range based on the 0.1% concentration limit of detection estimated. These results are very good in laser microprobe analysis. It is worth comparing with atomic absorption detection of Si, in which the limits of detection reported were only 1% and 10^{-7} g. Quantitation by chemiluminescence with acoustic normalization was quite satisfactory at approximately ±5%, in contrast to ±20 - 30% without normalization.

Literature Cited

1. Laqua, K. In Analytical Laser Spectroscopy; Omenetto, N., Ed., Wiley: New York, 1979; Chapter 2.
2. Dittrich, K.: Wennrich, R. Prog. Analyt. Atom. Spectrosc. 1984, 7, 139.

3. Korolev, N. V.; Faililevich, G. A. Zavodsk. Lab. 1964, 30, 557.

4. Klein, P.; Banatz, J.; Frensenius Z. Anal. Chem. 1981, 308, 283.

5. Deloule, E.; Floy, J. F. Chem. Geol. 1982, 37, 192.

6. Ryan, J. R.; Ruh, E.; Clark, C. B. Am. Cram. Soc. Bull. 1966, 45, 260.

7. Conzemius, R. J.; Capellen, J. M. Inter. J. Mass Spectro. and Ion Phys. 1980, 34, 197.

8. Hein, S. J.; Piepmeier, E. H. Trends Analy. Chem. 198, 7, 137.

9. Deijck, W. V.; Balke, J.; Maessen, F. J. M. J. Spectrochim. Acta 1979, 34B, 359.

10. Talmi, Y. Anal. Chim. Acta 1981, 127B, 71.

11. Quentmeier, A.; Laqua, K.; Hagenah, W. D. Spectrochim. Acta 1980, 35B, 139.

12. Mossotti, V. G.; Laqua, K.; Hagenah, W. D. Spectrochim. Acta 1967, 23B, 197.

13. Pasteris, J. D.; Kuehn, C. A.; Bodnar, R. J. Econ. Geol. 1986, 81, 915.

14. Ishizuka, T.; Uwamino, Y. Spectrochim. Acta 1983, 38B, 519.

15. Thompson, M.; Goulter, J. E.; Sieper, F. Analyst 1981, 106, 32.

16. Dreyfus, R. W.; Kelly, R.; Walkup, R. E. Appl. Phys. Lett. 1986, 49, 1478.

17. Rosano, W. J.; Parson, J. M. J. Chem. Phys. 1983, 76, 2696.

18. Luria, M.; Eckstrom, D. J.; Edelstein, S. A.; Perry, B. E.; Benson, S. W. J. Chem. Phys. 1976, 64, 2247.

19. Brayman, H. C.; Fishell, D. R.; Cool, T. A. J. Chem. Phys. 1980, 73,

4247.

20. Rosenwaks, S. Chem. Phys. Lett. 1979, 64, 352.
21. Schwenz, R. W.; Parson, J. M. J. Chem. Phys. 1982, 76, 4439.
22. Rosenwaks, S. J. Chem. Phys. 1976, 65, 3668.
23. Baltayan, P.; Hartmann, F.; Pebay-Peyroula, J. C.; Sadeghi, N. Chem. Phys. 1988, 120, 123.
24. Schwenz, R. W.; Parson, J. M. J. Chem. Phys. 1980, 73, 259.
25. Armstrong, R. A.; Davis, S. J. J. Chem. Phys. 1979, 71, 2433.
26. Conner, C. P.; Stewart, G. W.; Lindsay, D. M.; Gole, J. L. J. Am. Chem. Soc. 1977, 99, 2540.
27. Webb, M. S. W.; Webb, R. J. Anal. Chim. Acta 1971, 55, 67.
28. Kirchheim, R.; Nagorny, U.; Maier, K.; Tolg, G. Anal. Chem. 1976, 48, 1505.
29. Peppers, N. A.; Scribner, E. J.; Alterton, L. E.; Honey, R. C.; Beatrice, E. S.; Harding-Barlow, I.; Rosan, R.C.; Glick, D. Anal. Chem. 1968, 40, 1178.
30. Morton, K. L.; Nohn, J. D.; Macken, B. S. Appl. Spectrosc. 1973, 27, 109.
31. Piepmeier, E. H.; In Analytical Applications of Lasers, Piepmeier, E. H. Ed.; Wiley: New York, 1986; Chapter 19.
32. Carr, J. W.; Horlick, G. Spectrochim. Acta 1982, 37B, 1-15.
33. Chen, G.; Yeung, E. S. Anal. Chem. 1988, 60, 2258.
34. Rosano, W. J.; Parson, J. M. J. Chem. Phys. 1986, 84, 6250.
35. James, E. H.; Inorganic Chem., 3rd Ed.; Harper & Row: New York, 1983.
36. Verdasco, E.; Rabanos, V. S.; Aoiz, F. J.; Urena, A. G. J. Phys.

Chem. 1987, 91, 2073.

37. Dickson, C. R.; George, S. M.; Zare, R. N. J. Chem. Phys. 1977, 67, 1024.

38. Ottinger, C.; Zare, R. N. Chem. Phys. Lett. 1970, 5, 243.

SECTION FOUR:

FACTORS AFFECTING GAS-PHASE CONTINUOUS WAVE INFRARED LASER SENSITIZED PYROLYSIS

Introduction

The use of lasers for inducing chemical reactions is a mature field (1). One application involves the excitation of gaseous reactants by an infrared laser, with or without a sensitizer. Of interest is the comparison with traditional thermal reactions, since the hot reactants can be generated by a laser away from the walls of the cell, avoiding contributions from hot surfaces. Even though the early work on homogeneous pyrolysis by Shaub and Bauer (2) is based on a CW infrared laser and a sensitizer,much more work has been done using pulsed infrared lasers (3). The latter approach even allows direct pumping of the reactant in the absence of a sensitizer. While very often the laser-induced reactions are shown to closely parallel thermal reactor or shock tube results (2,3), there are also examples of significant differences in rate parameters and branching ratios in these studies (4).

To obtain reliable information about the rate parameters, the spatial and temporal distribution of temperature in the cell must be known. The problem is simplified if an internal standard is used, similar to the well-established comparative rate single-pulse shock tube methods (5). Then, only rough quantitative models are needed for the temperature

distribution (4a). For pulsed experiments, it is necessary to consider the gas dynamics involved in the expansion of the heated column to the rest of the cell (3b). The model is much simpler for CW experiments, since a steady-state temperature profile can be established in the cell. Such a simulation has been attempted previously (2), but the results do not compare well with measured conversion for standard test reactions. Despite the lack of a semiquantitative model, CW laser induced comparative rate studies have been quite successful (2).

In this article, we present results from a refined model for establishing the temperature profiles in a cell for CW laser sensitized pyrolysis. No adjustable parameters are used. The results are compared to experimental measurements of transmittance as well as unimolecular decomposition rates in a well-known test system. Transmittance turns out to be a sensitive and independent check of the gas temperature. The various features and experimental conditions that influence the determination of rate parameters can thus be depicted.

Model

Temperature distributions due to heating by a Gaussian beam have been treated before in conjunction with the thermal lens effect (6). Those results, however, are not applicable to the present problem because the temperature changes are large. This leads to variations in the absorption coefficient, thermal conductivity, and number density in different regions. Fortunately, it is possible to account for these variations by

using data from the literature.

For CW excitation, one can consider the steady-state heat flow through cylindrical segments of the gas of thickness dr from r = 0 (center of cell and axis of the laser beam) to r = R′ (inside cell wall). Since the highest intensity is at r = 0, only heat flow outward (radially) is important. Within each segment dr, the temperature can be considered to be constant. At the first level of approximation, we assume that the gas density is uniform throughout the cell and that the laser beam is not depleted as it travels along the cell. Initially, we also neglect heat flow in the axial direction. For a Gaussian beam, the amount of heat deposited per second in the cylinder a distance r from the axis is given by

$$Q = \frac{I}{4.184}\left[1 - \exp\left(-2\left(\frac{r}{w}\right)^2\right)\right] \qquad (1)$$

where w is the laser beam radius, I is the absorbed laser intensity per unit length in watts, and Q is in calories. Naturally, one can measure the exact distribution of the laser intensity and consider heat flow in infinitesimal cylinders if the distribution is irregular. Finally, if the light beam is attenuated significantly as it passes along the cell, one can repeat these calculations for each part of the path length by allowing I to vary in equation 1. The temperature difference between two consecutive cylinders is then

$$\Delta T = T_2 - T_1 = Q_1\, dr/\lambda A \qquad (2)$$

where A is the area of the boundary between cylinders in cm^2, and λ is the

thermal conductivity of the gas in cal/(cm s). The latter can be calculated in the hard-sphere approximation (zeroth order) as (7)

$$\lambda = (1.9891 \times 10^{-4}) \frac{(T/M)^{1/2}}{\sigma^2} \left(\frac{4}{15}\frac{C_v}{R} + \frac{3}{5}\right) \quad (3)$$

where M is the molecular weight, σ is the molecular radius, C_v is the heat capacity at constant volume, and R is the universal gas constant. We can also use the first approximation, i.e., divide by $\Omega^{(2,2)*}(T^*)$ according to Hirschfelder et al. (7). C_v can be derived from standard tables (8) for the temperature of interest via $C_v = C_p - R$.

As the temperature increases significantly above room temperature T_R, the gas density $\rho(T)$ can no longer be assumed to be uniform across the cell. The lower gas density at the center of the cell plus a lower absorption coefficient ε results in a lower amount of heat deposited. So eq 1 has to be modified by a factor T_R/T for each cylinder. So

$$Q(T) = Q(T_R)[T_R/T][\varepsilon(T)/\varepsilon(T_R)] \quad (4)$$

Values for $\varepsilon(T)$ have been reported in the literature (9). We note that even though there is a density gradient in the cell, there is not enough refractive index change to create a thermal lens that will change w in eq 1.

Actual temperature calculations can be done numerically. The cylindrical zones can be treated consecutively starting at the cell wall at T_R. For a unit length of the gas, the area A is simply given by $2\pi r$. So eq 1 through 3 can be used to calculated the temperature of the next inner zone by using the constants C_v, λ, $\varepsilon(T)$, gas density) associated

with the present zone. If the zones are thin enough, as in the present case, the temperature differences are small between zones, and the errors are negligible.

Finally, if the light beam is attenuated significantly as it passes along the cell, one can repeat these calculations for each part of the path length Δx by allowing I to vary in eq 1. The amount of light passing onto the next segment (Δx) can be treated exactly since the amount of light absorbed in the previous segment is governed by the temperature, and thus defining $\varepsilon(T)$ and $\rho(T)$. It can be seen that the beam does not remain Gaussian as it propagates through the gas. Also, there is a second boundary condition at the cell windows (entrance and exit of the laser) that requires the temperature to be at $T = T_R$. Rather than to treat the axial heat flow exactly, an approximation can be made by considering a "buffer" zone near the windows. We therefore treat the middle 3.6 cm of the cell as being free from conduction to the windows. The buffer zones at both ends then follow a linear temperature drop to T_R over 0.1 cm to the windows. As can be seen below, the exact details of the buffer zone do not influence the determination of activation energies much, since most of the reaction occurs in the small region where T is the largest.

Experimental Section

The laser used is a grating-tuned CO_2 laser (Molectron C250). By proper tuning, it is possible to produce a homogeneous beam about 1.5 mm in diameter. Occasionally, there appear stray modes that are well-

separated from the main beam. These are removed completely by a diaphragm without truncating the main beam. The beam size and shape are then measured by translating a 50- μm pinhole across the beam on a stage (Aerotech) and measuring the power (Coherent 210). The laser wavelength is determined by a spectrum analyzer (Optical Engineering).

The glass cell used is cylindrical (3.8 cm long and 4-cm i.d.) and is fitted with polished NaCl windows (0.5 cm thick) by epoxy (Eccobond). The cell is connected to a GC sampling septum and then to a grease-free stopcock. The connections only add 2 cm^3 to the total volume. Pumping to 10^{-6} Torr is possible on a grease-free vacuum system operated by a turbomolecular pump (Pfeiffer TPU). Pressures are measured on a manometer (MKS 221AHS-F) with 10-Torr full scale. In all experiments, 6 Torr of SF_6 (Matheson) and 1 Torr of C_2H_5Cl (Matheson) are introduced into the cell. After irradiation, a gas-tight syringe (Hamilton) withdraws 1 mL of gas through the septum. Since several minutes elapse between irradiation and withdrawal, uniformity of product distribution is assured provided there is no adsorption. The sample is injected into a gas chromatograph (Tracor 550) with an FID detector. Only the C_2H_4 peak is measured as it elutes off the column (packed 60/80 Carbosieve G, Supelco). Reactions at lower incident laser powers are run for longer times to allow better determinations of the conversions. Transmission of the laser beam was determined by measuring the power before or after the cell, which is fixed throughout the series of runs. The evacuated cell was also probed to determine the transmission of the windows, so that a correction to the measured laser power can be made. There is normally a 5% variation of the

measured power over the active area of the thermopile. So, the maximum registered power near the center of the sensor was used.

Calculations were done on a microcomputer (Atari 1200 XE) with BASIC programming. Initially, tables of density-weighted absorption coefficients, heat capacities, and thermal conductivities are generated as a function of temperature for SF_6. The small amount of C_2H_5Cl makes only a minor contribution and is neglected here. This is justified because the measured transmitted intensity (which is a sensitive probe of the temperature, vide infra) was found to be unaffected by this amount of C_2H_5Cl. Then, for a given disk in the cell 0.2 cm thick, 400 radial zones (0.05 mm each) are considered. Temperatures are propagated from the outside (T_R) to the center of the cell by use of eq 1 and 2 based on an estimate of Q_R, the total heat deposited in this disk by the laser. From the actual incident laser power and the temperature profile calculated, a refined estimate of absorption can then be obtained. A new Q_R is then used for a second iteration. Convergence to a stable temperature profile is obtained in three or fewer iterations. The next disk is then considered given the transmitted laser intensity in each radial zone. For the buffer zones at the beginning and the end of the cell, radial temperature profiles are not determined by eq 1 and 2. Instead, a linear interpolation to T_R at the windows for each radial zone is used, starting from the disks at 0.1 and 3.7 cm into the cell. For each temperature zone i in the cell, the value $(T_R/T_i)\exp(-E_a/RT_i)$ can be calculated to determine the conversion as a function of laser power and E_a.

Results and Discussion

Temperature Profile. The radial temperature distribution for a disk 0.2 cm thick receiving 2 W of incident laser power (1.5-mm diameter, Gaussian) and insulated longitudinally is shown in Figure 1. Although the general shape resembles the results of previous studies (6), the maximum temperature here (1144°K) is much lower than that from the simple model (2260°K). This is because the thermal conductivity increased by a factor of about 4 over this temperature range, the density decreased by a factor of 4, and the molar absorptivity decreased by a factor of 15. The importance of having reliable data on heat capacities (for calculating thermal conductivities via eq 3) and on absorptivities can be appreciated. The exact model for eq 3, however, is less important. The zeroth-order approximation gives a maximum temperature of 1149°K. This only has a small effect on the calculation of rate parameters. The temperatures are also substantially lower than previous computer models (2) although a different laser line was involved. Even the P(28) line used there bleaches eventually (9). Worse still, no experimental data on $\ddot{Y}$ are available in the high-temperature ranges. This may be why previous computer models (2) have not been successful.

The longitudinal temperature profile is shown in Figure 2. As discussed previously, exact radial temperatures were determined only for the central 3.6 cm, and the buffer zones at either end were interpolated from the boundary conditions. The effect of the entrance buffer zone is to lower the maximum temperature due to preabsorption and heat conduction

Figure 1. Radial temperature profile in a disk (0.2 cm thick, 2-cm radius) irradiated by a 2-W laser beam (1.5-mm diameter). $P(SF_6)$ = 6 Torr, P(20) CO_2 line.

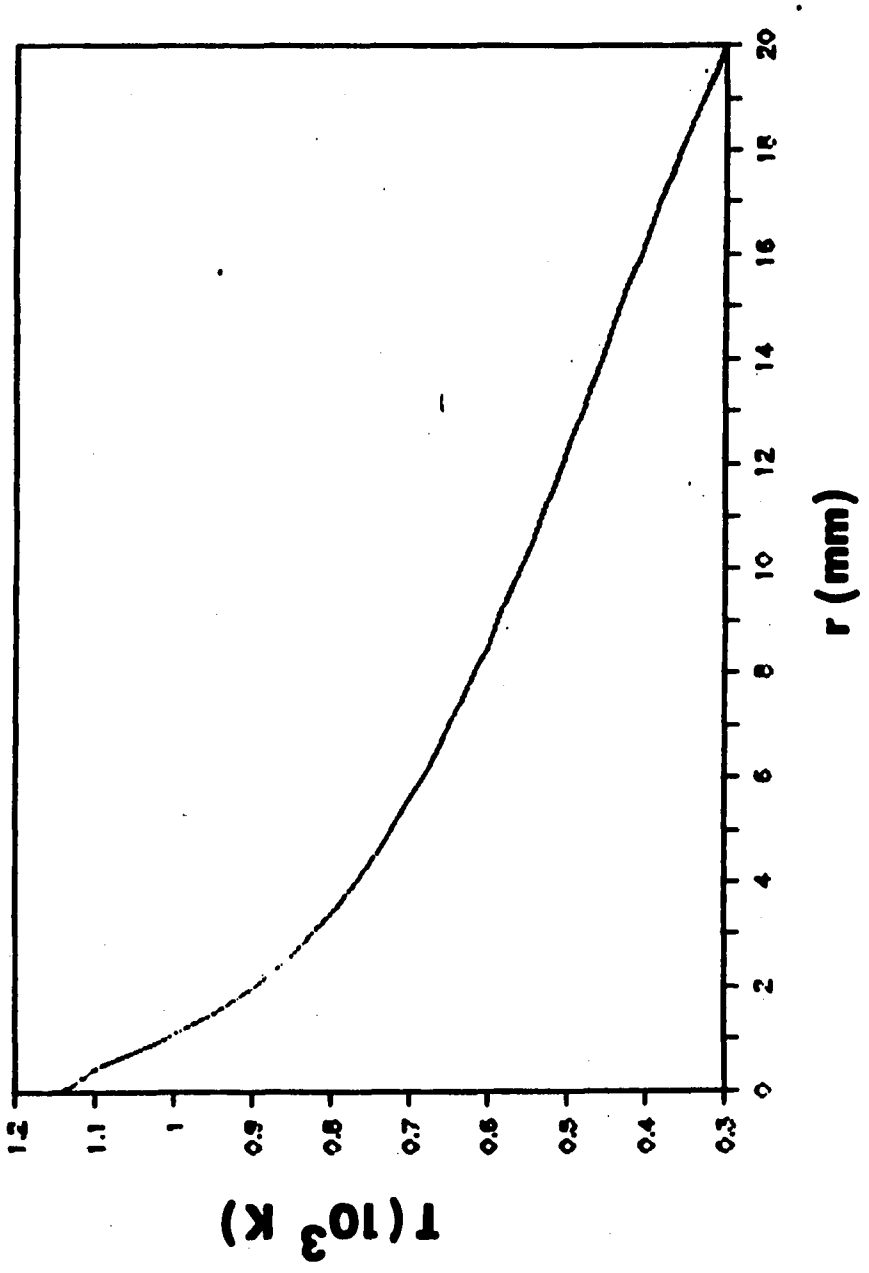
T(10³ K)
1.2
1.1
1
0.9
0.8
0.7
0.6
0.5
0.4
0.3
r (mm)
0
2
4
6
8
10
12
14
16
18
20

Figure 2. Longitudinal temperature profile along the axis of a cell (3.8 cm long, 2-cm radius) irradiated with 2.23 W under the same conditions as in Figure 1. The first and last 1 mm are buffer zones as defined in the text.

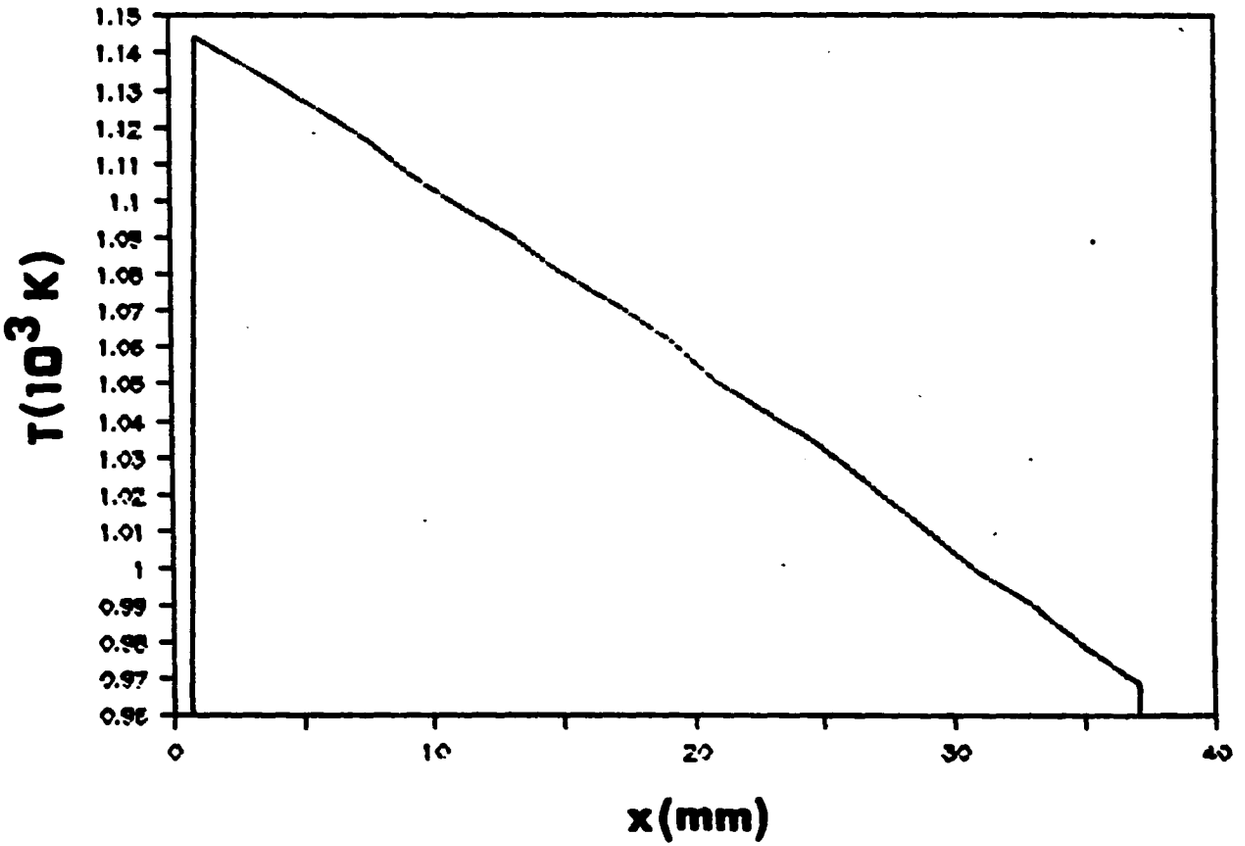
T(10^3 K)
1.15
1.14
1.13
1.12
1.11
1.1
1.09
1.08
1.07
1.06
1.05
1.04
1.03
1.02
1.01
1
0.99
0.98
0.97
0.96
0
10
20
30
40
x(mm)

to the windows. For example, for 2 W to reach the central zones, one needs to send 2.23 W into the cell. Without the buffer zone, the same power would have created a maximum temperature of 1166°K instead. The effect of the exit buffer zone can be neglected, since most of the reaction (vide infra) occurs toward the front of the cell. It can be observed from Figure 2 that the temperature drops roughly linearly in the central region, and only by a small amount. This is again a result of increased thermal conductivity, decreased density, and decreased ε, at higher temperatures.

The effect of the details of the cross-sectional laser intensity distribution on the temperature profile can also be examined. From Figure 1, most of the temperature rise from T_R to T_{max} is from the region outside the laser beam. So, the details of the laser beam are not very important in determining T_{max}. Equation 1 is more a convenience in defining a diameter than a critical assumption. On doubling the beam half-width (same total power), we obtain a maximum temperature of 1106°K. Even though uneven absorption causes the laser beam to deviate from a Gaussian shape as it propagates, an effect that is fully accounted for in our calculations, there is little loss in accuracy if a Gaussian shape is assumed throughout the cell because the size of the beam hardly changes.

Finally, it should be noted that no part of the cell, including the windows, feels warm to touch even after lengthy exposures. The boundary conditions are justified. This is not necessarily true for higher laser powers or for smaller diameter cells. For example, at 10 W, the windows start to feel warm, indicating that the boundary conditions are no longer

correct. Such conditions probably existed in earlier work (2) to make comparisons with models difficult.

Transmission. Figure 3 shows the laser power (integrated over its cross section) as the beam propagates through the cell. The details in the buffer zones naturally depend on the interpolation procedure, but the effects are not large. In the central zone, the laser power decreases roughly linearly and not exponentially. This is from bleaching due to ρ and ε. We note that, at low powers, 6 Torr of SF_6 will absorb 99% of the light in a path length of 1.5 cm.

A real test of the model is the comparison between calculated and measured transmittance through the cell. This is shown in Figure 4. Considering the lack of any adjustable parameters except for the choice of the buffer zones, the agreement is good. To evaluate the contributions from the choice of the buffer zones, we also present the results when the zones are absent. The fit becomes worse. Buffer zones have to exist because the windows are cold. Our interpolation procedure seems to be a reasonable one. Figure 4 depends greatly on the laser beam parameters, since ε changes rapidly in this temperature range (9). Also plotted are calculated transmittance for a beam twice the diameter but at the same power. This shows the best agreement with experiment. Our laser beam is multimode and falls off slower than a Gaussian shape. The improved fit is not unexpected. In fact, transmittance measurements for well-characterized laser beams may prove to be a good probe of gas temperatures. Naturally, the probe will have to be at low powers to avoid contributions to the local temperature. These results also imply that

Figure 3. Integrated laser power along the longitudinal axis of the cell in Figure 2.

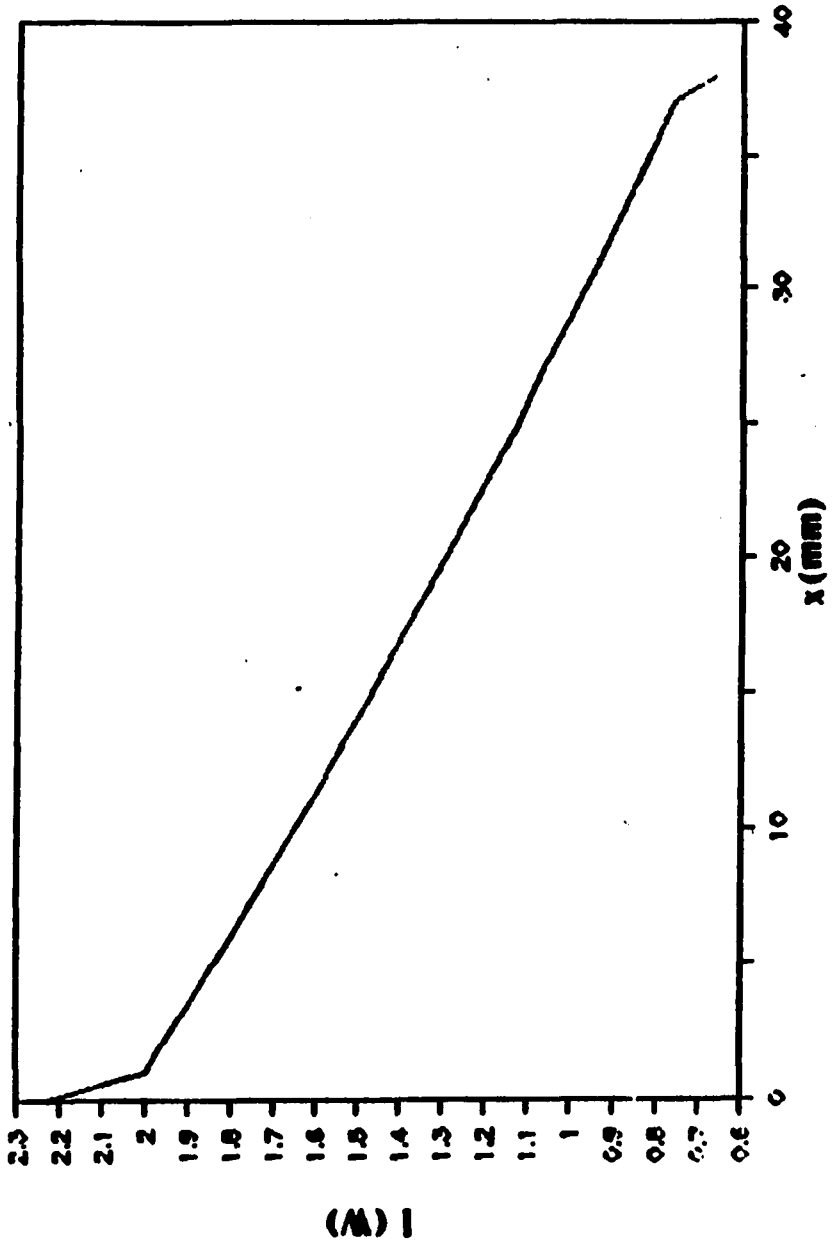
x(mm)
0
10
20
30
40
I (A)
2.3
2.2
2.1
2
1.9
1.8
1.7
1.6
1.5
1.4
1.3
1.2
1.1
1
0.9
0.8

Figure 4. Calculated (solid lines) and experimental (points) transmittance through the cell at various incident laser powers:

(a) parameters as in Figure 2;

(b) buffer zones absent;

(c) for a beam with twice the Gaussian beam waist.

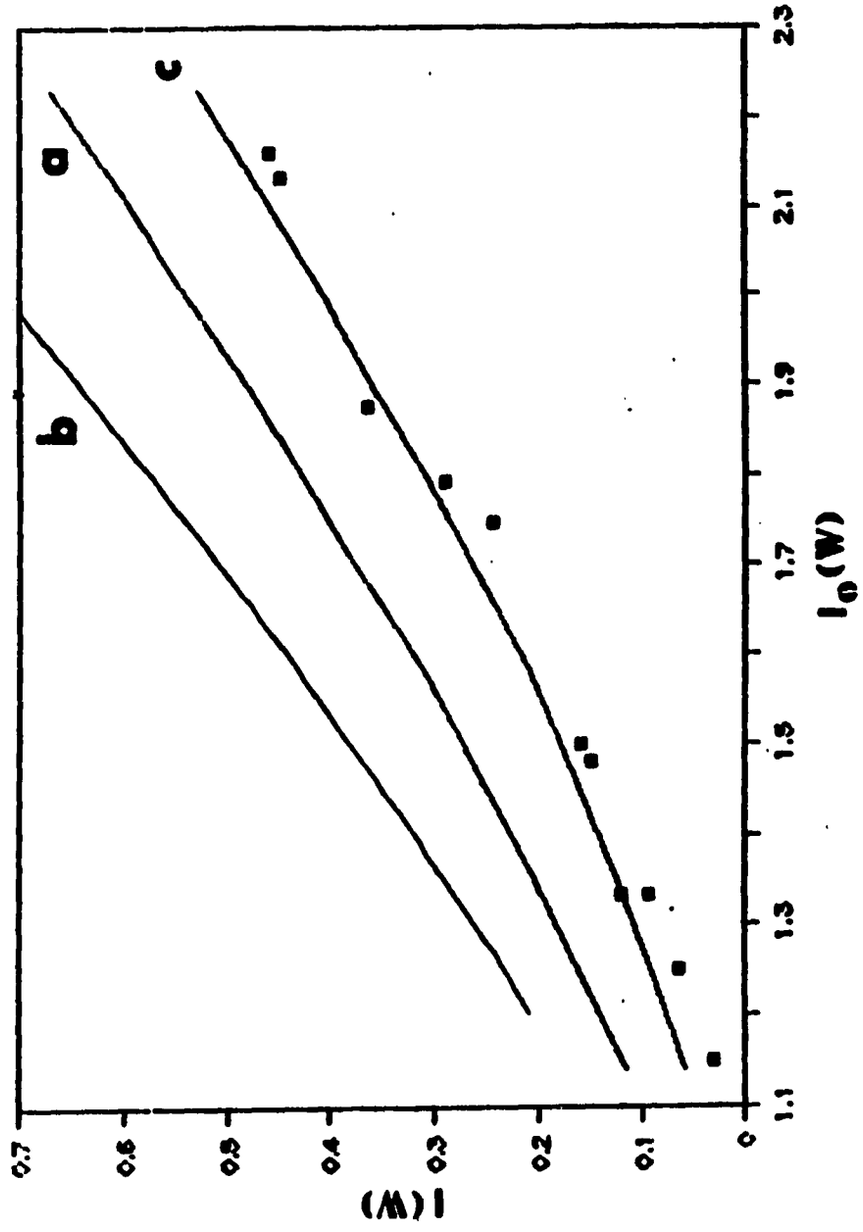
a
b
c
0.7
0.6
0.5
0.4
0.3
0.2
0.1
0
I (W)
1.1
1.3
1.5
1.7
1.9
2.1
2.3
I_0(W)

caution must be taken in interpreting laser transmittance measurements for determining gaseous concentrations whenever the absorption per unit length is high.

Kinetic Parameters. One of the major incentives for predicting temperature profiles is to compare laser-induced pyrolysis with thermal experiments. Some success has been reported for pulsed excitation (3b). However, the steady-state temperature distribution of CW excitation requires fewer assumptions and should make predictions easier. For excitation periods longer than 1 s, such a steady-state condition will be achieved (6). The relative fraction converted per unit volume per unit time, i.e., $(T_R/T_i)\ \exp\text{-}(-E_a/RT_i)$, is plotted in Figure 5 as a function of radial distances from the cell axis for the data in Figure 1. Since this has a logarithmic ordinate, contributions outside the laser beam are essentially negligible. Also plotted in Figure 5 are cumulative yields for each cylindrical zone. The volume-weighted values drop off similarly, but a maximum exists slightly away from the axis. Therefore, most of the reaction occurs near but not at the maximum temperature. The longitudinal distribution of reaction yields is shown in Figure 6. It is clear that 90% of the reaction occurs in the first half of the cell, and increasing the cell length further should not affect the total yield. Another consideration is the effect of the laser beam shape and size. For conditions identical with those in Figure 5, doubling the beam half-width (constant power) only increases the integrated yield in that disk by 30%. Lower temperatures are compensated somewhat by larger volumes in the high-temperature zones. Naturally, this only holds if the laser beam is still

Figure 5. Relative conversion in the disk in Figure 1: (a) fractional conversion per second per unit volume, and (b) fractional conversion per second in each cylindrical volume element. E_a = 57.4 kcal/mol.

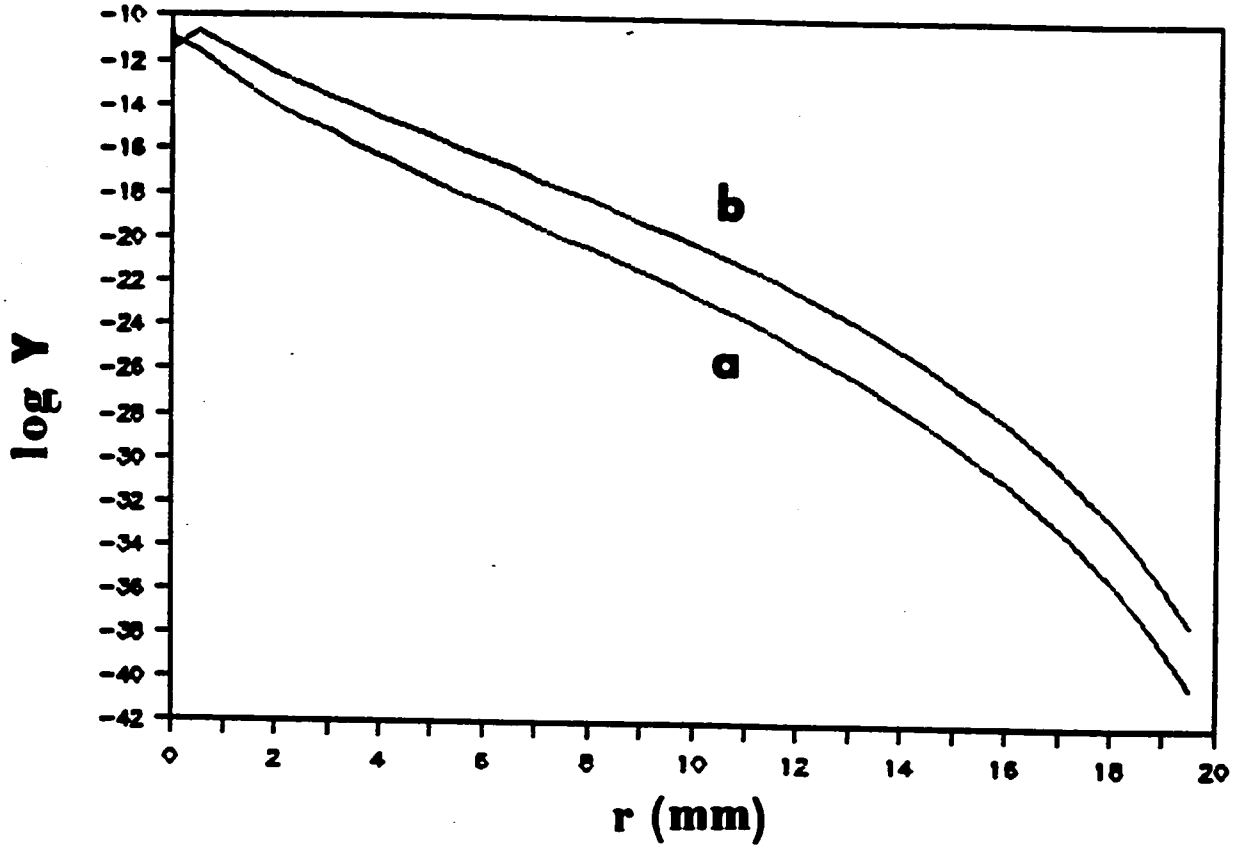
log Y
-10
-12
-14
-16
-18
-20
-22
-24
-26
-28
-30
-32
-34
-36
-38
-40
-42
0
2
4
6
8
10
12
14
16
18
20
r (mm)
b
a

Figure 6. Relative conversion along the cell in Figure 2, integrated over each disk. E_a = 57.4 kcal/mol.

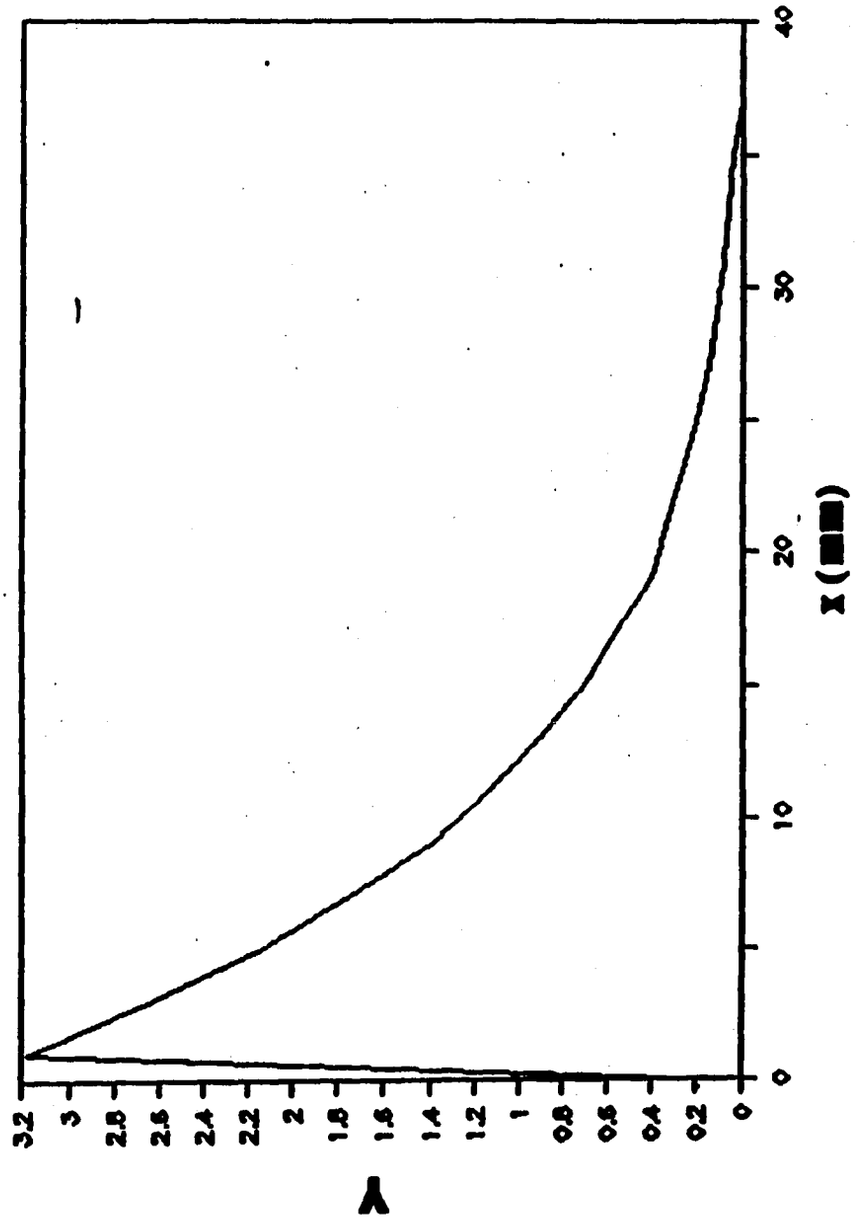
A
3.2
3
2.8
2.6
2.4
2.2
2
1.8
1.6
1.4
1.2
1
0.8
0.6
0.4
0.2
0
0
10
20
30
40
x (■■)

compared to the cell diameter. Otherwise the details of the temperature profile will become important. The increased beam diameter does mean lower transmittance and thus lower powers for the trailing sections of the cell. But since most of the reaction occurs toward the front of the cell (Figure 6), the total yield is affected less, changing by 20% in this case.

The above calculations can be repeated for a series of incident laser powers and a series of E_a values. Two of these calculations of total yields are plotted in Figure 7. A normalization factor was used to allow displaying these on the same scale; i.e., the frequency factor is allowed to vary. The experimental values are also plotted there. The variation of reaction yield as a function of laser power is a result of the differences in temperature in the cell. So, Figure 7 allows us to use C_2H_5Cl as a chemical thermometer to compare with the calculations. Naturally, both the frequency factor and the activation energy contribute to the rates of reaction. The temperature dependence, however, is dominated by the latter. Furthermore, the frequency is influenced by activation efficiencies that can cause a falloff from the high-pressure limit (10). Even though it has been shown (11) that at these pressures C_2H_5Cl (in traditional thermal experiments) approaches the high-pressure limit, there is no corresponding verification for activation by SF_6. Also, activation at lower temperatures, where literature values for the accepted Arrhenius parameters are obtained, may be quite different than activation at the higher temperatures here (12). Finally, very low C_2H_4 pressures are formed in these experiments, and standards are difficult to

Figure 7. Relative conversions in the entire cell in Figure 2 as a function of incident laser power:

(a) Ea = 57.4 kcal/mol;

(b) E_a = 65 kcal/mol;

(c) experimental points.

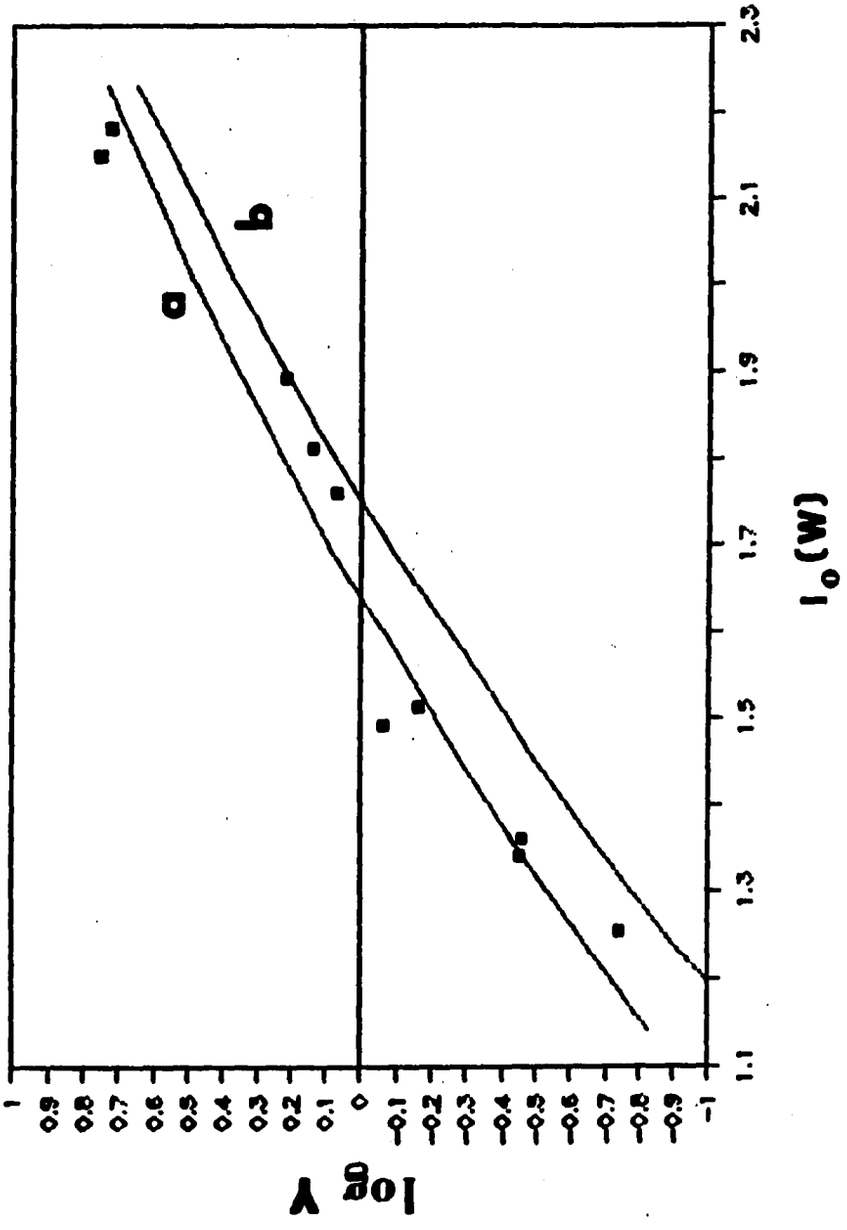
log Y
1
0.9
0.8
0.7
0.6
0.5
0.4
0.3
0.2
0.1
0
-0.1
-0.2
-0.3
-0.4
-0.5
-0.6
-0.7
-0.8
-0.9
-1
1.1
1.3
1.5
1.7
1.9
2.1
2.3
I_o(W)
a
b

prepare and to sample. Because of these uncertainties, only the relative yields for a series of incident laser powers rather than the absolute yields are determined in these studies.

Although the trends in Figure 7 are nonlinear, an objective way to compare these is to use the slopes of linear regression lines through each data set. The experimental data in Figure 7 do not justify fitting to the very slight curvatures of the lines. Since the frequency factor and the activation energy can be considered as independent parameters, as in conventional Arrhenius plots, it is appropriate to assign these to the intercept and the slope of the linear regression lines, respectively. The measured "slopes" for the experimental data, the theoretical results for E_a = 65 kcal/mol, and the theoretical results for E_a = 57.4 kcal/mol are 1.432, 1.617, and 1.433, respectively. One can conclude that the best fit is E_a = 57 ± 2 kcal/mol. The agreement (which must be considered fortuitous) with the literature value (13) of E_a = 57.4 kcal/mol is good, especially since the calculations are essentially absolute. The calculations were again repeated for the absence of the buffer zones. The best fit then becomes E_a = 58.8 kcal/mol. This results from higher temperatures predicted, but still the effect is not a substantial one.

The comparative rate method (5) has been very useful for obtaining rate parameters without knowing the actual temperatures. In shock tubes (5), one essentially has a single uniform temperature. It is easy to see that the derived slopes and intercepts follow rigorously. If the temperature varies as a function of space and/or time, the comparative rate method leads to errors that are determined by the dissimilarity

between the two reactions. The case of having two discrete temperature zones (in space or in time) has been discussed previously (4a). A gas dynamic model allowing for continuous temperature variations has been used to determine Arrhenius parameters for unknown reactions based on an internal standard (3b). It is useful to see how well the comparative rate method in the linear equation form (5) works for a cell with such a large variation in temperatures as here. The theoretical curves in Figure 7 (solid lines) can be used. At each laser power, one can fine the relative rates of the two hypothetical reactions with E_a = 57.4 and 65 kcal/mol. These relative rates can be treated in a log-log plot following comparative rate methods (5). From the slope of that plot, we find that the ratio of the two E_a is 1.118. This is to be compared to the correct ratio of 1.132. The agreement is not bad. Naturally, similar errors will be introduced in the corresponding frequency factors. This shows that even though there is a large variation in local temperatures, only a few zones with the highest temperatures are responsible for most of the reaction yields, so that linear comparative rate methods can be used under these conditions when ΔE_a is small. In other words, the relevant temperature range is actually quite narrow.

The importance of convection under these conditions can be experimentally assessed. From the above, it has already been shown that the transmission of the laser beam provides a sensitive probe for the temperature distributions. We have thus performed parallel transmission measurements at various laser powers for a cell containing 6 Torr of SF_6, once with the cell placed horizontally and once with the cell placed

vertically with the laser beam entering from the top. The former case maximizes convective contributions to heat transfer away from the irradiated central zone, and the latter case minimizes these contributions. From 2- to 9-W input power, we cannot observe any noticeable differences in the transmitted intensities regardless of cell orientation. This confirms that convection can be neglected for the range of conditions used in this study. The fact that the transmitted intensity always reaches a final value after less than 2 s indicates that a steady-state temperature distribution has indeed been achieved for our experiments.

We have developed a reasonable model for temperature distributions in a cell containing an absorber under irradiation by a CW laser beam. Both the transmitted intensity and the yields in a sensitized pyrolysis reaction compare favorably with experiments. The implication is that the reaction pathway parallels that under thermal excitation. Since the main reaction zone is away from the cell walls, surface effects are minimized. At least for the conditions here, that the surfaces are cold (required by the model) is confirmed experimentally. We find that despite the large variation in temperatures, the traditional (linear) comparative rate method should give reliable predictions. In fact, because of the lack of good data on absorptivities at high temperatures, the comparative rate method with an appropriate internal standard is the method of choice for higher excitation powers (required for studying reactions with larger E_a). Apparently, neglecting convection did not lead to serious errors here, but that may have to be considered for faster reactions (depleting reactants

in the high-temperature zone) or for substantially different cell pressures. Finally the high-pressure limit (11) of gas-phase reactions needs to be accounted for to refine similar calculations. For C_2H_5Cl, ref 11 does show that we are at the high-pressure limit, assuming activation by SF_6 is comparable to activation by C_2H_5Cl. The results here admittedly must be used with caution to predict kinetic parameters in the absence of internal standards, but they do offer good insight into the nature of CW laser sensitized gas-phase reactions.

Literature Cited

1. Steinfeld, J. I., Ed. Laser-Induced Chemical Processes; Plenum: New York, 1981.
2. Shaub, W. M.; Bauer, S. H. Int. J. Chem. Kinet. 1975, 7, 509.
3. (a) Tsang, W.; Walker, J. A.; Braun, W. J. Phys. Chem. 1982, 86, 719. (b) Dai, H.-L; Specht, E.; Berman, M. R.; Moore, C. B. J. Chem. Phys. 1982, 77, 4494.
4. (a) McMillen, D. F.; Lewis, K. E.; Smith, G. P.; Golden, D. M. J. Phys. Chem. 1982, 86, 709. (b) Moylan, C. R.; Brauman, J. I. Int. J. Chem. Kinet. 1986, 18, 379. (c) BErman, M. R.; Comita, P. B.; Moore, C. B.; Bergman, R. G. J. Am. Chem. Soc. 1980, 102, 5692. (d) Comita, P. B.; Berman, M. R.; Moore, C. B.; Bergman, R. G. J. Phys. Chem. 1981, 85, 3266.
5. Tsang, W. J. Chem. Phys. 1964, 41, 2487.
6. (a) Gordon, J. P.; Leite, R. C. C.; Moore, R. S.; Porto, S. P. S.;

Whinnery, J. R. J. Appl. Phys. 1965, 36, 3. (b) Stone, J. J. Opt. Soc. Am. 1972, 62, 327. (c) Hu, C.; Whinnery, J. R. Appl. Opt. 1973, 12, 72. (d) Whinnery, J. R. Acc. Chem. Res. 1974, 4, 225.

7. Hirschfelder, J. O.; Curtiss, C. F.; Bird, R. B. Molecular Theory of Gases and Liquids; Wiley: New York, 1954.
8. JANAF Thermochemical Tables, Supplement; National Bureau of Standards, Washington, DC, 1978, 917.
9. Nowak, A. V.; Lyman, J. L. J. Quant. Spectrosc. Radiat. Transfer 1975, 15, 945.
10. Slater, N. B. Proc. R. Sopc. London. A 1953, A218, 224.
11. Howlett, K. E. J. Chem. Soc. 1952, 3695.
12. (a) Hassler, J. C.; Setser, D. W. J. Chem. Phys. 1966, 45, 3246. (b) Dees, K.; Setser, D. W. J. Chem. Phys. 1968, 49, 1193.
13. Robinson, P. J.; Holbrook, K. A. Unimolecular Reactions; Wiley: New York, 1972. This is an average value of two separate reports of 56.5 and 58.4 kcal/mol.

SECTION FIVE:

LASER-INDUCED THERMAL DECOMPOSITION OF TETRALIN AT LOW EXCITATION TEMPERATURE AND LOW CONVERSION

Introduction

The thermal chemistry of tetralin (1) (1) has generated much recent interest because of its role as a hydrogen-donor solvent in coal liquefaction and because, as the simplest hydroaromatic compound, 1 models one of the important structural features of coal (2). The decomposition of tetralin has been studied using a variety of techniques including conventional flash vacuum pyrolysis (FVP) and techniques that utilize a laser, infrared multiphoton dissociation (MPD) and SiF_4 sensitized thermal activation (1,3). The major products that have been reported (1,3) are benzocyclobutene (2), styrene (3), o-allyltoluene (4), indene (5), 1,2-dihydronaphthalene (6), and naphthalene (7).

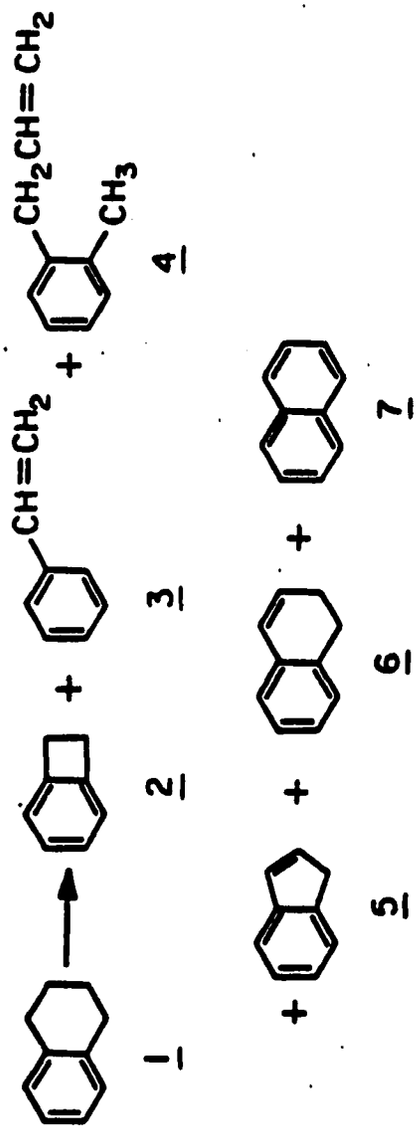
CH2CH=CH2
CH3
CH=CH2
1
2
3
4
5
6
7

It is generally accepted that the loss of ethylene gives rise to 2 and 3 while the loss of hydrogen gives rise to 6 and 7. There is good evidence that the primary products are 2, 4, and 6, and these give rise to secondary products 3, 5, and 7, respectively. While FVP (700-900°C, 0.1 torr) (1i) leads primarily to dehydrogenation, laser-induced decomposition (3) has been reported to result in primarily ethylene loss. The implication is that the FVP results may be influenced by surface catalytic effects. We report here new results, which are at variance with previous work (3), on the laser-induced decomposition of tetralin.

Experimental Section

Apparatus

The experimental arrangements were very similar for the three types of studies: infrared laser multiphoton dissociation, infrared pulsed laser SF_6 (or SiF_4)-sensitized pyrolysis and infrared cw laser SF_6 (or SiF_4)-sensitized pyrolysis. The schematic diagram of the experimental arrangement for the pulsed laser-sensitized pyrolysis is shown in Figure 1. A grating-tuned TEA CO_2 laser (Lumonics, Model 102) was used as the pulsed laser. The laser beam was defined with a 0.8 cm pinhole. The intensity profile was tophat shaped with variations of 30% across the beam. The laser pulse had a 150-ns peak and a 2-μs tail. The unattenuated energy of the laser beam was 0.11 J/pulse at 1027.4 cm^{-1}, and 0.26 J/pulse at 944.2 cm^{-1} and 933.0 cm^{-1}. The pulse-to-pulse variation was ±15% at 1027.4 cm^{-1} and ±5% at the other two lines.

The pulsed laser beam was attenuated by a 10-cm long cell filled with

Figure 1. The schematic diagram of the experimental arrangement for laser induced pyrolysis of tetralin.

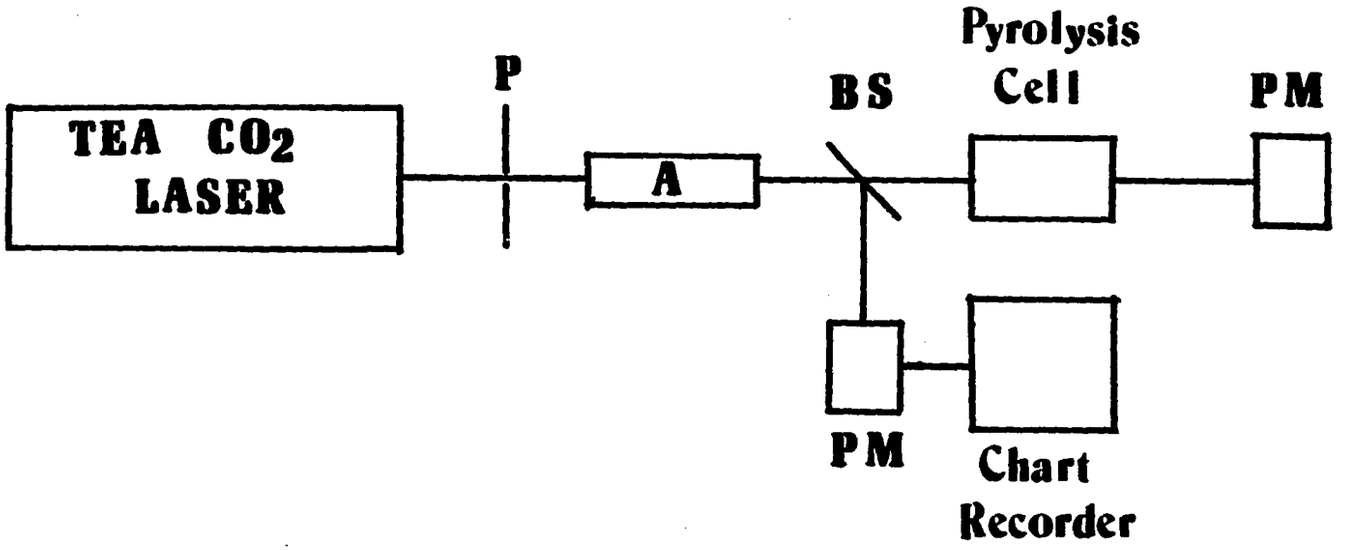
TEA CO_2
LASER
P
A
BS
Pyrolysis
Cell
PM
PM
Chart
Recorder

0-10 torr of SF_6 or SiF_4 depending on the wavelength used. The laser beam was unfocused. Around 10% of the laser energy was directed into a power meter (Laser Precision, Model RJ7200) for monitoring the laser energy continually during the pyrolysis. The incident laser energy (I_0) was measured with no pyrolysis cell in the beam path. For multiphoton excitation, a BaF_2 lens with 6.0 cm focal length was placed before the pyrolysis cell and no pinhole or attenuation cell were used. The laser beam was focused in the center of the pyrolysis cell. The P(20) line at 944.2 cm^{-1} was used with a square beam size of 1.6 cm and an energy of 1.6 J/pulse. The energy density at the focal point has not been evaluated. The pulsed laser was operated at 0.4 Hz for all experiments. Higher repetition rates produce poor pulse-to-pulse reproducibility.

The cw laser-sensitized pyrolysis was performed with a Molectron C250 grating-tuned CO_2 laser. The experimental setup was similar to the pulsed laser sensitized pyrolysis as shown in Figure 1, except that no attenuation cell was used. The laser power was controlled directly by the laser operating current. The laser beam was near Gaussian in profile with power levels stable to ±1% throughout the experiment. The maximum power obtained was 18 W at 933.0 cm^{-1}, 21 W at 944.2 cm^{-1} and 5 W at 1027.4 cm^{-1}. The laser power was measured by a power meter (Coherent, 1 W = 1 mV).

For both pulsed and cw lasers, the wavelength was calibrated by a spectrum analyzer (Optical Engineering). The transmission was about 20-40% in the 3.8 cm long cell with 6.0 torr of SF_6. Higher laser powers resulted in more fraction of the light transmitted. A chart recorder (Fisher 5000) was used to monitor the laser power throughout the

experiment.

Several Pyrex sample cells, fitted with KBr windows at normal incidence, were used as the pyrolysis cell. MPD experiments were carried out in a 10 cm x 2 cm (i.d.), 4 cm x 3.8 cm (i.e.) or 4 cm x 3.5 cm (i.d.) cell. The windows were attached with 5-minute epoxy (Devcon). A 2.8 cm i.d. Pyrex cell with an adjustable length to 1, 2 and 4 cm was used in the study of surface effects. All the cells were fitted with two stopcocks and two O-ring joints: one connected to a sampling glass tube (2 cm x 0.2 cm i.d.) and the other connected to the vacuum line. In the kinetic study with cyclopropane as a chemical thermometer, the sampling tube was 3 cm x 0.7 cm (i.d.) and fitted with a gas-sampling septum.

A dye laser (Spectra Physics, Model 380) pumped by an argon ion laser was used for I_2 excitation at 576.601 nm. The wavelength was monitored by a wavemeter (Burleigh). The I_2 absorption was confirmed by the strong reddish fluorescence from a second (low pressure) I_2 cell which was placed in the laser path during irradiation.

In the experiments involving UV photolysis, HI was excited by an excimer laser (Lambda Physik) at 308 nm. The laser beam was focused with a BaF_2 lens (f.l. = 15 cm). For both HI and I_2 photolysis experiments, the 4 cm x 3.8 cm (i.d.) cell with two quartz windows was used.

Sample Handling

Samples were prepared in a turbomolecular pump (Pfeiffer, TPU 40) vacuum system, with grease-free stopcocks and O-ring joint connections. The base pressure was less than 10^{-6} torr. The pyrolysis cell and the

vacuum manifold were heated by a heat gun to clean the walls under vacuum before the sample was prepared. Pressure was measured by a manometer (MKS 221 AHS-F) with 10 torr f.s.

Tetralin, freshly purified, was stored in a side-arm of the vacuum manifold. Air was evacuated while tetralin was frozen with liquid N_2. The pyrolysis cell was cleaned with HNO_3, water and acetone and the windows were repolished after I_2, HI or deuterium experiments were undertaken.

The sample preparation procedure was the same in both cw and pulse-sensitized pyrolysis. First a sensitizer was expanded into the cell and was frozen into the sample tube. Next, the stopcock to the sample tube was closed and the cell was evacuated. Then tetralin was allowed to expand into the cell until the pressure was 0.325 torr. The sensitizer was then warmed up to expand back to the cell as the stopcock was opened. Five minutes was allowed for equilibration of the gases before irradiation. When an additional gas was required for the sample mixtures, it was usually introduced after the sensitizer and was condensed in the sample tube before tetralin was introduced. For MPD experiments, the cell contains only 0.325 torr tetralin.

The pyrolysis cell was irradiated immediately after sample preparation. The reaction time was 1-2 hours for a pulsed laser experiment and 1-2 minutes for a cw laser experiment. After the reaction, the condensable materials were frozen into the sample tube. Then the sample tube was warmed up in a Dry Ice-1-propanol bath and the sensitizer was evacuated. The tube was then detached from the cell. 50 μl of n-

hexane with biphenyl as an internal standard was added along the wall by a 50 μl syringe (Hamilton). GC analysis was done immediately. The cell mixtures with non-condensable gases were taken to a mass spectrometer for H_2, HD and D_2 analysis in a continuous flow system as needed.

In the kinetic studies, cyclopropane and its products were sampled by a gas-tight 2 ml syringe (Anspec) from a sample tube with a gas sampling septum. This sampling process took place after the products were frozen into and then warmed up to room temperature in the sample tube. After gas sampling, the sample tube was frozen again for tetralin product analysis. The gas sampling septum was changed for each sample.

Analysis

The pyrolysis products of tetralin were analyzed by gas chromatography. A Hewlett Packard 5840 gas chromatograph equipped with a DB-1701 capillary column (J & W Scientific) and a flame ionization detector was used. The oven was programmed at 80°C initially for 10 min, and then the temperature rose by 3°C/min for another 15 min. The over heating rate was changed to 15°C/min until the temperature reached 250°C. All compounds determined were eluted before 25 min and were baseline resolved.

The response factors for 1, 2, 3, 4, 6, 7 and biphenyl were 0.82, 0.57, 0.57, 0.65, 0.76, 0.80 and 1.0. The response factor of o-allyltoluene was assumed to be 0.82 on a weight-to-weight basis. The product peak areas relative to tetralin were calibrated. In most cases, 2 μl was injected by a 10 μl syringe (Hamilton). Results agreed among injections within ±3%.

The reproducibility for an overall experiment including product transfer procedure was checked by 1, and 3 and was within ±5%. All products were identified by GC-MS (Finnegan 4500) with the same GC conditions. The GC retention times of products except 5 were also compared with standards.

Isotopic analysis and I_2 or HI product analysis were made by GC-MS. The non-condensable gas products were analyzed on a Kratos MS50 mass spectrometer. The responses of H_2 and D_2 were almost the same in a H_2:D_2 (1:1) mixture. HD was assumed to produce the same response.

The analysis of cyclopropane products was performed on a Tracor 550 gas chromatograph with a porapak Q column at a constant oven temperature of 40°C. 1.0 ml gas samples were directly injected by a gas-tight syringe with a reproducibility of ±4%. The GC peak area was measured by the cut-and-weigh procedure. The linearity of this method was checked by known amounts of cyclopropane and propylene.

The infrared spectra of 1 and SF_6 were taken by FTIR with 0.3 cm^{-1} resolution. The 4 cm x 3.8 cm (i.d.) cell was used. Both 1 and SF_6 were at the same pressure as in the pyrolysis experiment (1:0.325 torr, SF_6:6 torr).

Materials

Preparation of ammonium tetralin-6-sulfonate. Commercial tetralin was washed with successive portions of concentrated sulfuric acid until the acid layer was no longer colored. Then it was continually washed with water, 10% Na_2CO_3, and water, and was dried with $MgSO_4$. The tetralin was distilled from clean sodium through vigreux column at reduced pressure.

a quantity of 30 ml of concentrated sulfuric acid was added slowly to the pre-purified tetralin (46 ml) with vigorous stirring. The mixture was heated on a steam-bath for 2 hr. and then poured into a water solution (80 ml) of ammonium chloride (24 g). The white solid formed was filtered and recrystallized in a minimum amount of boiling water. The precipitate, ammonium-tetralin-6-sulfonate was washed with small quantities of 50% aqueous ethanol and dried. The yield of ammonium tetralin-6-sulfonate was about 50% (39 g).

Decomposition of ammonium tetralin-6-sulfonate. Ammonium tetralin-6-sulfonate (23 g) was mixed with 27 ml concentrated sulfuric acid and the mixture was steam-distilled in an oil-bath at 165-179°C. The distillate was extracted with ether and the ether layer was washed with 1-% Na_2CO_3 in water. Then the ether layer was dried with $MgSO_4$ and concentrated.

Purification of tetralin. Purification of tetralin was carried out by the method of Bass (1) and followed by column chromatography on alumina (Woelm Activity I, hexanes). The crude tetralin was distilled from clean sodium at reduced pressure and purified by column chromatography on alumina. Analysis of a neat sample by GC showed that the sample was >99.8% pure.

General. o-allyltoluene, indene, styrene, benzocyclobutene, 1,2-dihydronaphthalene, naphthalene and diphenyl were obtained from Aldrich and used without pretreatment. The hexane used as a solvent was HPLC grade.

Gases. All gases used in this experiment were obtained from Matheson Co., Inc.: SiF_4 (99.99%), SF_6 (99.99%), H_2 (99.99%), D_2 (99.5%),

cyclopropane (99.0%), propylene (99.0%) and HI (98%). They were used as received. The purity of cyclopropane was checked by the Tracor GC and about 0.3% of propylene was found. A correction was applied in the calculation of cyclopropane conversion to propylene.

Results and Discussion

Laser-induced pyrolysis

The reaction conditions and analytical procedures (4) were chosen to closely match those reported earlier (3). Three types of studies are reported in Table I: MPD, SiF_4- or SF_6-sensitized thermal activation by cw IR laser excitation, and SiF_4- or SF_6-sensitized thermal activation by pulsed IR laser excitation. For MPD (5), it is clear that ethylene loss (2 and 3) is the major reaction channel (A and B in Table I). It is difficult to compare the fluence of these MPD experiments (6) with previous work, but considering the beam properties and the optical arrangements, we conclude they are quite comparable. Even though we find less of 5 and more of 6 than previous work (3), the conclusion that ethylene loss is the main decomposition channel in MPD is confirmed.

Tetralin decomposition sensitized by SiF_4 or SF_6 based on cw IR laser excitation has not been reported previously. A major consideration is that one can control the power levels and the power densities much more reliably than with the corresponding pulsed lasers (7). One expects to find a steady-state temperature gradient starting at a high level at the center of the laser beam (due to cumulative absorption), dropping quickly

outside the irradiated region, and eventually equilibrating with the cell walls along a slower temperature gradient (8). In our experiments, no part of the cell felt warm to touch even at the highest powers used, so that reactions on hot surfaces can be neglected. No decomposition products were found when the reaction mixture was left in the cell for 28 hours without laser irradiation.

To assess the contributions of surface reactions to the overall decomposition process, we studied the dependence of the absolute yields of products on the size and shape of the sample cell at a fixed input laser power of 9 W. Under these conditions, the major reaction products are 6 and 7. For cylindrical cells of length (cm) x diameter (cm) of 4x3.8, 4x2.8, 2x2.8 and 1x2.8, the measured formation rates (10^{-12} mole s^{-1}) for 6 + 7 are 121, 52, 1.9, and 0.21, respectively. The KBr windows in every case should contribute roughly the same amount of surface reactions since the contact areas as well as the distances from the hot gas column are comparable. In fact, since less depletion of laser light and less area for thermal conduction exist in the smallest cell, surface temperatures at the windows there should be the highest. The fact that the decomposition rates decrease substantially in this series of experiments indicate that surface reactions at the cell windows cannot be important in the cw laser-induced decomposition. As for the pyrex cell walls, the first two absolute yields show a decrease that is better explained by the decrease in the volume of gas heated (3.8^2:2.8^2) than by the decrease in available surface area (3.8:2.8). The pyrex surface area decreased by a factor of 4 in the last 3 cells but the yields decreased by a factor of 360. It has

been shown (8) that smaller cells provide shorter distances for heat conduction from the center of the cell to the cell walls. Since the cell walls are at room temperature, this implies that the heated gas column has a lower temperature in smaller cells for the same incident laser power. This then accounts for the dramatic decrease in absolute rates in this series of experiments. One can therefore conclude that neither the pyrex cell walls nor the KBr windows contribute to the dehydrogenation of tetralin via surface reactions.

The results of cw laser-induced thermal decomposition is shown in Table I, C-E. Invariably, the major products (6,7) are associated with dehydrogenation. The difference in absorption coefficients for SiF_4 and SF_6 accounts for the reaction times needed to achieve similar conversions. When the reaction yields are high, substantial conversion to secondary products (3,7) occurred as expected. The two studies involving SF_6 show that energy density, and not just total energy deposited, is important to the extent of reaction, as has been pointed out previously (3) in the concept of a maximum temperature. The long duration needed for the SiF_4 reaction also rules out the contribution of window heating (hot surface catalysis) in the decomposition of tetralin. These results, plus the fact that no fluorinated hydrocarbons were found in GC-MS analysis, show that the sensitizer only acts as a heat-transfer agent in tetralin decomposition.

For pulsed laser excitation (sensitized), a representative selection of results is shown in Table I, F-I. Regardless of the sensitizer, at low excitation energies and at low conversions dehydrogenation is the dominant

channel. This is in line with the cw laser results. At higher pulse energies, contributions from dehydrogenation and ethylene loss channels then become comparable. The pulse energies for SF_6-sensitization and for SiF_4-sensitization cannot be compared directly, since absorption coefficients are quite different. For experiments H and I, the cell lengths are different, but the surface area to volume ratios are similar. So, the results cannot be explained on the basis of surface-catalyzed reactions. Other experiments not shown also confirm that the change in cell length from 10 cm to 5 cm does not influence the product distributions. Rather, the difference in laser powers is responsible for the results in H and I. Even though 0.11 J does not seem too different from 0.09 J, our laser shows large pulse-to-pulse variations at the maximum output range. With the average energy per pulse of 0.11 J there, individual pulses as high as 0.15 J are actually present throughout the experiment. It is the pulses with the highest power that dominate the pyrolysis process, since yields are exponentially dependent on temperature. Unfortunately, we were not able to obtain still higher output levels from our laser at the SiF_4 wavelength to observe a clear-cut cross-over of the two reaction channels.

Both the cw and the pulsed sensitized reactions are in disagreement with previous results (3), which show the ethylene loss (2 and 3) is the main decomposition channel. The fact that our MPD results agree with previous work (3) indicates that tetralin purity, analytical procedures, and nonhomogeneous reactions cannot account for the discrepancies in the pulsed-laser sensitized experiments.

Activation energies

To resolve these apparent inconsistencies, we determined the Arrhenius parameters for the two decomposition channels over the range of 5-10 W input laser power (6 torr SF_6, P(20), 2.6 mm beam, 4 cm x 3.8 cm cell) using as an internal thermometer (9) the isomerization reaction cyclopropane to propylene (E_a = 65 kcal/mol, log A (s^{-1}) = 15.2). The comparative rate method for cw sensitized pyrolysis has been discussed earlier (8). For dehydrogenation (6 + 7), from the log-log plot of conversions (9), the slope gives E_a = 72 ± 3 kcal/mole and the intercept gives log A (s^{-1}) = 15.2 ± 0.5 (10). A separate series of runs was made without cyclopropane over the same range of laser powers but over longer times to allow better determination of the rates for the ethylene loss channel (2 + 3). The dehydrogenation channel (6 + 7) was used there as the internal thermometer. The results are shown in Figure 2. In this way, we found for ethylene loss E_a = 79 ± 3 kcal/mole and log A (s^{-1}) = 16.8 ± 0.5. The Arrhenius parameters do not suggest the presence of any unusual reaction mechanisms.

As with all comparative rate methods, the absolute values of the Arrhenius parameters are subject to various systematic errors (10). The relative values between the dehydrogenation channel and the ethylene-loss channel should however be quite reliable. These relative values allow one to determine the trend of the competition between the two channels as a function of temperature with confidence, in contrast to simply plotting the relative yields versus the laser powers used. Figure 2 shows a linear

Figure 2. Comparative rate plot of the ethylene loss (2 + 3) vs. the dehydrogenation (6 + 7) channels in tetralin.

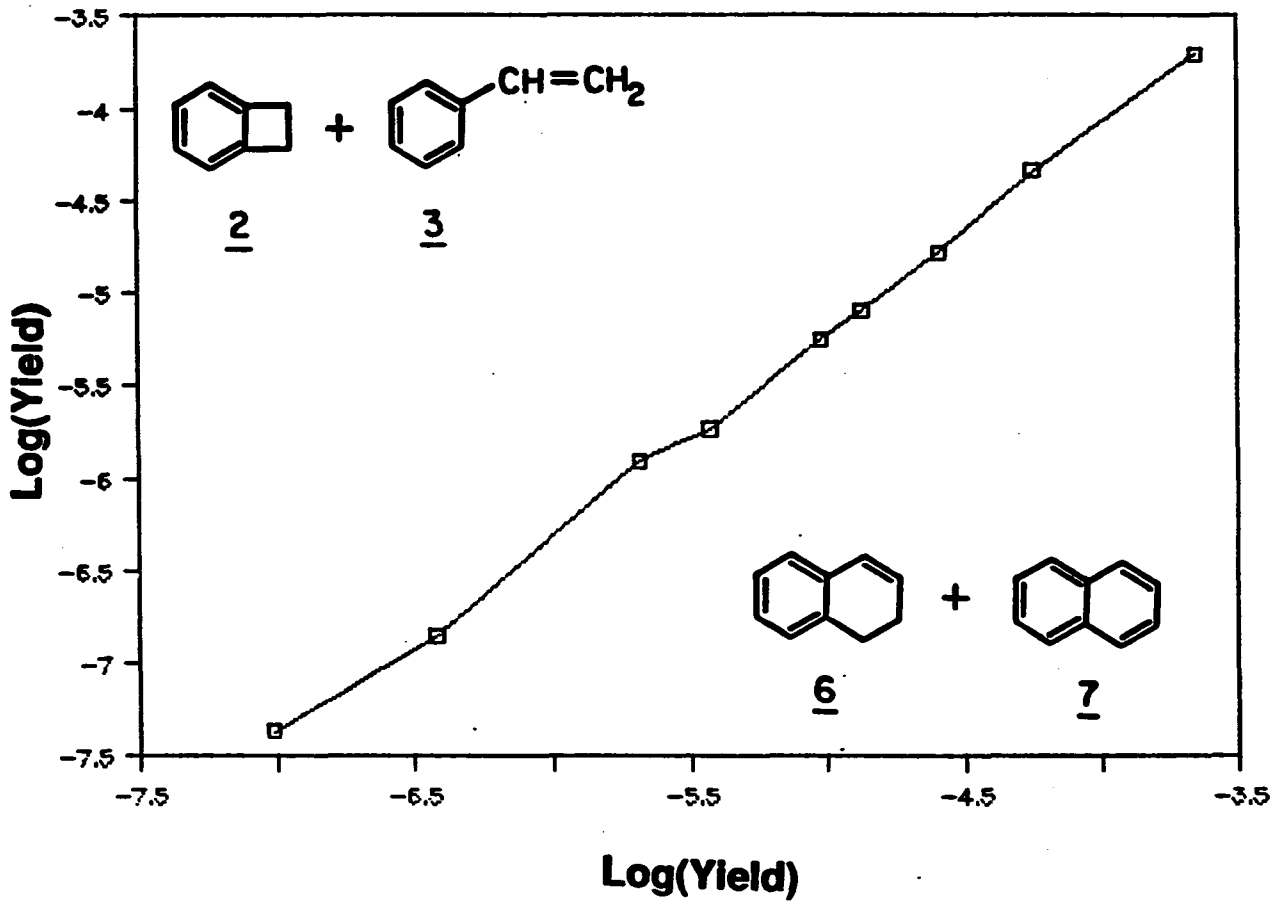
-3.5
-4
-4.5
-5
-5.5
-6
-6.5
-7
-7.5
Log(Yield)
CH=CH2
2
3
6
7
-7.5
-6.5
-5.5
-4.5
-3.5
Log(Yield)

plot with a correlation coefficient of $r^2 = 0.998$, with the uncertainties increasing at low yields due to increased errors in product quantitation. One can predict from these Arrhenius parameters a cross-over temperature for the two decomposition channels of 1000 °K. The implication is that the pulsed sensitized reactions reported earlier (3) are actually performed at an effective temperature higher than either the pulsed or the cw experiments reported here. Since the sensitizer is excited to high vibrational levels following multiphoton absorption (pulsed experiments), and since V → V energy transfer to the reactant is highly favored (compared to V → T), the calculated maximum temperature (9b) for pulsed experiments does not adequately describe the non-Boltzmann excitation of the reactants.

Reaction kinetics

Although the analysis of reaction kinetics often does not lead to an unambiguous determination of reaction mechanisms, it is still useful as a check for consistency. We have studied the yields of the dehydrogenation channel (6 + 7), under conditions where these are the major decomposition products, over the range of 0.35 torr to 0.10 torr tetralin (1). The upper limit is determined by the room-temperature vapor pressure of tetralin and the lower limit is determined by the amount of products needed for accurate quantitation. The total conversion is kept below 1% to reduce secondary effects, and the laser power and the reaction period are kept constant to avoid correction terms. We found that the reaction rate is first order with respect to tetralin concentration.

If the loss of hydrogen from tetralin is via concerted molecular dissociation or stepwise (non-chain) loss of hydrogen atoms, the kinetics must necessarily be first order with respect to tetralin concentration. If the loss of hydrogen is aided by radical chains, the reaction kinetics is more complicated. Let us consider the many possible elementary reactions involved. For clarity, we shall abbreviate tetralin (1) as AH_2. So, A is dihydronaphthalene (6) and AH is the radical intermediate.

$$AH_2 \rightarrow AH + H \quad (1)$$

$$H + AH_2 \rightarrow AH + H_2 \quad (2)$$

$$H + AH_2 \rightarrow AH + H + H \quad (3)$$

$$AH \rightarrow A + H \quad (4)$$

$$H + AH \rightarrow AH_2 \quad (5)$$

$$H + AH \rightarrow A + H_2 \quad (6)$$

$$H + H\ (+ M) \rightarrow H_2 \quad (7)$$

The initial loss of a H atom, reaction (1), must be common to all radical reaction schemes. If reaction (3) is important in the net production of A, then reaction (7) must also be involved for mass balance. For chain propagation in the combination (1), (3), (4), and (7), the rate of production of A is second order with respect to $[AH_2]$, which is inconsistent with the experimental observations. The apparent activation energy (11) for that chain process is given by $E_a = (2E_3 - E_7)$, which is too low compared to the observed value of 72 kcal/mol. Furthermore, at these total pressures and these concentrations, reaction (7) is highly unlikely to be important. Also, reaction (3) is likely to have a higher activation energy than reaction (2) and is thus less probable. A similar

conclusion is reached if one considers the combination (1), (2), (4), and (7), where chain propagation results in a rate of production of A that is 3/2 order with respect to $[AH_2]$ and an apparent activation energy of $E_a = (E_2 + \frac{1}{2}E_1 - \frac{1}{2}E_7) \approx \frac{1}{2}E_1$, which is too low compared to the observed value of 72 kcal/mol.

Other possible chain processes involve either reactions (1), (2), (4), and (5) or (1), (2), (4), and (6). Either scheme gives a rate of production of A that is first order with respect to $[AH_2]$. In the former case, one has an apparent activation energy $E_a = \frac{1}{2}(E_1 + E_2 + E_4 - E_5)$. In the latter case, $E_a = \frac{1}{2}(E_1 + E_2 + E_4 - E_6)$. We estimate that the upper limits for E_1 and E_4 are 81.6 and 49.1 kcal/mol respectively. Also, $(E_2 - E_5)$ and $(E_2 - E_6)$ should both be close to zero. So these schemes give an upper estimate of the apparent activation energy of 65 kcal/mol. Even though (as discussed above) the absolute value of the activation energy determined here for hydrogen loss has large uncertainties, it was measured relative to that for cyclopropane isomerization ($E_a = 65$ kcal/mol). The fact that the experimental value is found to be significantly larger than 65 kcal/mol is thus inconsistent with the upper limit indicated by the above kinetic analysis. Obviously, we have assumed that activation of cyclopropane and tetralin by SF_6 is similar. So, kinetic analysis gives additional evidence against, but cannot rule out the participation of chain propagation in the production of A.

Radical chains

The observation of an excess of dehydrogenation products (6 + 7) over ethylene-loss products (2 + 3) in itself cannot confirm that the former is the dissociation channel with the lower energy barrier. It is possible that dehydrogenation products are formed as a result of radical chains, which magnify the contributions from that channel. We have already shown above that surface-catalyzed reactions are not important in the production of 6 + 7. The isotopic studies indicate that hydrogen atoms are formed during pyrolysis. Presumably these can cycle (by reaction with tetralin) to produce more dehydrogenation products. However, it is not clear why such chains should be more important here than in previous work (3). In pulsed laser experiments, the hot zone quickly expands and is cooled by the surrounding gas to quench long chain processes. In cw laser experiments, gases in the heated zone migrate outwards and are also cooled by the surrounding gas. Although the temperature profiles are different in the two cases, the time periods involved for migration from the heated zone to the cold walls are quite similar.

We studied the effect of potential chain terminators on the cw pyrolysis of 1. If in the presence of known chain terminators the contribution of the dehydrogenation channel decreases, one can conclude that radical chains are important in the overall reaction. However, if known chain terminators do not affect the pyrolysis yields, one cannot conclude that radical chains are unimportant. Unfavorable competition for the radical intermediates may have been responsible for the negative results. Table II shows sets of experiments involving the addition of

potential chain terminators. Ideally, the species added should be in large excess. However, there is a secondary effect that the maximum temperature may change due to the change in the effective thermal conductivity of the gas (8). One also has to maintain a low total conversion to avoid secondary reactions. At the second time, enough products must be formed to allow reliable product analysis.

Table II A, B show that the addition of toluene as a potential chain terminator (9b) to the pyrolysis mixture did not alter the fraction of dehydrogenation products. There is a noticeable decrease in the total conversion. That observation is consistent with a decrease in temperature of the heated gas due to the higher thermal conductivity of toluene. This is confirmed independently by the fact that there is a simultaneous decrease in the transmission through the cell (8).

HI was used as a potential chain terminator in the pyrolysis reaction. The relevant reaction is $H + HI \rightarrow H_2 + I$. Table II C, D show that the addition of HI decreases the total conversion slightly, presumably due to a decrease in reaction temperature. The relative contributions of the two channels, however, remain similar to A. We found also that deposits of I_2 are visible on the cell walls after these pyrolysis experiments, showing that HI does participate somehow. On the other hand, laser excitation of a mixture of HI and SF_6 alone did not produce any observable I_2 deposits under similar conditions. So, the uptake of H by HI did not affect the dehydrogenation channel.

I_2 was then used as a potential chain terminator. The relevant reaction is $H + I_2 \rightarrow HI + I$. This also serves as a check that the I_2

produced in the HI experiments above did not bias the results. Table II A and E show that the absolute yield for ethylene loss did not change but the absolute yield for dehydrogenation increased markedly. This is contrary to what one expects if hydrogen atoms are assisting in the dissociation of 1. Rather, the increase in dehydrogenation yield is consistent with either I-atom initiated dissociation ($I + AH_2 \rightarrow AH + HI$) or competition with the reverse reaction $AH + H \rightarrow AH_2$ ($I_2 + H \rightarrow HI + I$ or $I + AH \rightarrow HI + A$). The direct production of I atoms at room temperature by laser photolysis (45 mW, 576.601 nm, 20 min) of I_2[14] did not produce any dissociation in 1. This is not unexpected since there should exist a reasonable energy barrier for the reaction $I + AH_2$.

We also studied the effect of potential chain assisted dissociation of 1. H atoms can be produced either by room temperature laser photolysis or by cw laser-sensitized reaction at high temperatures. Photolysis of HI at 308 nm produces visible deposits of I_2 on the cell walls, indicating dissociation of HI to generate H atoms. To confirm that one can in fact initiate radical chains this way at room temperature, we studied the H-atom assisted dissociation of ethane and propylene. These involve well known H-atom chain mechanisms (15). Table III shows the result of irradiation of the two hydrocarbons in the presence of HI at 308 nm. The results indicate that the normal (thermal) dissociation products are formed via H-atom chain propagation under these conditions. A mixture of 1 (0.325 torr), SF_6 (6.0 torr) and HI (3.7 torr) was then irradiated by the same laser (308 nm, 147 mJ/pulse, 3000 pulses) in the gas cell used in the laser-sensitized experiments after installing quartz windows. Only

four product peaks were found by GC-MS analysis, giving total conversion of 1.4% of 1. These have masses of 134 (30%), 136 (10%), 136 (10%) and 138 (50%), respectively. These are clearly hydrogen addition products of 1, presumably hexalin, combinations of octalin, and decalin. One can conclude that the reaction between H atoms and 1 is one of addition rather than abstraction. Even though these results are for room temperature reaction, one expects addition to dominate also at high temperatures. This is because the pre-exponential factors for abstraction and for addition should be similar (both are biomolecular processes). A reversal in the relative importance of the two processes is not likely.

We have also studied the reaction between H atoms and 1 at elevated temperatures. Hexamethylethane decomposes thermally to produce H atoms as an intermediate (16). When a mixture of hexamethylethane (2.0 torr) and SF_6 (6.0 torr) was irradiated by a cw laser (944.2 cm^{-1}, 5.0 W, 180 s), isobutene (6.5%) was found as a product, indicating that H atoms were actually produced. Under the identical conditions, only a trace of 6 was found in the product analysis for the sensitized pyrolysis of 1. When hexamethylethane (2.0 torr) was copyrolyzed with 1 (0.30 torr) under these conditions, hexalin (mass = 134) was the primary product (1.1%). Again only a trace of 6 was found. This confirms that addition rather than abstraction is the main reaction pathway between H atoms and 1.

Related reactions

The cw laser-sensitized decomposition of cyclohexane was studied. When cyclohexane (0.3 torr) and Sf_6 (6.0 torr) were irradiated by the same cw

laser (944.2 cm^{-1}, 45 W, 30 min.), the total conversion was 65%. The four products formed are ethylene (60%), butadiene (14%), cyclobutane (18%) and cyclohexene (9%). The first three products are from the ethylene loss channel and secondary reactions (83% of each mole of cyclohexane dissociated) and the last one is from dehydrogenation (17% of each mole of cyclohexane dissociated). When cyclohexene (0.3 torr) was pyrolysis with SF_6 (6.0 torr) for 15 min., the total conversion was 82%. The three products are ethylene (84%), butadiene (0.7%), and cyclobutane (15%). So, in fact there is a substantial contribution from the dehydrogenation channel (>>17%) in the pyrolysis of cyclohexane. Electronic effects in 1 should make dehydrogenation even easier when compared to cyclohexane. In other words, the importance of dehydrogenation in the pyrolysis of 1 is not surprising based on these results.

We also studied the cw laser-sensitized pyrolysis of cyclodecane. The results are shown in Table IV, together with a parallel study using flash-vacuum pyrolysis . The six major product peaks are identified by the masses of the molecular ions. Mass 140 results from the breaking of a C-C bond to form decene. The location of the double bond formed causes the separation into 3 GC peaks. Clearly the breaking of a C-C bond is more favorable here than the breaking of a C-H bond, which leads to the two mass 138 peaks. Unlike 1 or cyclohexane, no ethylene loss products are found. Mass 247 is probably a result of condensation of the intermediates. One can rule out concerted ethylene loss from cyclohexane. Apparently, after the first C-C bond is broken, there is enough stabilization to prevent further dissociation to produce ethylene. It is

noteworthy that the dehydrogenation products are not the dominant ones here. If H atom chain propagation were important in the dissociation of 1 or of cyclohexane, it would also have been a major contributor in cyclodecane pyrolysis. So, our cw sensitized experiments do not seem to particularly favor radical chain reactions. It is also interesting that FVP gives similar product distributions as the laser experiments. This strengthens the thesis that cw laser-sensitized pyrolysis mimics traditional thermal activation. Since surface effects are unimportant in the laser experiments, vide supra, the similarity in products produced also argues for the lack of surface effects in FVP.

It is also useful to investigate the FVP of 1 at low pressures and short contact times. These are conditions which should eliminate the contributions from any radical chain reactions. The results are summarized in Table IV. Clearly dehydrogenation is still the major decomposition pathway. We can conclude that the dominance of dehydrogenation products cannot be attributed to radical (H atom) chain propagation.

Another important reaction investigated is the pyrolysis of 2-benzocyclohepenone which produces the same diradical intermediate as that produced by tetralin. The results should show the low energy channel of this intermediate. The yields of these products at various FVP temperatures and the laser-induced pyrolysis are given in table VI.

The following scheme accounts for the products 2, 3, 4, 7. Notice that as the FVP temperature is lowered, more 6 relative to 7 is obtained which is consistent with the conversion of 6 to 7 as a secondary reaction. As

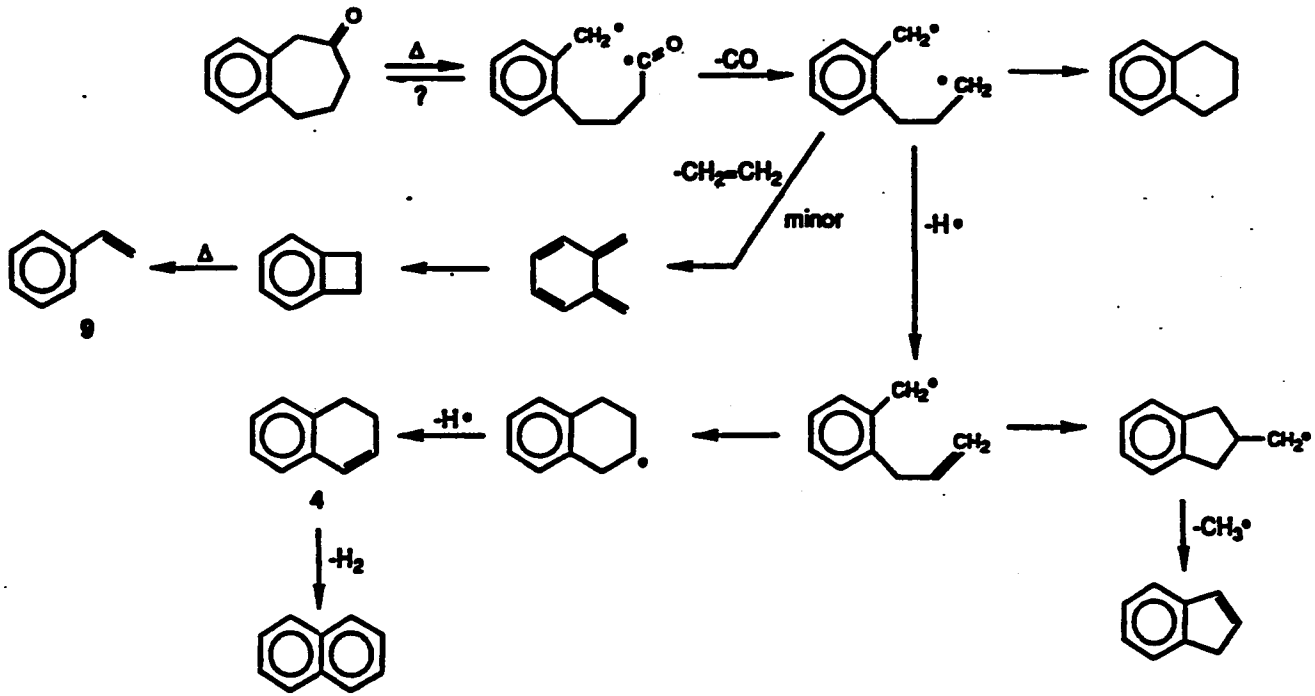
Δ
?
-CO
-CH₂=CH₂
minor
-H•
Δ
-H•
-H₂
-CH₃•
9
4

the temperature is raised, there is more 2 relative to 1, 4, 6, and 7 and the ratio of 3 to 2 increases. The laser-induced reaction shows the similar results.

This is consistent with the loss of ethylene being a higher energy pathway and with styrene being a secondary product.

Isotopic studies

Deuterium labeling can provide additional insight into the mechanism of cw laser sensitized dehydrogenation. Two types of studies were performed. In all cases, the laser power and the total conversion were kept low to avoid secondary effects. Under these conditions, dehydrogenation was the main reaction channel. First, the deuterium distribution in 6 was determined for the pyrolysis of 1,1,3,3-d_4-tetralin. The relative amounts of d_0, d_1, d_2, d_3, and d_4 in 6 were found to be 2.0%, 0.8%, 10.9%, 80.2%, and 6.2% respectively. These distributions are comparable to those obtained in pulsed laser-sensitized pyrolysis. They indicate that dehydrogenation is primarily via 1,2 elimination. However, contributions from the loss of hydrogen from other positions cannot be ruled out. Second, the deuterium distribution in the hydrogen gas formed during the pyrolysis of 1:1 mixtures of h_{12} and d_{12} (liquid) tetralin was measured. The relative amounts of H_2, HD, and D_2 found were found to be 53:35:12 at a laser power of 8.6 W and a 3 min. irradiation time. These results are consistent with those reported earlier. A significant amount of the hydrogen is formed via intermolecular pathways. This indicates that concerted molecular elimination is not the major pathway for the

dissociation of tetralin. It is however not possible to conclude whether the loss of hydrogen from tetralin involves intermolecular processes (e.g. abstraction) or whether isotopic scrambling occurs after decomposition.

Our deuterium labeling results indicate that 1,2-elimination is the primary mode (ca. 80%) of dehydrogenation but that ca. 10% 1,4- and ca. 10% 2,3-elimination are also involved and that these eliminations take place by a combination of 20% concerted and 80% stepwise loss. The previous workers also studied the decomposition of cis-1,2-diprotio-tetralin-d_{10} and concluded that results from this compound are also consistent with a combination of 20% concerted and 80% stepwise elimination. Thus, all of these results indicate that the primary mode of hydrogen loss is stepwise but that there is also significant loss of molecular hydrogen by concerted pathways. Because the temperature of these experiments is uncertain, it is possible that at lower effective temperatures, the amount of concerted elimination would be even more important.

From study of the thermal decomposition of 3,3,6,6-tetradeuteriocyclohexene (8) at ca. 500°C (12), it is concluded there are four primary unimolecular processes: the retro Diels-Alder reaction (ca. 95%), D_2 (a 1,4) elimination (ca. 5%), HD (a 1,2) elimination (<0.5%), and H_2 (a 1,2) elimination (<0.5%). The activation energies for these processes are given over the arrows.

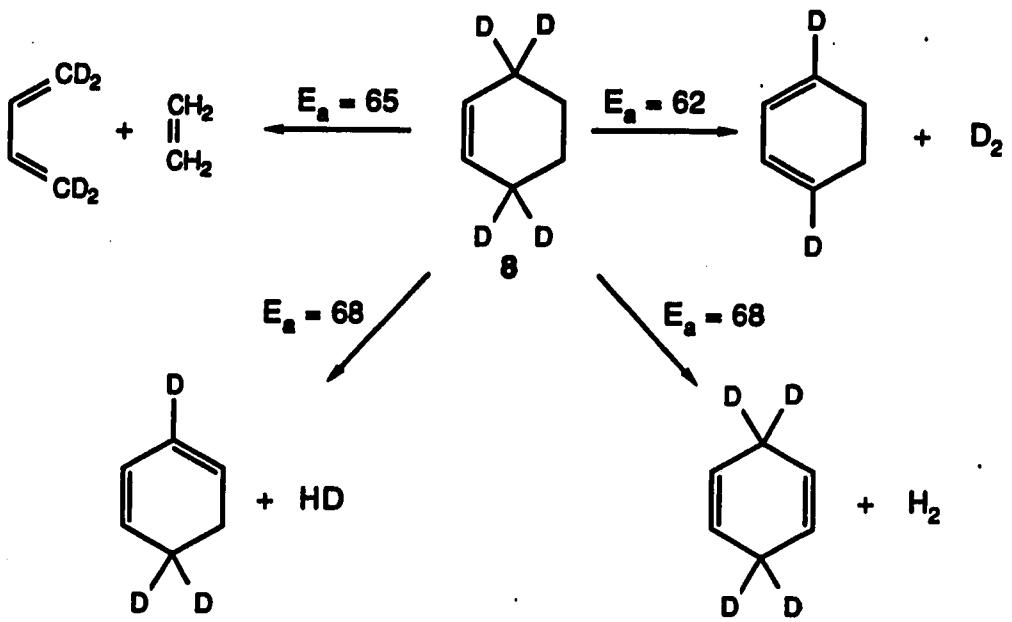
CD2
CD2
+
CH2
CH2
Ea = 65
D
D
D
D
8
Ea = 62
D
D
+ D2
Ea = 68
D
D
D
+ HD
Ea = 68
D
D
D
D
+ H2

Although the reliability of the activation energies for the two minor pathways is questionable because so little of the decomposition occurs by these reactions and the analysis is complicated by secondary processes, the results do provide some evidence for the concerted 1,2-elimination of molecular hydrogen.

Additional support for the 1,2-elimination of molecular hydrogen has also been obtained from a study of the thermal decomposition of 4-deuteriocyclopentene (9) at 550°C (13).

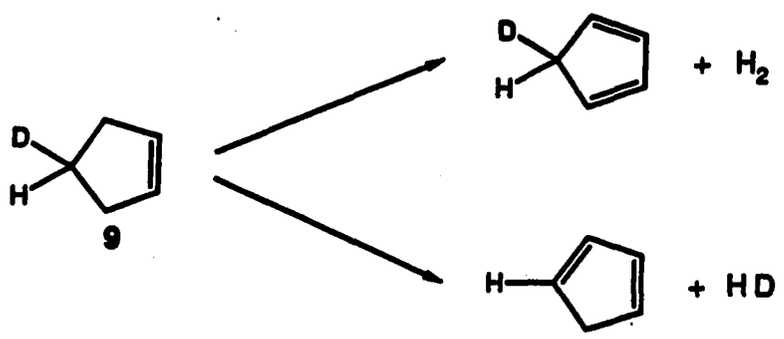

It is concluded that the ratio of 1,4- to 1,2-elimination is 12:1.

The expected activation energies for the retro Diels-Alder reaction and the 1,4-loss of hydrogen should be greater for tetralin than for cyclohexene because these reactions disrupt the aromaticity of the benzene ring. Comparison of model reactions shows that the tetralin transition state should be 8 kcal/mol higher than the corresponding cyclohexene transition states to account for the loss of benzene resonance energies (3). However, the activation energies for the 1,2-eliminations should be

comparable for cyclohexene and tetralin since these reactions do not disrupt the benzene ring of tetralin. This analysis suggests that for tetralin the concerted 1,2-elimination of hydrogen should be competitive with 1,4-elimination of hydrogen and the elimination of ethylene by a retro Diels-Alder reaction.

Our observed values for the activation energies for loss of ethylene, 79 kcal/mol, and dehydrogenation, 72 kcal/mol, are similar to those calculated from the cyclohexene values, 73 (65 + 8) kcal/mol and 68 kcal/mol (the 1,2-elimination value), respectively. However, the experiments indicate that stepwise elimination is the primary pathway. The activation energy for loss of a benzylic hydrogen atom should be 80-85 kcal/mol and although this value would allow the stepwise loss of hydrogen to be significant in the 1000 °K range, it would not be expected to be the primary mode of dehydrogenation if reasonable A factors are used for the different channels.

Previous workers have estimated that the activation energy for the loss of ethylene should be 75 kcal/mol for a concerted process but only ca. 67 kcal/mol for a stepwise process. However, on the basis of products from substituted tetralins, it was concluded that the retro Diels-Alder reaction is concerted, not stepwise (1i), and this conclusion appears to be consistent with the results of the present study. Possibly the estimate of E_a = 67 kcal/mol for the stepwise process is several kcal/mol too low due to unaccounted for conformational effects in the fragmentation reaction.

Although there are still unexplained facets of the laser-induced

decomposition of tetralin, the present study strongly supports dehydrogenation as the lowest energy channel, a result consistent with the numerous studies of the pyrolysis of tetralin using conventional techniques. A consequence of this agreement is that it is not necessary to invoke surface-catalyzed reactions to explain the FVP results.

The discrepancies between the previous laser-induced decomposition study (3) and the present study and the unanswered questions of the present study show how difficult and tricky these laser studies are. On the other hand, the results of the present study reduce the concern that surface-catalyzed reactions are dominant under FVP conditions and thus reestablishes FVP as an attractive technique for studying the true thermal reactions of organic compounds.

Literature Cited

1. (a) Franz, J. A., Camaioni, D. M. J. Org. Chem., 1980, 45, 5247; (b) Benjamin, B. M., Hagaman, E. W., Raaen, V. F., and Collins, C. J. Fuel, 1979, 58, 386; (c) Hooper, R. J., Battaerd, H. A. J., and Evans, D. G. ibid., 1979, 58, 132; (d) Bredael, P., and Vinh, T. H. ibid., 1979, 58, 211; (e) Tominaga, H., and Tahagi, V. J. Fac. Eng. Univ. Tokyo Ser. A, 1977, 15, 68; (f) Loudon, A. G., Maccoll, A., and Wong, S. K. J. Chem. Soc. B., 1970, 1733; (g) Badger, G. M., Kimber, R. W. L., Novotny, J. Aust. J. Chem., 1962, 15, 616; (h) Gangwer, T., MacKenzie, D., and Casano, S. J. Phys. Chem., 1979, 83, 2013; (i) Trahanovsky, W. S., and Swenson, K. E. J. Org. Chem., 1981, 46, 2984.

2. Whitehurst, D. D. "Organic Chemistry of Coal," J. W. Larson, Ed., ACS Symposium Series 71, American Chemical Society, Washington, 1978, pp. 1.

3. (a) Berman, M. R., Comita, P. B., Moore, C. B., and Bergman, R. G. J. Am. Chem. Soc., 1980, 102, 5692; (b) Comita, P. B., Berman, M. R., Moore, C. B., and Bergman, R. G. J. Phys. Chem., 1981, 85, 3266.

4. Several pyrex sample cells, fitted with KBr windows at normal incidence are used. The cells were pumped to $<10^{-5}$ torr on a grease-free vacuum line and was filled to 0.325 torr of 1 for all experiments. All gas pressures were measured with a capacitance manometer. After photolysis, the products are condensed in a side-arm with liquid N_2, warmed to dry-ice temperature and pumped to remove the sensitizer, and dissolved in hexane for analysis.

5. (a) Rosenfield, R. N., Brauman, J. I., Barker, J. R., and Golden, D. M. J. Am. Chem. Soc., 1977, 99, 8063; (b) Danen, W. C., Koster, D. F., and Zitter, R. N. Ibid., 1979, 101, 4281; (c) Reiser, C. Lussier, F. M., Jensen, C., and Steinfield, J. I. Ibid., 1979, 101, 350; Golden, D. M., Rossi, M. J., Baldwin, A. C., and Barker, J. R. Acc. Chem. Res., 1981, 14, 56.

6. The intensity profile here is tophat shape with variations of 30% across the beam, compared to a near Gaussian beam in previous work. A 6-cm f.l. BaF_2 lens is used here while a 15-cm f.l. NaCl lens was used previously. The laser pulse here had a 150-ns peak and a 2-μs tail, compared to a 100-ns peak and 1-μs tail in previous work.

7. The cw beam is near Gaussian in profile with power levels stable to $\pm$1%

throughout the experiment, compared to ±5% pulse-to-pulse variations in the P(20) CO_2 line (MPD and SF_6 sensitization) and ±15% pulse-to-pulse variations in the P(40) CO_2 line (SiF_4 sensitization).

8. Zhu, J., and Yeung, E. S. J. Phys. Chem.. Int. J. Chem. Kinetics, 1975, 7, 509; (b) Dai, H. L., Specht, E., Berman, M. R., and Moore, C. B. J. Chem. Phys., 1982, 77, 4494; (c) McMillen, D. F., Lewis, K. E., Smith, G. P., and Golden, D. M. J. Phys. Chem., 1982, 86, 709.

10. The possible sources of error include uncertainties in the exact temperature profile in the cell, dissimilarity in Arrehenius parameters between the internal standard tetralin, and deviations from the high pressure limit.

11. Laidler, K. J., "Chemical Kinetics," 2nd Ed., McGraw-Hill, New York, 1965, p. 388.

12. Tardy, D. C., Ireton, R., and Gordon, A. S. J. Am. Chem. Soc., 1979, 101, 1508.

13. Baldwin, J. E. Tetrahedron Lett., 1966, 2953.

14. Yappert, M. C., and Yeung, E. S. J. Am. Chem. Soc., 1986, 108, 7529.

15. Rice, F. O., and Herzfeld, K. J. Am. Chem. Soc., 1934, 56, 284.

Table I. Product distribution of decomposition of 1

Conditions	Products, %							% Conversion of 1
	2	3	4	5	6	7	Others	
A. multiphoton excitation, 1.6 J/pulse, 950 pulses[c]	54.1[a,b]	11.0	0	0	25.1	4.4	5.4	1.3
B. multiphoton excitation, 1.6 J/pulse, 2812 pulses[c]	48.2	9.0	7.5	0	26.0	8.9	0.4	2.3
C. cw laser excitation, 6 torr SiF_4 sensitized, 5.0 W, 12 hours[d]	trace	0	0	0	100	trace	0	2.1
D. cw laser excitation 6 torr, SF_6 sensitized, 6.6 W, 5 min.[d]	14.7	0	0	0	70.6	14.6	0.1	1.1
E. cw laser excitation, 6 torr, SF_6 sensitized, 14.5 W, 1 min.[d]	1.8	31.9	7.6	0.5	3.1	55.5	0	58.2
F. pulsed excitation, 3 torr SF_6 sensitized, 0.04 J/pulse, 3420 pulses[d]	0	0	0	0	75.8	24.2	0	0.09
G. pulsed excitation, 3 torr SF_6 sensitized, 0.26 J/pulse, 5 pulses[d]	14.9	24.5	12.4	1.6	19.1	22.7	4.8	0.7

H.	pulsed excitation, 6 torr SiF_4 sensitized, 0.09 J/pulse, 2000 pulses[d]	trace	trace	0	0	63.4	36.5	0.1	0.4
I.	pulsed excitation, 6 torr SiF_4 sensitized, 0.11 J/pulse, 1000 pulses[c]	53.4	0	0	0	46.6	trace	0	0.56
J.	flash vacuum pyrolysis[e]	6	10	f	5	55	10	13	6

[a]Numbers are percent of total products found.

[b]All data have been corrected for FID response.

[c]10-cm cell.

[d]5-cm cell.

[e]Reference 11.

[f]Not determined.

Table II. Effect of radical scavenger on the product distribution from cw laser-sensitized pyrolysis of 1[a]

	power (W)	time (S)	HI (torr)	I_2 (torr)	toluene (torr)	1 conv%	Products % 2	3	4	5	6	7	others
A	9.0	120	0	0	0	2.7	19.2	11.0	4.8	1.8	56.6	6.6	
B	9.0	120	0	0	1.0	0.9	35.7	6.0	0	0	53.5	4.7	
C	9.0	60	1.0	0	0	0.4	30	trace	-	-	70	trace	
D	9.0	60	0.2	0	0	0.75	11.2	9.2	-	-	70	9.2	
E	9.0	60	0	0.25	0	7.0	1.3	-	-	-	50.7	44.0	3.6[b]

[a]3.5 (i.d.) x 4.0 cm cell, Sf_6 = 6.0 torr, and 1 = 0.325 torr.

[b]The 3.6% of products consist of two peaks with longer retention times than product 7. The structures were not determined. These are likely to be iodine substitution products.

Table III. H-atom induced decomposition of ethane and propylene[a]

UV Laser Power (mJ/pulse)	Number of Pulses	Sample	HI (torr)	Conversion (%)	Products		
					CH_4	C_2H_4	C_2H_2
147	6000	ethane or propylene 2.0 torr	0	0	0	0	0
147	6000	ethane[b] 2.0 torr	5.0	0.99	0.66	0.66	0
147	12000	ethane 2.0 torr	5.0	1.8	1.4	1.1	0
143	6000	propylene 2.0 torr	5.0	4.5	1.5	1.3	2.5
0	0	ethane or propylene	5.0	0	0	0	0

[a]Cell: 2.0 (i.d.) x 5.0 cm, Injection: 0.2 ml, Column Temperature: 60½C.

[b]Ethane contains 0.5% of ethylene, which has been corrected for in the results.

Table IV. Pyrolysis of cyclodecane in SF_6-sensitized cw laser experiment[a]

power (W)	time (s)	cyclodecane (torr)	SF_6 (torr)	conversion (%)	Products %[b]					
					247[c]	140A	140B	140C	138A	138B
10	600	0.4	6.5	0	-	-	-	-	-	-
14.5	600	0.4	6.0	<0.5	-	>80	-	-	-	-
17.5	600	0.4	6.0	5.2	7.2	45.8	18.0	7.2	12.0	9.6
FVP[d]				7.8	7.3	63.3	11.9	5.5	6.4	5.5

[a]Cell: 3.5 (i.d.) x 4.0 cm, P(20). Purity of cyclodecane: 93.3% (used as received).

[b]Six largest peaks were selected and placed in the order of GC retention time. The GC response factor was assumed to be the same for all peaks. These six peaks contained more than 90% of the products.

[c]Number represent the mass.

[d]Data provided by L. Su and W. S. Trahanovsky.

Table V. Yields of Pyrolysis Products of 2-Benzocycloheptenone

Experiment	T (°C)	P(torr)	Conv%[a]	Products%								
				3	2	4	1	6	7	A	B	others
Flash Vacuum Pyrolysis	700	3×10^{-5}	10.1	trace	trace	2.1	2.6	6.5	4.1	7.6	21.0	56.1[b]
	750	5×10^{-5}	17.0	trace	trace	5.3	9.4	11.7	7.3	10.5	27.4	28.4[c]
	800	5×10^{-5}	32.8	0.6[d]	1.4	9.6	20.2	13.3	7.3	6.3	15.8	25.5[e]
	850	3×10^{-4}	60.4	1.2	2.1	11.3	24.6	8.0	7.2	6.6	16.3	22.7[f]
	900	3×10^{-4}	90.4	4.6	4.5	18.8	25.4	5.0	12.5	3.1	6.5	19.6[f]
Laser Induced Pyrolysis[g]		2×10^{-2}	7.8	trace	trace	18.2	57.3	12.4	12.2	--	--	--
		8×10^{-2}	22.8	8.8	trace	7.7	20.6	13.7	20.7	--	8.4	19.8[h]

[a]Amount in % of Ketone recovered subtracted from 100.A: 1-methylnapthalene, B: 2-methylnapthalene.

[b]Two products, with retention times near those of the methylnapthalenes, constitute 30.1% of the products. Flash vacuum pyrolysis data provided by J. L. Malandra and W. S. Trahanovsky.

[c]One product, with retention time near those the methylnapthalenes, constitutes 8.8% of products.

[d]Relative GC yields in %, uncorrected.

[e]Yields of individual products were <5%.

[f]Yields of individual products were <3%.

[g]Conditions are SF_6 = 6 torr, laser power = 9.5 W and reaction time = 180 s.

[h]Yields include 5 peaks.

GENERAL SUMMARY

New applications of laser-based techniques have been investigated in this dissertation in three major areas: thin-layer chromatography, microprobe elemental analysis and gas phase pyrolysis.

A new quantitation method, laser pyrolysis with the use of a CW infrared laser, is demonstrated for thin-layer chromatography. No spray reagent or "color" developing process is necessary for detecting any organic compound. A complete analysis including sample introduction, separation and detection takes less than 20 min. Two amino acids, serine and phenylalanine, and two pesticides, p,p-DDT and methoxychlor were used as the test samples. The sensitivity and linearity compare favorably to conventional densitometry. The detection limit for phenylalanine with flame ionization detection was 100 ng and foe methoxychlor with electron-capture detection was 20 ng. This technique combine the advantages of the separation power of TLC and the broad spectrum of detection methods of gas chromatography.

Another new method of laser application demonstrated is direct coupling of TLC to GC with the use of a excimer pulse laser. Laser desorption with a special TLC cell was used for the interface. Factors affecting the transfer efficiency and the parent peak ratio were studied. The fragmentation pattern in the gas chromatogram provides a fingerprint for each TLC separated compound. For TLC separations of complex mixtures, GC provides one more dimension of separation and sensitive detection. Laser desorption with electron capture detection(no GC column) was also

investigated as a universal quantitative technique for TLC. The limit of detection was in the low nanogram range. The scan speed was five times faster, the detection limit was 20 times lower, and the resolution was two times better than the analogous laser pyrolysis method. It, actually, demonstrated that pulse laser is better than CW infrared laser in the application of vaporization scanning TLC plates.

Chemiluminescence produced by the reactions of Si, Ge, Al and Cu atoms with F_2 or fluorine containing compounds such as SF_6 and NF_3 was observed in laser generated plume. The emission spectra correspond to the individual monofluorides. The reaction of Si with SF_6 was examined and the chemiluminescence intensity was found to be first order with respect to SF_6 pressure for low pressure. Chemiluminescence as elemental detection method for laser microprobe analysis was evaluated. The limit of detection of Si was around 10 pg. The acoustic signal associated with the laser generated plume was linearly related to the chemiluminescence intensity over two orders of magnitude. The acoustic signal can thus be used as an internal standard for chemiluminescence determination of elements, even through the amount of material vaporized is different for each laser pulse.

For the gas phase pyrolysis, a model is developed for predicting temperature profiles in a gas cell containing absorbing gas when irradiated by a CW laser beam with well defined parameters. The model takes into account the explicit temperature dependence of heat capacities, thermal conductivities, molar absorptivities, and gas densities. The predicted transmittance of the laser beam as a function of incident power

agrees with experimental values. The model is further used to predict rate parameters of a standard homogeneous pyrolysis reaction that is sensitized by the heated gas. The results provide insight into the comparison between the traditional thermal processes and CW laser sensitized pyrolysis.

The laser-induced decomposition of tetralin was investigated under conditions at which both the excitation temperatures and the conversions of reaction are minimized. The major products were found to be 1,2-dihydronaphthalene and naphthalene. Arrhenius parameters were determined for the two channels, hydrogen loss and ethylene loss, to be E_a = 72 Kcal/mole, log A(s^{-1}) = 15.2, and E_a = 79 Kcal/mole, log A(s^{-1}) = 16.8, respectively. Surface reactions and radical chain reactions were determined to be unimportant. The results indicate that dehydrogenation is the lowest energy homogeneous decomposition channel.

REFERENCES

1. Piepmeier, E. H. Ed. Analytical application of Lasers, Wiley: New York. 1986.
2. Dittrich, K., and Wennrich, R. Prog. Analyt. Atom. Spectrosc., 1984, 7, 139.
3. Laqua, K. Analytical Laser Spectroscopy, Wiley: 1979; Chapter 2, p47
4. Berman, M. R., and Zare, R. N. Anal. Chem., 1975, 47, 1200.
5. Bicking, M. K. L., Kinseley, R. N., and Svec, H. J. Anal. Chem., 1983, 55, 200.
6. Huie, C. W., and Williams, W. R. Anal. Chem., 1989, 61, 2288.
7. Personor, R. I. "Laser Fluorescence Analysis of Organic Molecules in Solid Solutions" Ed. Letokhvo, V. S., Laser Analytical Spectroscopy, IOP: New York, 1986.
8. Hurtubise, R. J. Anal. Chem., 1989, 61, 889A
9. Chen, I. T., and Morris M. D. Anal. Chem., 1984, 56, 19
10. Scudieri, F. "Photoacoustic Analysis in Condensed Matter", Ed. Martallucci, S., Chester, A. N. Analytical Laser Spectroscopy; Plenum Press: New York, 1985.
11. Chen, I. I., and Morris, M. D. Anal. Chem., 1984, 56, 19.
12. Fishman, V. A., and Barda, J. Anal. Chem., 1981, 51, 102.
13. Rosencwaig, A. and Nall S. S. Anal. Chem., 1975, 47, 548.
14. Eloy, J. F. C.E.A. Report, Grenoble, No. 4777, 1976.
15. Lincoln, K. A. Int. J. Mass Spectrom. Ion Phys., 1974, 45, 13.

16. Selter, K. P., and Kunze, H. J. Physica Scripta, 1982, 25, 929.

17. Tembreull, R., and Lubman, D. M. Anal. Chem., 1984, 56, 19.

18. Shibanov, A. N. "Laser Desorption Spectrometry of Nonvolatile Organic Molecules", Ed. Letokhov, V. S. Laser Analytical Spectroscopy, IOP: New York, 1986.

19. Baldwin, M. A. and Mclafferty, F. W. Org. Mass Spectrom., 1973, 7, 1353.

20. Lee, T. D., Anderson, W. R. Jr.,and Daves, G, D. Jr. Anal. Chem., 1981, 53, 304.

21. Cotter, R. J., and Fenshelan, C. Biomed. Mass Spectrom., 1979, 6, 287.

22. Haverkamp, J., and Kistemaker, P. G. Int. J. Mass Spectrom. Ion Phys., 1982, 45, 275.

23. Vanderborgh, N. E. "Laser Induced Pyrolysis Techniques", Ed. Jones, C. E. R., and Cramers, C. A. Analytical Pyrolysis, Elsevier, New York, 1977, 235.

24. Posthumus M. A., Kistemaker, P. G., Meuzelaar H. L. C., and Ten Noever De Brauw M. C. Anal. Chem., 1978, 50, 985.

25. Means, J. C., and Perkins, E. G. "Laser pyrolysis GC/MS of Membrane Components", Ed. Jones, C. E. R., and Cramers, C. A. Analytical Pyrolysis, Elsevier: New York, 1977, 249.

26. Madison, S. A., and Keehn, P. M. J. Anal. Appl. Pyrol., 1986, 9, 237.

27. Fanter, D. L., Levy, R. L. and Wolf, C. J. Anal. Chem., 1972, 44, 43.

28. Basov, N. G., Boiko, V. A., Krokhin, O. N., Semenov, O. G., and Skilizkov, G. V. Zh. Tekh. Fiz., 1968, 38, 1973.

29. Shu, V. H., Kivel, B., and Weyl, G. M. J. Quant. Spectrosc. Radiat.

Transfer, 1978, 20, 627.

30. Dpauszky, I. Pure Appl. Chem., 1982, 54, 879.

31. Howe, J. A. J. Chem. Phys., 1963, 39, 1362.

32. Dimitrov, G., Nikolova, L. and Vassiler, Y. Mikrochim. Acta(wien), Suppl., 1979, I, 503.

33. Brech, F. Appl. Spectrosc., 1962, 16, 59.

34. Lambert, D. J. Chem. Soc., Faraday Trans. II, 1972, 68, 364.

35. Shaub, W. M. and Bauer S. H. Int. J. Chem. Kinet., 1975, VII, 509.

36. Touchstone, J. C., and Dobbins M. F. Practice of Thin Layer Chromatography; Wiley: New York, 1983.

37. Kirchner, J. G. Thin Layer Chromatography; Wiley: New York, 1978.

38. Drug Testing and Research Program, New York State Racing & Wagering Board, Cornell University, 1981.

39. Touchstone J. C., and Sherma J. Densitometry in Thin layer Chromatography Practice and Applications; Wiley: New York, 1979.

40. Hiemenz, P. C. Principles of Colloid and Surface Chemistry, Dekker, New York, 1977.

41. Ma, Y., and Yeung, E. S. Anal. Chem., 1988, 60, 722.

41a. Raglione, T. V.; Hartwick, R. A. Anal. Chem. 1986, 58, 2680.

41b. Hofstraat, J. W.; Engelsma, M.; Van De Nesse, R. J.; Gooijer, C.; Velthorst, N. H.; Brinkman, U. A. Anal. Chim. Acta 1986, 186, 247.

41c. Casu, B.; Cavallotti, L. Anal. Chem. 1962, 34, 1514.

41d. Janak, J. J. Gas Chromatogr. 1964, 15, 15.

41e. Humphrey, A. M. J. Chromatogr. 1970, 53, 375.

42. Okumura, T., Kadono, T., and Iso'o A. J. Chromatogr., 1975, 102, 329.

43. Ranny, M. Thin-Layer Chromatography With Flame Ionization Detection; Reidel: New York, 1987.

44. Ma, Y., Koutny, L. B., and Yeung, E. S. Anal. Chem., 1989, 61, 1931.

45. Sanders, M. J., Cooper, R. S., and Small, G. J. Anal. Chem., 1986, 54, 816.

46. Colling, E., Burda, B. H., and Kelley, P. A. J. Chromatogr. Sci., 1986, 24, 7.

47. Ready, J. F. J. Appl. Phys., 1965, 36, 462.

48. Spitzer, L. In Physics of Fully Ionized Gases; Interscience: New York, 1962, Chapter 5.

49. Pang, H. M., and Yeung, E. S. Anal. Chem., in press.

50. Nikolaev, G. I., and Podgornaja, V. I. Zh. Prikl. Spektrosk., 1972, 16, 911.

51. Petrakiev, A., Jotov, T., and Georgieva, L. 8th Nat. Conf. Spectrosc., Verna, 1968, 165.

52. Conzemius, R. J., and Capellen, J. M. Int. J. Mass Spectrom. Ion Phys., 1980, 34, 197.

53. Schaden, G. J. Anal. Appl. Pyroly., 1985, 8, 135.

54. Kelly, J. D., and Wolf, C. J. J. Chromatogr. Sci., 1970, 8, 583.

54a. Loudon, A. G., Maccoll, A., and Wong, S. K. J. Chem. Soc. (B), Phys. Org., 1970, 1733.

55. Carlsen, L., and Egsgaard, H. Thermochim. Acta, 1980, 38, 47.

56. Egsgaard, H., Larsen, E., and Carlsen, L. J. Anal. Appl. Pyroly., 1982, 4, 33.

57. Egsgaard, H., and Carlsen, L. J. Anal/ Appl. Pyroly., 1984, 7, 1.

58. Carlsen, L. "Gas Phase Gurie Point Pyrolysis", Ed. Voorhees, K. J. Analytical Pyrolysis; Butterworth: London, 1984.

59. Egsgaard, H., and Carlsen, L. J. Anal. Appl. Pyroly., 1986, 10, 83.

60. Egsgaard, H., and Carlsen, L. J. Anal. Appl. Pyroly., 1983, 5, 257.

61. Barlow, A., Lehrle, R. S., Robb, J. C., and Sunderland, D. Polymer, 1967, 8, 523.

62. Meier, J., Akermann, F., and Guenthard, H. H. Chim. Acta, 1968, 51, 1686.

63. Moylan, C. R., and Brauman, J. I. Int. J. Chem. Kinet., 1986, 18, 379.

64. Holbrook, K. A., Ddershaw, G. A., and Mathews, M. Int. J. Chem. Kinet., 1985, 17, 1275.

65. Pola, J. Collect. Czech. Chem. Commun., 1981, 46, 2860.

66. Pola, J., and Vcelak, J. J. Anal. Appl. Pyrolysis, 1987, 10, 257.

67. Tsang, W., Walker, J. A. and Braun, W. J. Phys. Chem., 1982, 86, 719.

68. Perettie, D. J., Khan, S. M., Clark, J. B., and Grzybowski, J. M. "Laser induced Selective Decomposition Reactions", Ed. Kompa, K. L., and Wanner, J. Laser Application in Chemistry; Plenum: New York, 1984.

69. Harrison, R. G. "Infrared Laser induced Energy Distributions in Polyatomic Molecules", Ed. Kompa, K. L., and Wanner J. Laser Applications in Chemistry; Plenum: New York, 1984.

70. Olszyna, K. J., Grunwald, E., and Keehn, P. M. Tetrahedron Letters, 1977, 19, 1609.

71. Comita, P. B. Ph.D. Thesis, University of California, Berkeley, 1981.

ACKNOWLEDGEMENT

I would like to express my thanks and appreciation to Dr. Edward S. Yeung for the opportunity to do the research in the field of laser spectroscopy and for providing invaluable insight at crucial times during the course of this work.

All the members of my research group also deserve my thanks for their fellowship and support, especially Patrice, who has been so helpful in the past years.

I am also grateful to Dr. W. S. Trahanovsky and his students: S. Lee, D. R. Fisher, L. Su, and J. L. Malandra for collaborators in the tetralin experiment.

I would like to acknowledge my ten-day-old daughter, Kathy, who is so cute and has given me so much joy and trouble.

Finally, I wish to express my especial appreciation to my wife, Quanhong, for her love, understanding and tremendous support.